NASA TECHNICAL
MEMORANDUM

DYNAMIC STABILITY CHARACTERISTICS
OF THE COMBINATION SPACE SHUTTLE
ORBITER AND FERRY VEHICLE

Delma C. Freeman, Jr., and Richmond P. Boyden

Langley Research Center
Hampton, Va. 23665

1. Report No. NASA TM X-3497	2. Government Accession No.	3. Recipient's Catalog No.
4. Title and Subtitle DYNAMIC STABILITY CHARACTERISTICS OF THE COMBINATION SPACE SHUTTLE ORBITER AND FERRY VEHICLE		5. Report Date May 1977
		6. Performing Organization Code
7. Author(s) Delma C. Freeman, Jr., and Richmond P. Boyden		8. Performing Organization Report No. L-11131
9. Performing Organization Name and Address NASA Langley Research Center Hampton, VA 23665		10. Work Unit No. 506-26-30-04
		11. Contract or Grant No.
12. Sponsoring Agency Name and Address National Aeronautics and Space Administration Washington, DC 20546		13. Type of Report and Period Covered Technical Memorandum
		14. Sponsoring Agency Code

15. Supplementary Notes

16. Abstract

Subsonic forced-oscillation tests of a 0.015-scale model of the space shuttle orbiter/747 ferry vehicle were conducted in the Langley high-speed 7- by 10-foot tunnel. The tests were made at Mach numbers of 0.2, 0.4, and 0.5 for angles of attack up to 12°. Tests were made of the basic 747 airplane, of the modified 747 (tip fins and struts added), of the ferry configuration (747 plus orbiter at an incidence angle of 3°), and of the approach and landing test configuration (747 plus orbiter at an incidence angle of 6°).

17. Key Words (Suggested by Author(s)) Space shuttle Dynamic stability Shuttle ferry vehicle	18. Distribution Statement Unclassified - Unlimited Subject Category 15	
19. Security Classif. (of this report) Unclassified	20. Security Classif. (of this page) Unclassified	21. No. of Pages 113	22. Price* $5.50

DYNAMIC STABILITY CHARACTERISTICS OF THE COMBINATION

SPACE SHUTTLE ORBITER AND FERRY VEHICLE

Delma C. Freeman, Jr., and Richmond P. Boyden
Langley Research Center

SUMMARY

Subsonic forced-oscillation tests of a 0.015-scale model of the combination space shuttle orbiter and ferry vehicle were conducted in the Langley high-speed 7- by 10-foot tunnel. These tests were made at Mach numbers of 0.2, 0.4, and 0.5 to measure the pitch, yaw, and roll damping, the normal force due to pitch rate, and the cross derivatives, namely, yawing moment due to roll rate and rolling moment due to yaw rate. The results of this investigation showed that the model exhibited large positive damping in pitch, yaw, and roll throughout the test ranges of angle of attack and Mach number for all configuration variables tested.

INTRODUCTION

In support of the space shuttle development effort, the Langley Research Center has sponsored a program to measure experimentally the dynamic stability characteristics of space shuttle vehicles. The aerodynamic damping derivatives have been determined for the orbiter at speeds ranging from subsonic to hypersonic (refs. 1 to 3), and for the launch vehicle from lift-off to staging of the solid rocket boosters (refs. 4 and 5). As a continuation of this work, forced-oscillation dynamic-stability tests of a 0.015-scale model of the combination space shuttle orbiter and ferry vehicle (hereinafter referred to as the space shuttle orbiter/747 ferry vehicle) were made in the Langley high-speed 7- by 10-foot tunnel.

The space shuttle orbiter/747 ferry vehicle has been developed as a part of the shuttle program to provide a transport for the shuttle orbiter vehicle. The carrier aircraft was developed from a commercial Boeing 747 airplane and was modified by the addition of both tip fins to the horizontal tail to augment the directional stability and fore and aft support struts for the orbiter. In addition to the ferry mission, the carrier aircraft will also be used in the orbiter approach and landing tests (ALT configuration) to carry the orbiter to an altitude of approximately 7000 m, at which point the orbiter will be separated for a gliding flight to touchdown.

In the present investigation, tests were made at Mach numbers of 0.2, 0.4, and 0.5 to measure the pitch, yaw, and roll damping, the normal force due to pitch rate, and the cross derivatives, namely, for yawing moment due to roll rate and for rolling moment due to yaw rate. Tests were made of the basic 747 airplane, of the modified 747 (tip fins and struts added), of the ferry configuration (747 plus orbiter at an incidence angle of 3°), and of the approach and

landing test configuration (747 plus orbiter at an incidence angle of 6°). The addition of a tail-cone fairing to the orbiter base for ferrying and the deployment of the 747 wing spoilers for orbiter separation in the approach and landing tests were also investigated.

SYMBOLS

All aerodynamic parameters presented are referred to the body axes system except for the static longitudinal data which are referred to the stability axes system. (See fig. 1.) The origin of the axes corresponded to the center-of-gravity position shown in figure 2 (x_{cg} = 51.13 cm or $0.255\bar{c}$). The dimensional parameters of the basic 747 were used as reference for the aerodynamic coefficients.

b reference span for 747, meters

C_D drag coefficient, $\dfrac{F_D}{q_\infty S}$

C_L lift coefficient, $\dfrac{F_L}{q_\infty S}$

C_l rolling-moment coefficient, $\dfrac{\text{Rolling moment}}{q_\infty S b}$

C_{l_p} $= \dfrac{\partial C_l}{\partial\left(\dfrac{pb}{2V}\right)}$, per radian

$C_{l_{\dot{p}}}$ $= \dfrac{\partial C_l}{\partial\left(\dfrac{\dot{p}b^2}{4V^2}\right)}$, per radian

$C_{l_p} + C_{l_{\dot{\beta}}} \sin\alpha$ damping-in-roll parameter, per radian

C_{l_r} $= \dfrac{\partial C_l}{\partial\left(\dfrac{rb}{2V}\right)}$, per radian

$C_{l_{\dot{r}}}$ $= \dfrac{\partial C_l}{\partial\left(\dfrac{\dot{r}b^2}{4V^2}\right)}$, per radian

$C_{l_r} - C_{l_{\dot{\beta}}} \cos\alpha$ rolling moment due to yaw-rate parameter, per radian

C_{l_β} $= \dfrac{\partial C_l}{\partial\beta}$, per radian

$C_{l_{\dot{\beta}}}$ $= \dfrac{\partial C_l}{\partial\left(\dfrac{\dot{\beta}b}{2V}\right)}$, per radian

$C_{l_\beta} \cos \alpha + k^2 C_{l_{\dot{r}}}$ effective dihedral parameter, per radian

$C_{l_\beta} \sin \alpha - k^2 C_{l_{\dot{p}}}$ rolling moment due to roll-displacement parameter, per radian

C_m pitching-moment coefficient, $\dfrac{\text{Pitching moment}}{q_\infty S \bar{c}}$

$C_{m_q} = \dfrac{\partial C_m}{\partial\left(\dfrac{q\bar{c}}{2V}\right)}$, per radian

$C_{m_{\dot{q}}} = \dfrac{\partial C_m}{\partial\left(\dfrac{\dot{q}\bar{c}^2}{4V^2}\right)}$, per radian

$C_{m_q} + C_{m_{\dot{\alpha}}}$ damping-in-pitch parameter, per radian

$C_{m_\alpha} = \dfrac{\partial C_m}{\partial \alpha}$, per radian

$C_{m_{\dot{\alpha}}} = \dfrac{\partial C_m}{\partial\left(\dfrac{\dot{\alpha}\bar{c}}{2V}\right)}$, per radian

$C_{m_\alpha} - k^2 C_{m_{\dot{q}}}$ oscillatory longitudinal-stability parameter, per radian

C_N normal-force coefficient, $\dfrac{\text{Normal force}}{q_\infty S}$

$C_{N_q} = \dfrac{\partial C_N}{\partial\left(\dfrac{q\bar{c}}{2V}\right)}$, per radian

$C_{N_{\dot{q}}} = \dfrac{\partial C_N}{\partial\left(\dfrac{\dot{q}\bar{c}^2}{4V^2}\right)}$, per radian

$C_{N_q} + C_{N_{\dot{\alpha}}}$ normal force due to pitch-rate parameter, per radian

$C_{N_\alpha} = \dfrac{\partial C_N}{\partial \alpha}$, per radian

$C_{N_{\dot{\alpha}}} = \dfrac{\partial C_N}{\partial\left(\dfrac{\dot{\alpha}\bar{c}}{2V}\right)}$

$C_{N_\alpha} - k^2 C_{N_{\dot{q}}}$ normal force due to pitch-displacement parameter, per radian

C_n yawing-moment coefficient, $\dfrac{\text{Yawing moment}}{q_\infty S b}$

C_{n_p} $\quad = \dfrac{\partial C_n}{\partial\left(\dfrac{pb}{2V}\right)}$

$C_{n_{\dot{p}}}$ $\quad = \dfrac{\partial C_n}{\partial\left(\dfrac{\dot{p}b^2}{4V^2}\right)}$, per radian

$C_{n_p} + C_{n_{\dot{\beta}}}\sin\alpha$ $\qquad$ yawing moment due to roll-rate parameter, per radian

C_{n_r} $\quad = \dfrac{\partial C_n}{\partial\left(\dfrac{rb}{2V}\right)}$, per radian

$C_{n_{\dot{r}}}$ $\quad = \dfrac{\partial C_n}{\partial\left(\dfrac{\dot{r}b^2}{4V^2}\right)}$, per radian

$C_{n_r} - C_{n_{\dot{\beta}}}\cos\alpha$ $\qquad$ damping-in-yaw parameter, per radian

C_{n_β} $\quad = \dfrac{\partial C_n}{\partial\beta}$, per radian

$C_{n_{\dot{\beta}}}$ $\quad = \dfrac{\partial C_n}{\partial\left(\dfrac{\dot{\beta}b}{2V}\right)}$, per radian

$C_{n_\beta}\cos\alpha + k^2 C_{n_{\dot{r}}}$ $\qquad$ oscillatory directional-stability parameter, per radian

$C_{n_\beta}\sin\alpha - k^2 C_{n_{\dot{p}}}$ $\qquad$ yawing moment due to roll-displacement parameter, per radian

C_Y $\qquad$ side-force coefficient, $\dfrac{\text{Side force}}{q_\infty S}$

C_{Y_β} $\qquad = \dfrac{\partial C_Y}{\partial\beta}$, per radian or per degree

$\bar{c}$ $\qquad$ reference chord for 747, meters

F_D $\qquad$ drag force, newtons

F_L $\qquad$ lift force, newtons

f $\qquad$ frequency of oscillation, hertz

i $\qquad$ incidence angle, degrees

k $\qquad$ reduced-frequency parameter, $\omega\bar{c}/2V$ in pitch and $\omega b/2V$ in roll and yaw, radians

M $\qquad$ free-stream Mach number

4

M_Y	pitching moment, newton-meters
M_Z	yawing moment, newton-meters
p	angular velocity of model about X-axis, radians per second
q	angular velocity of model about Y-axis, radians per second
q_∞	free-stream dynamic pressure, pascals
R	Reynolds number, based on $\bar{c}$ of 747
r	angular velocity of model about Z-axis, radians per second
S	reference area, meters^2
V	free-stream velocity, meters per second
X,Y,Z	body system of axes
X_s,Y_s,Z_s	stability system of axes
x_{cg}	center of gravity along X-axis
z_{cg}	center of gravity along Z-axis
α	angle of attack, degrees or radians
β	angle of sideslip, radians
δ_s	spoiler deflection, degrees (numbers used as subscripts depict spoiler segments)
ω	angular velocity, $2\pi f$, radians per second

Subscript:

o	orbiter

A dot over a quantity indicates a first derivative with respect to time.

APPARATUS AND MODEL

A three-view drawing of the 0.015-scale model used in the investigation is presented in figure 2(a). The model consisted of the space shuttle orbiter mounted "piggyback" on the 747 carrier vehicle. The model was constructed to enable tests of the basic 747, the modified 747 (tip fins and struts added), the ferry mode (orbiter incidence angle of 3°), and the approach and landing test mode (orbiter incidence angle of 6°). Other configuration changes such as the

5

fairing of the tail cone on the orbiter base (fig. 2(b)), the installation of the rocket nozzle (fig. 2(c)), the fairing of support struts (fig. 2(d)), and deployment of the 747 wing spoilers to represent approach and landing test orbiter separation conditions (fig. 2(e)) were also duplicated. A drawing of the 747 tip fins is presented in figure 2(f).

In order to accommodate the support sting, the base of the 747 was modified as shown in figures 2(g) and 3. The modifications consisted of a fuselage cross section that is constant from a point just aft of the wing-body juncture to the end of the model. The span and geometry of the horizontal tail were maintained by removing area from the root. Although this modification would be expected to alter the aerodynamic and damping characteristics of the basic 747, it should not materially affect the incremental effect of the orbiter on the overall dynamic characteristics of the model; therefore, the addition of the measured increments to the damping extracted from flight tests of the basic 747 should give the correct damping values for the ferry and ALT vehicles.

The forced-oscillation tests were made in the Langley high-speed 7- by 10-foot tunnel. The operating characteristics of the tunnel are presented in reference 6. Photographs of the model are presented in figure 3. A description of the apparatus and data-reduction techniques is presented in reference 2.

TESTS

The forced-oscillation dynamic-stability tests were made to determine the pitch $C_{m_q} + C_{m_{\dot{\alpha}}}$, yaw $C_{n_r} - C_{n_{\dot{\beta}}} \cos \alpha$, and roll damping $C_{l_p} + C_{l_{\dot{\beta}}} \sin \alpha$; the normal force due to pitch rate $C_{N_q} + C_{N_{\dot{\alpha}}}$; and the cross derivatives, namely, yawing moment due to roll rate $C_{n_p} + C_{n_{\dot{\beta}}} \sin \alpha$ and the rolling moment due to yaw rate $C_{l_r} - C_{l_{\dot{\beta}}} \cos \alpha$. The values of the nominal amplitude of the oscillation and of the range of the reduced-frequency parameter k during the tests were:

Axis	Amplitude, deg	k, rad
Pitch	1	0.0058 to 0.0190
Yaw	1	0.0064 to 0.0159
Roll	2.5	0.0109 to 0.0195

Static force tests were made to determine the static longitudinal and lateral stability characteristics of the model to aid in the interpretation of the dynamic tests results. Both the static and dynamic force tests were made over an angle-of-attack range of approximately -4° to 12°. The static lateral stability characteristics were determined from incremental differences in C_n, C_l, and C_Y measured over the angle-of-attack range at fixed angles of sideslip of 0° and 2.5°. The test conditions were as follows:

Mach number, M	Dynamic pressure, q_∞, Pa	Reynolds number, R
0.2	2 758	0.56×10^6
.4	10 165	1.06
.5	14 948	1.27

For all tests, transition in the form of sparsely distributed No. 80 carborundum grains was applied in bands 0.16 cm wide located 1.5 cm streamwise from the leading edges of all lifting surfaces of both the 747 and orbiter. Similar bands were applied in rings 3.05 cm aft of the nose of the orbiter and the 747.

The static force data have been corrected for sting bending and all drag data are total drag in that the base drag has not been subtracted out.

PRESENTATION OF RESULTS

The contents of the figures presented in this paper are as follows:

RESULTS AND DISCUSSION

Static Longitudinal Stability

The static-longitudinal-stability data for the model are presented in fig-
ures 4 and 5. These static data, which were obtained by utilizing the same
model that was used for the dynamic tests, are presented to verify and aid inter-
pretation of the dynamic test results. The results of tests to determine the
effects of the addition of the orbiter support struts and the tip fins to the
basic 747 are presented in figure 4. Addition of the struts and tip fins
increased the static longitudinal stability; this indicated that the increased
horizontal tail effectiveness due to the end-plating effects of the tip fins
more than overpowered any strut drag effects on the model stability. Presented
in figure 5 are results of tests made to determine the effect of the orbiter and
orbiter incidence on the static longitudinal characteristics of the modified 747

(struts and tip fins added). Although the combination orbiter and 747 was less stable than the 747 alone at low angles of attack, the instability of the 747 alone above an angle of attack of 8° was eliminated by the addition of the orbiter. Increasing the orbiter incidence angle to 6° provided a positive trim increment at all angles of attack and increased the trim angle of attack from 3.5^O to 8°.

Static Lateral Stability

The static-lateral-stability data are presented in figures 6 and 7. The results of figure 6 show the effect of tip fins and struts on the static lateral characteristics of the basic 747 and indicated that, as expected, the addition of the tip fins resulted in an increase in $C_{n\beta}$ at low angles of attack because

of the increased side area of the tip fins. The fins had very little effect on $C_{l\beta}$. Results presented in figure 7 show the effect of the orbiter and orbiter

incidence on the static lateral characteristics of the modified 747. Adding the orbiter shielded the 747 vertical tail and resulted in a large decrease in $C_{n\beta}$

at angles of attack below 4°. As the angle of attack increased to 5° or 6°, the 747 vertical tail emerged from the wake of the orbiter and directional stability was essentially restored to the level of the 747 without the orbiter. This change in the level of $C_{n\beta}$ is generally above the cruise angle-of-attack range

(for example, at $M = 0.5$ for the ferry configuration ($i_O = 3^O$) the cruise angle of attack is 4.5^O). Results of figure 7 also indicate that the orbiter installation increased the level of the effective dihedral $\left(-C_{l\beta}\right)$.

Pitching Oscillation Test Results

The oscillatory-longitudinal-stability parameters measured in the pitching oscillation tests at Mach numbers of 0.2, 0.4, and 0.5 are presented in figures 8 to 17. The in-phase with displacement parameter $C_{m\alpha} - k^2 C_{m\dot{q}}$ and the

out-of-phase with displacement parameter $C_{m_q} + C_{m\dot{\alpha}}$ are presented in figures 8

to 12. A comparison of the in-phase $C_{m\alpha} - k^2 C_{m\dot{q}}$ with $C_{m\alpha}$ computed from the

static tests results is presented in figure 9. This comparison made for the ferry configuration ($i_O = 3^O$) shows reasonable agreement between the static and forced-oscillation test results.

In general, the model exhibited large positive pitch damping $\left(\text{negative val-}\right.$ ues of $C_{m_q} + C_{m\dot{\alpha}}\left.\right)$. The data of figure 8 show the effects of adding the tip

fins and struts to the basic 747 configuration. These results show significant increases in the damping of the 747 due to these additions. The increased damping results from increased horizontal tail effectiveness due to the end-plating

effect of the tip fins. The addition of the orbiter to the modified 747 generally increased the pitch damping. (See fig. 9.)

The effect of strut fairings (fig. 2(d)) and spoiler deployment (fig. 2(e)) is presented in figures 10 and 11, respectively. These configuration changes had no significant overall effect on the level of the pitch damping.

The results of figure 12 show the effect of the orbiter tail-cone fairing (fig. 2(b)) on the pitch damping. Even though the tail cone increased the orbiter length by approximately 25 percent, it had essentially no effect on the pitch damping of the ferry configuration because of the very large damping of the 747.

The normal force due to pitching velocity $C_{N_q} + C_{N_{\dot\alpha}}$ and the in-phase with displacement parameter $C_{N_\alpha} - k^2 C_{N_{\dot q}}$ are presented in figures 13 to 17. These results show $C_{N_\alpha} - k^2 C_{N_{\dot q}}$ is positive and decreases with angle of attack. Considerable scatter is seen in $C_{N_q} + C_{N_{\dot\alpha}}$ because the measurement of the secondary parameters is more difficult, as pointed out in reference 2. The comparison of the in-phase parameter $C_{N_\alpha} - k^2 C_{N_{\dot q}}$ with C_{N_α} determined from the static data presented in figure 14 shows good agreement.

Yawing Oscillation Tests

The oscillatory-stability parameters measured in the yawing oscillation tests are presented in figures 18 to 25. The in-phase with displacement parameter $C_{n_\beta} \cos \alpha + k^2 C_{n_{\dot r}}$ and out-of-phase with displacement parameter $C_{n_r} - C_{n_{\dot\beta}} \cos \alpha$ results are included in figures 18 to 21. The model had large positive damping in yaw $\left(\text{negative values of } C_{n_r} - C_{n_{\dot\beta}} \cos \alpha\right)$ throughout the test ranges of angle of attack and Mach number. Data showing the results of adding the tip fins and struts to the basic 747 are presented in figure 18. These results show a significant increase in the yaw damping due to the increased side area of the tip fins aft of the center of rotation. The effect of the orbiter and orbiter incidence on the yaw damping $C_{n_r} - C_{n_{\dot\beta}} \cos \alpha$ of the modified 747 and data showing a comparison of the in-phase parameter $C_{n_\beta} \cos \alpha + k^2 C_{n_{\dot r}}$ and $C_{n_\beta} \cos \alpha$ computed from the static test are presented in figure 19. There appears to be good agreement between the static and dynamic test results. The addition of the orbiter to the modified 747 had no adverse effects on the vehicle damping although the orbiter installation slightly increased the damping of both the ferry and ALT vehicle. The large decrease in C_{n_β} due to the blanket-

10

ing of the 747 vertical tail by the orbiter seen in the static data (fig. 7) also is seen in the in-phase parameter. Deploying the spoilers (fig. 20) and adding the tail cone (fig. 21) had no adverse effects on the combined vehicle damping.

The rolling moment due to yawing velocity $C_{l_r} - C_{l_{\dot{\beta}}} \cos \alpha$ is presented in figures 22 to 26. A comparison of the in-phase parameter $C_{l_\beta} \cos \alpha + k^2 C_{l_{\dot{r}}}$ with $C_{l_\beta} \cos \alpha$ computed from the static data (fig. 23) shows the static data to have the same trends with angle of attack and approximately the same level as the in-phase parameter. The measured value of $C_{l_r} - C_{l_{\dot{\beta}}} \cos \alpha$ is positive at zero angle of attack and increases with angle of attack. Configuration changes have little effect on the parameter.

Rolling Oscillation Tests

The oscillatory-stability parameters measured in the rolling oscillation tests are presented in figures 26 to 33. The in-phase with displacement parameter $C_{l_\beta} \sin \alpha - k^2 C_{l_{\dot{p}}}$ and out-of-phase with displacement parameter $C_{l_p} + C_{l_{\dot{\beta}}} \sin \alpha$ are presented in figures 26 to 29. Data showing the effect of orbiter and orbiter incidence on the roll damping of the basic 747 along with a comparison of $C_{l_\beta} \sin \alpha - k^2 C_{l_{\dot{p}}}$ with $C_{l_\beta} \sin \alpha$ computed from the static tests (fig. 27) indicate good agreement between the static and dynamic test results. The model exhibited large positive roll damping (negative values of $C_{l_p} + C_{l_{\dot{\beta}}} \sin \alpha$) throughout the test ranges of angle of attack and Mach number.

Except for the spoiler deployment at high angles of attack (fig. 28), the roll damping of the ferry and ALT configuration was insensitive to the configuration changes tested. The results of figure 28 show that, at the higher test angles of attack, the deployment of the spoiler did increase the roll damping. This increased damping is probably caused by the formation of regions of separated flow on the wing which lags the model motion and therefore increases the damping contribution of the wing.

The yawing moment due to rolling velocity $C_{n_p} + C_{n_{\dot{\beta}}} \sin \alpha$ data measured in the roll tests are presented in figures 30 to 33. The results of figure 31, which presents the effect of the orbiter and orbiter incidence on the yawing moment due to rolling velocity, show that the addition of the orbiter to the modified 747 resulted in a negative increment in $C_{n_p} + C_{n_{\dot{\beta}}} \sin \alpha$. Also presented in figure 31 is a comparison of $C_{n_\beta} \sin \alpha - k^2 C_{n_{\dot{p}}}$ with $C_{n_\beta} \sin \alpha$ computed from the static data. These comparisons show good agreement between the static and dynamic test results.

11

SUMMARY OF RESULTS

An investigation has been conducted to determine the subsonic dynamic stability characteristics of a 0.015-scale model of the combination space shuttle orbiter and ferry vehicle. The results of this investigation may be summarized as follows:

1. The model exhibited large positive damping in pitch, yaw, and roll throughout the test ranges of angle of attack and Mach number for all configuration variations.

2. There was generally good agreement of the in-phase dynamic parameters with the corresponding static data.

3. Addition of the orbiter to the modified 747 had no adverse effects on the damping over the test ranges of angle of attack and Mach number.

4. Addition of the orbiter to the modified 747 shielded the 747 vertical tail and significantly reduced the directional stability of the ferry and ALT configuration at angles of attack below 4°.

Langley Research Center
National Aeronautics and Space Administration
Hampton, VA 23665
February 28, 1977

REFERENCES

1. Boyden, Richmond P.; and Freeman, Delma C., Jr.: Subsonic and Transonic Dynamic Stability Characteristics of a Space Shuttle Orbiter. NASA TN D-8042, 1975.

2. Freeman, Delma C., Jr.; Boyden, Richmond P.; and Davenport, E. E.: Supersonic Dynamic Stability Characteristics of a Space Shuttle Orbiter. NASA TN D-8043, 1976.

3. Uselton, Bob L.; and Jenke, Leroy M.: Pitch-, Yaw-, and Roll-Damping Characteristics of a Shuttle Orbiter at $M_\infty = 8$. AEDC-TR-74-129, U.S. Air Force, May 1975. (Available from DDC as AD A011 648.)

4. Freeman, Delma C., Jr.; Boyden, Richmond P.; and Davenport, Edwin E.: Subsonic and Transonic Dynamic-Stability Derivatives of a Space Shuttle Launch Vehicle. NASA TM X-3336, 1976.

5. Boyden, Richmond P.; Freeman, Delma C., Jr.; and Davenport, Edwin E.: Supersonic Dynamic-Stability Derivatives of the Space Shuttle Launch Vehicle. NASA TM X-3315, 1976.

6. Schaefer, William T., Jr.: Characteristics of Major Active Wind Tunnels at the Langley Research Center. NASA TM X-1130, 1965.

Figure 1.- System of axes used in investigation. Arrows indicate positive
direction of moments, forces, and angles.

ORBITER DIMENSIONS

S_o .056 m^2

b_o 18.09 cm

$\bar{c}_o$ 35.69 cm

REFERENCE DIMENSIONS

x_{cg} 51.13 cm (Ferry config.)

z_{cg} 8.79 cm (Ferry config.)

S .115 m^2 (747)

b 89.46 cm (747)

$\bar{c}$ 12.49 cm (747)

$\bar{c}$

105.99

47.93

18.71

89.46

$x_{cg} = 51.13$

61.24

25.98

i_o

$z_{cg} = WL\ 8.79$
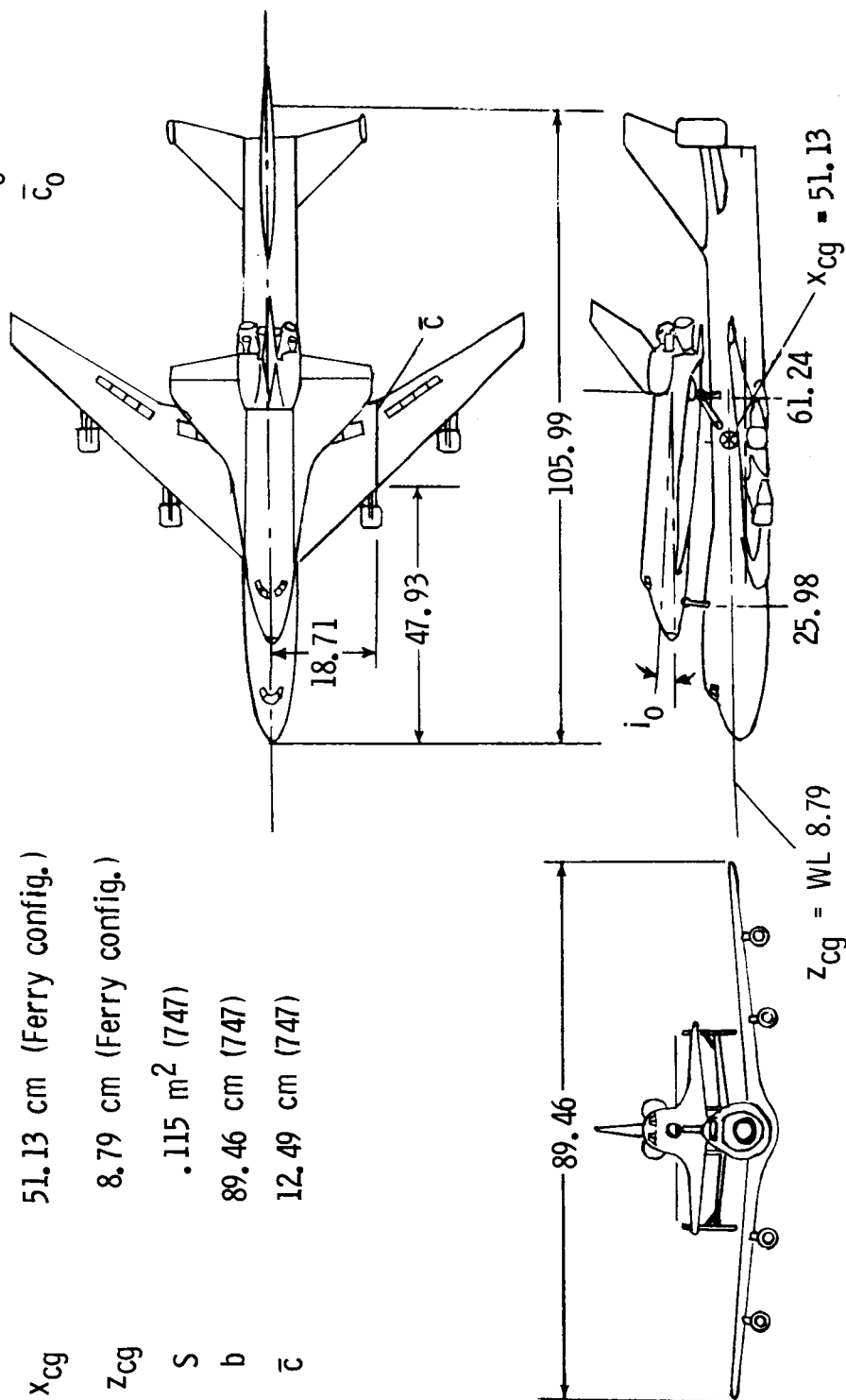
(a) Three-view drawing of model.

Figure 2.- Drawings of model used in investigation. All dimensions are in centimeters.

15

10.03

Rear view

15.49

Side view
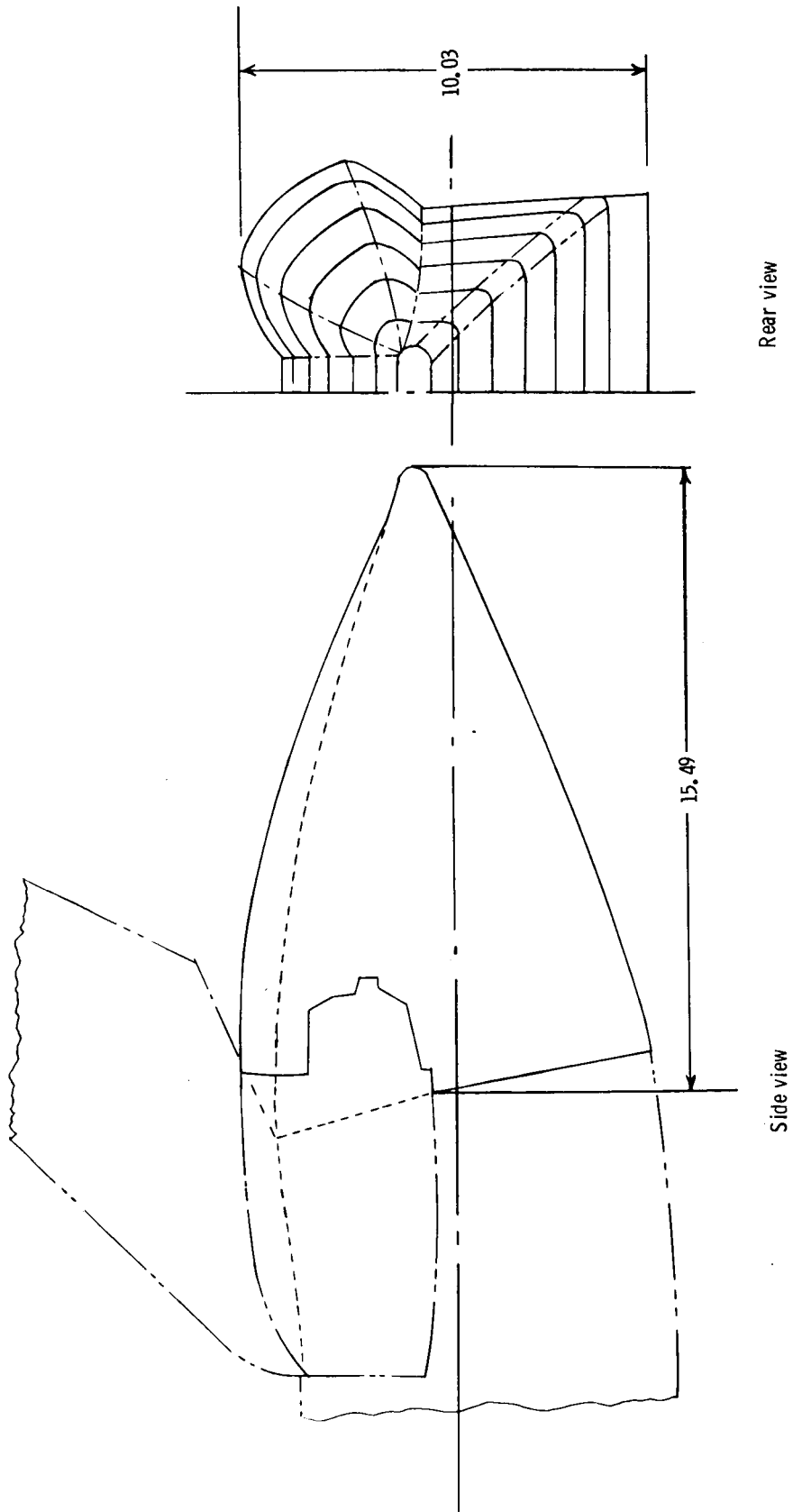
(b) Orbiter tail-cone fairing.

Figure 2.- Continued.

Top view

Orbiter base

3° 30′

Model center line

3° 30′

Side view

Orbiter base

16°

Model center line

10°
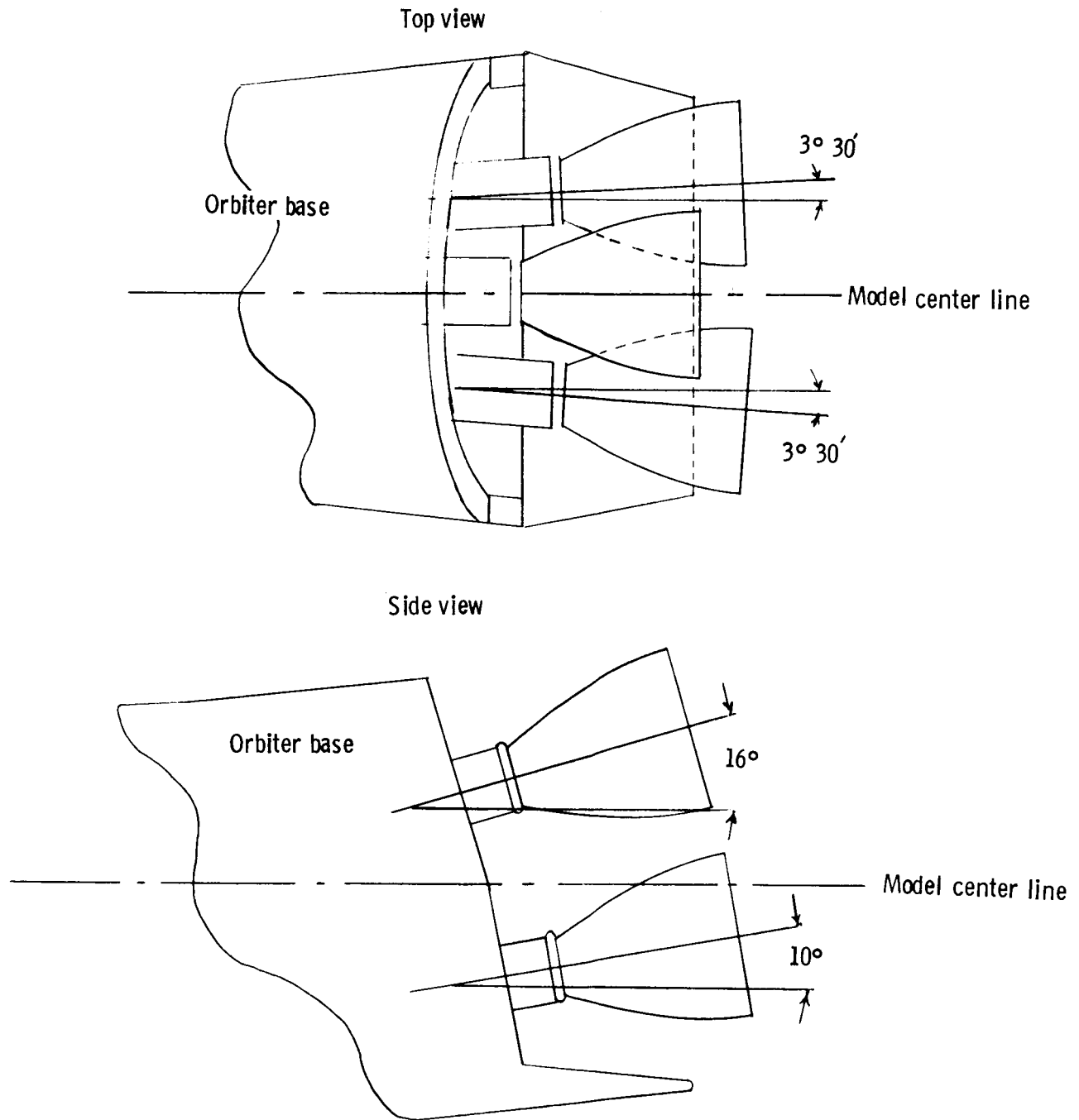
(c) Orbiter base with nozzles installed.

Figure 2.- Continued.

Unfaired cross section

Faired cross section

Section B-B

Unfaired cross section

Faired cross section

Section A-A
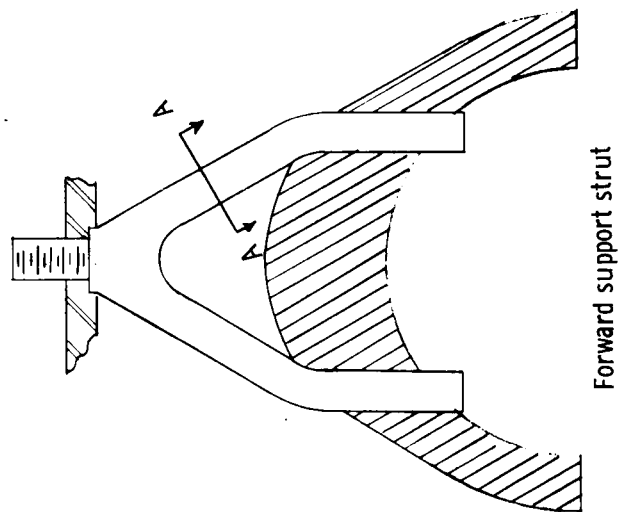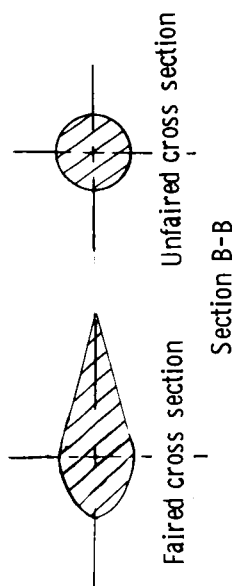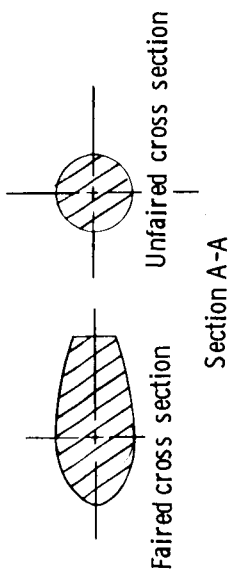
Aft support strut

Forward support strut
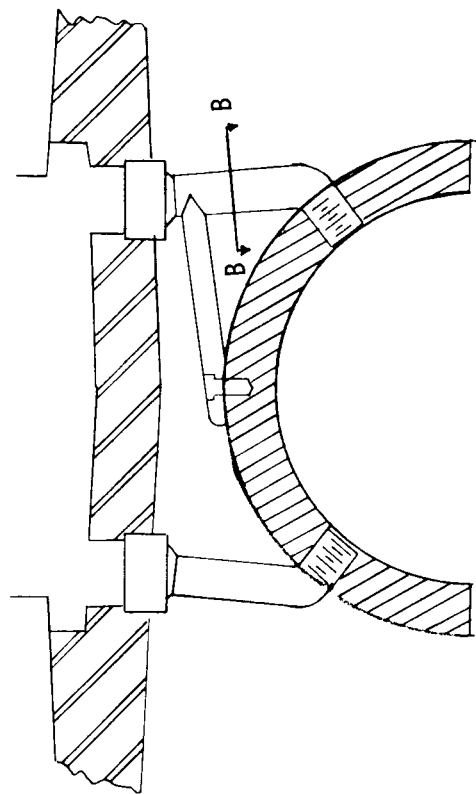
(d) Forward and aft support strut details.

Figure 2.- Continued.
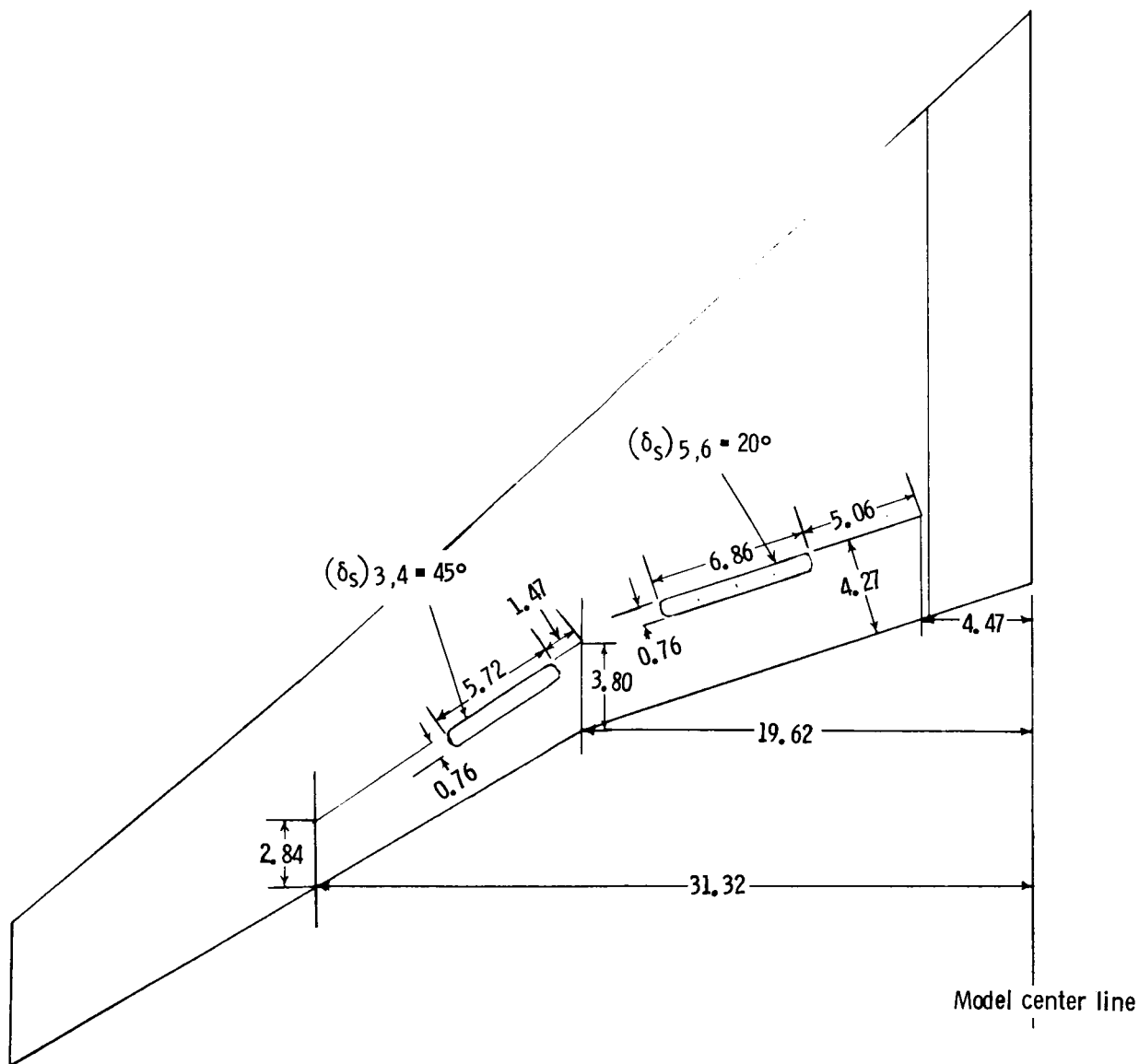
(e) Details of 747 spoiler deployment during orbiter separation.

Figure 2.- Continued.

Horizontal tail

.19

1.73

1.42

3.89

4.36

.91

.30

9.58

.71

1.21
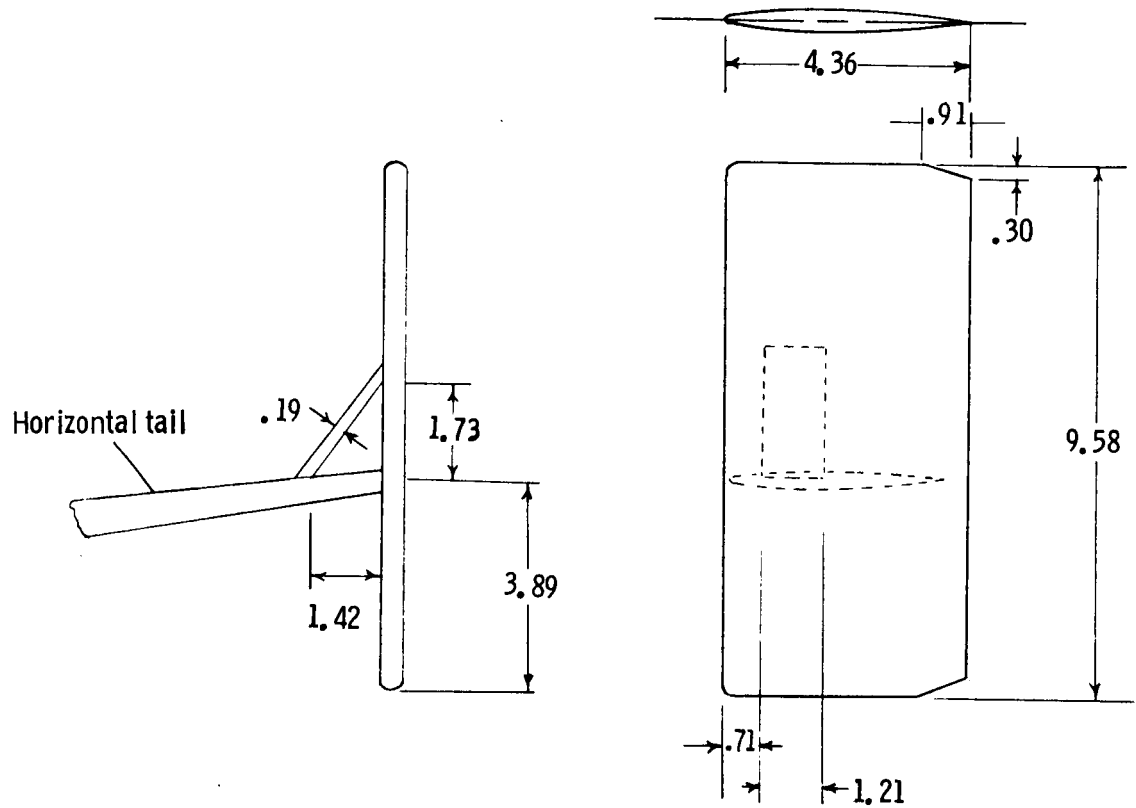
(f) Details of tip fins.

Figure 2.- Continued.

20
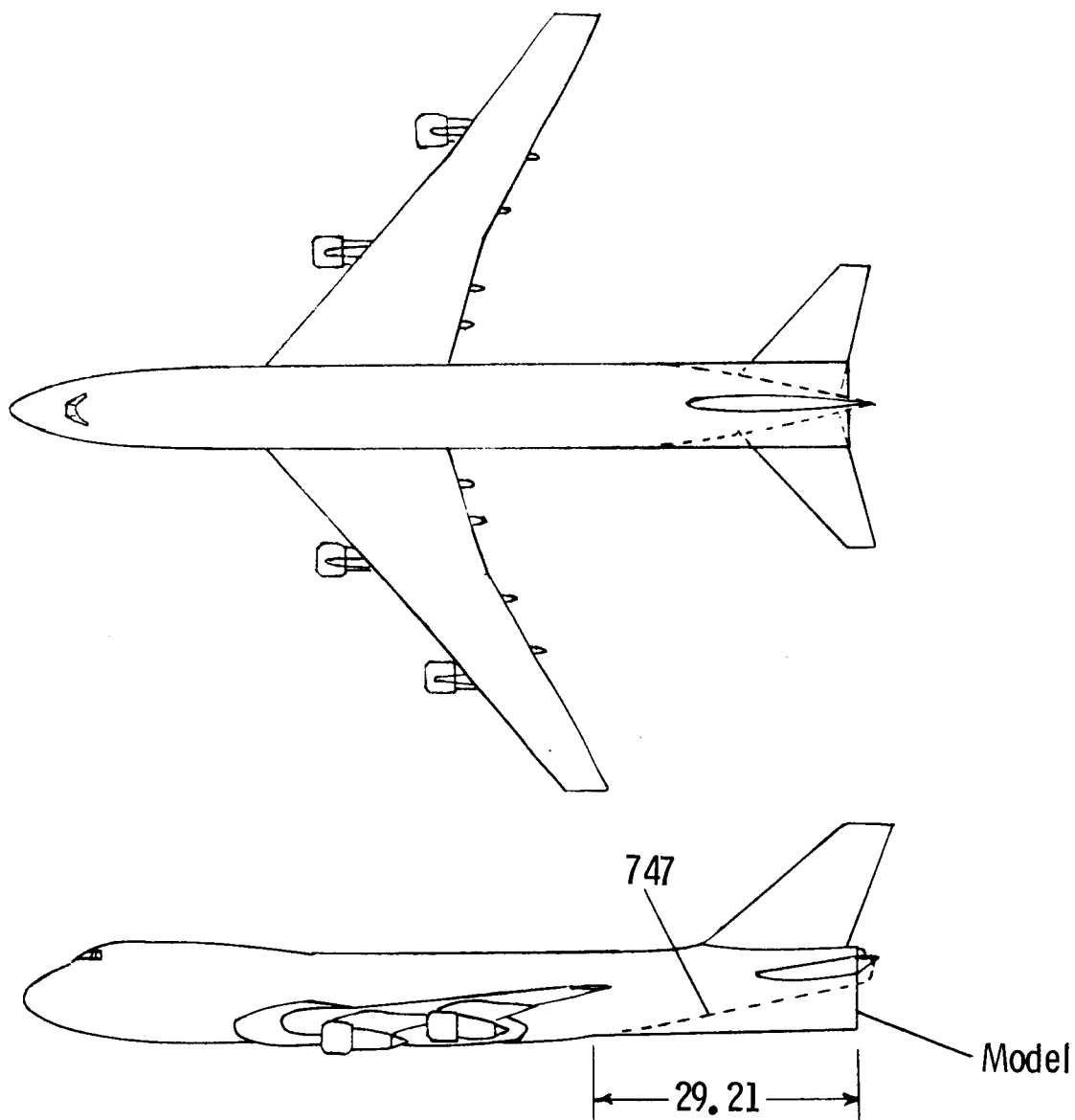
(g) Comparison of wind-tunnel model with basic 747.

Figure 2.- Concluded.

L-75-8426

(a) Front view.

Figure 3.- Model mounted for forced-oscillation tests in the Langley high-speed 7- by 10-foot tunnel.
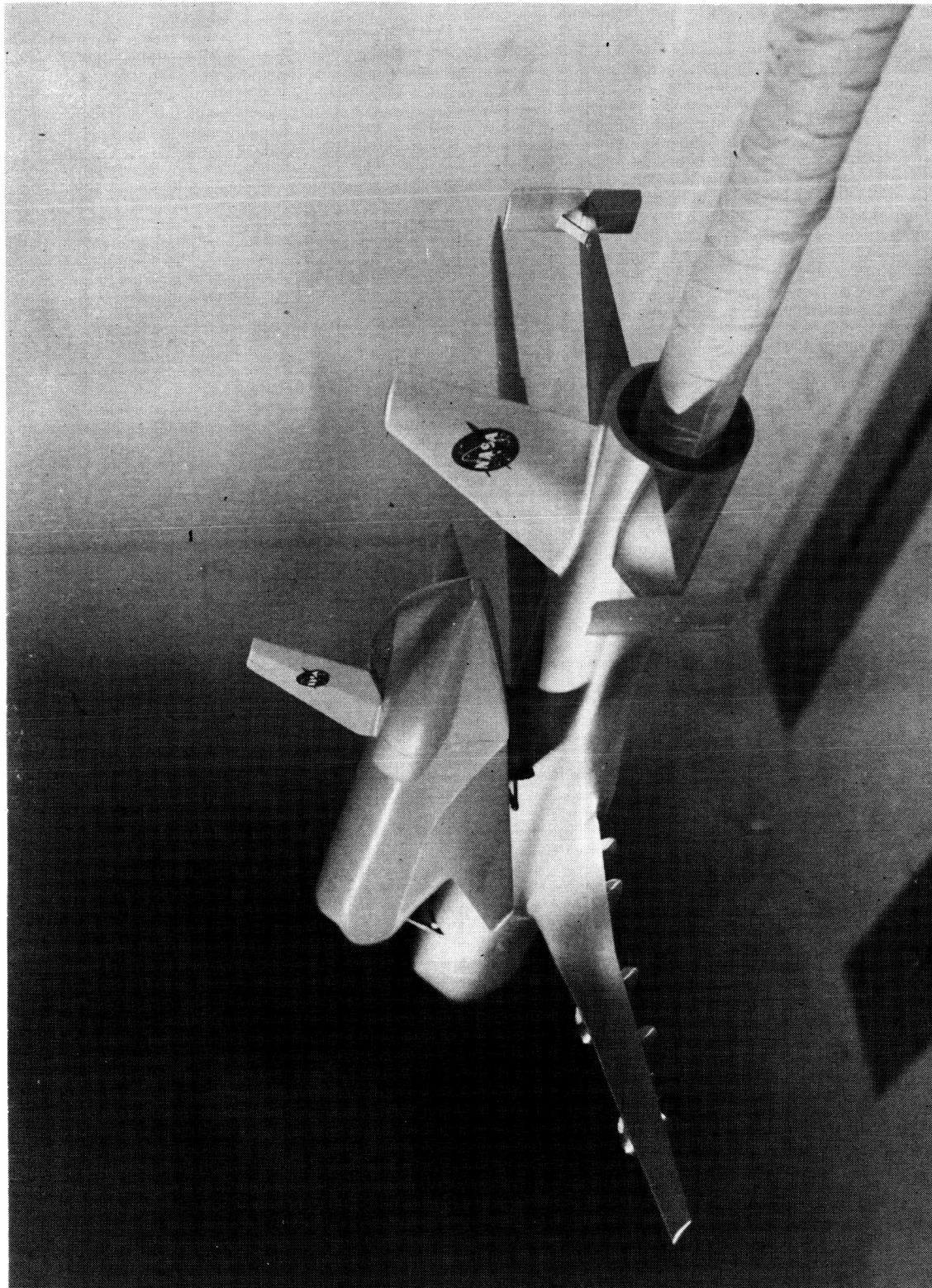
L-75-8423

(b) Rear view.

Figure 3.- Concluded.

23
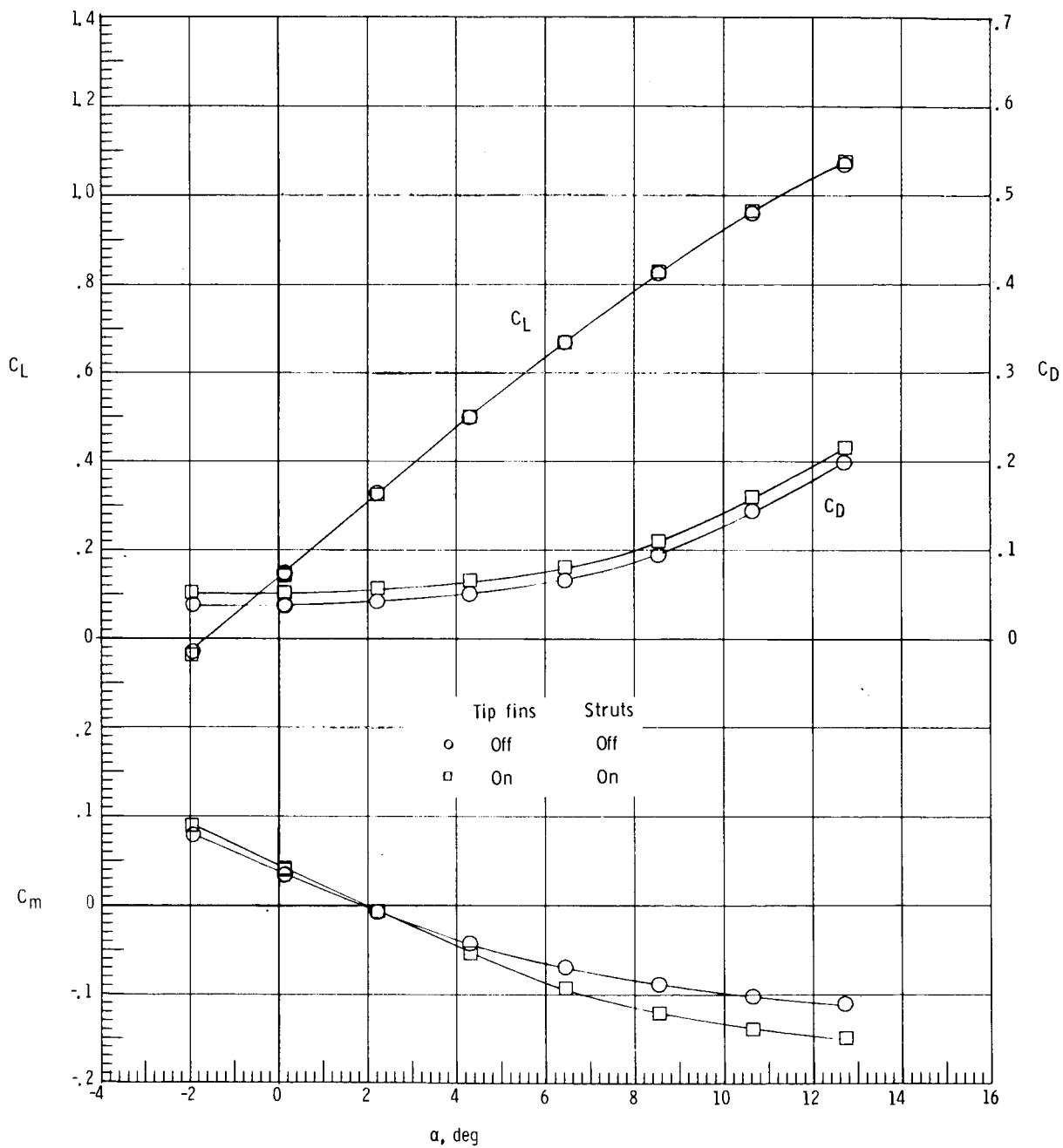
(a) M = 0.2.

Figure 4.- Effect of tip fins and struts on static longitudinal characteristics of basic 747. Faired struts.
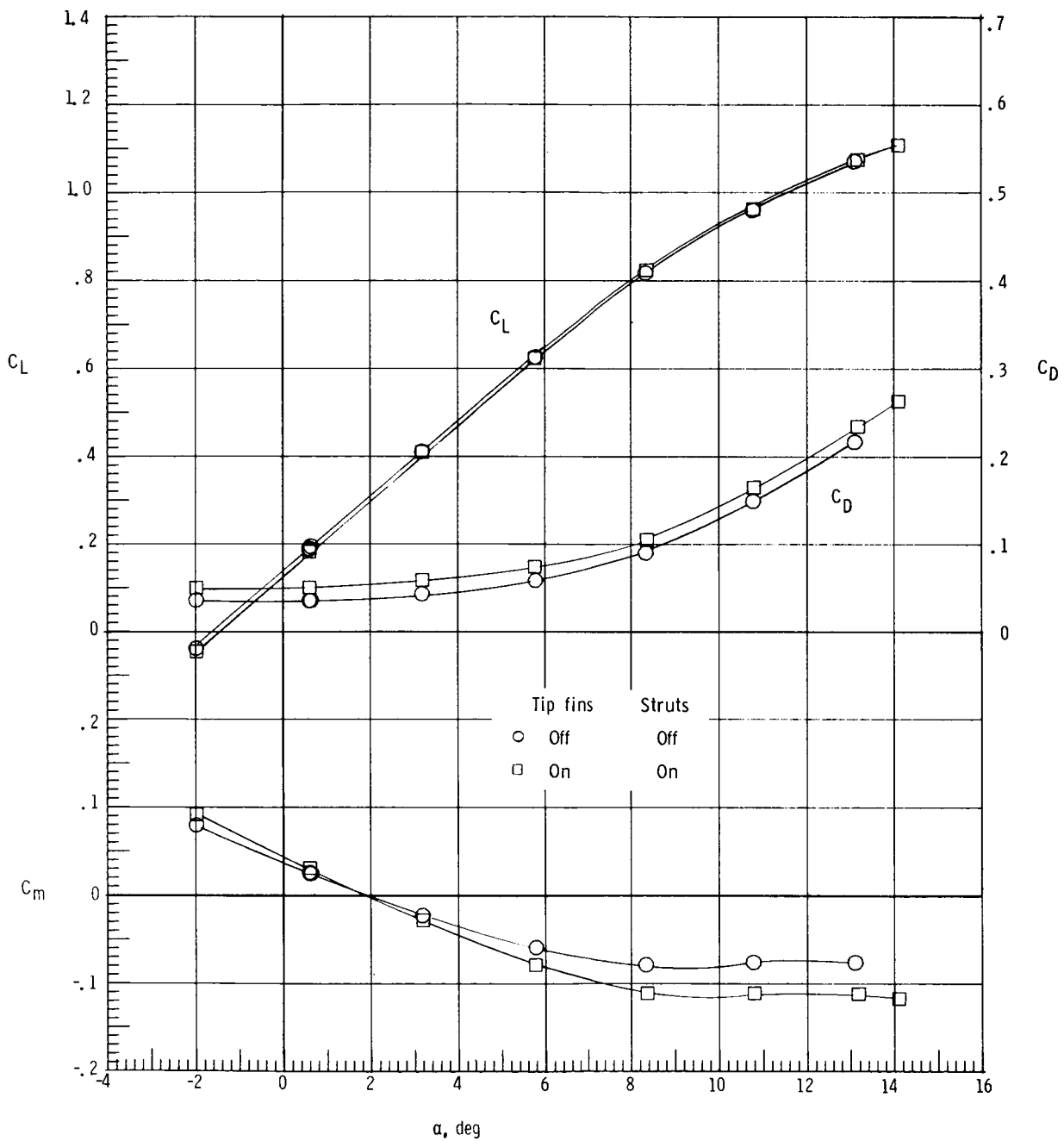
(b)   M = 0.4.

Figure 4.- Continued.
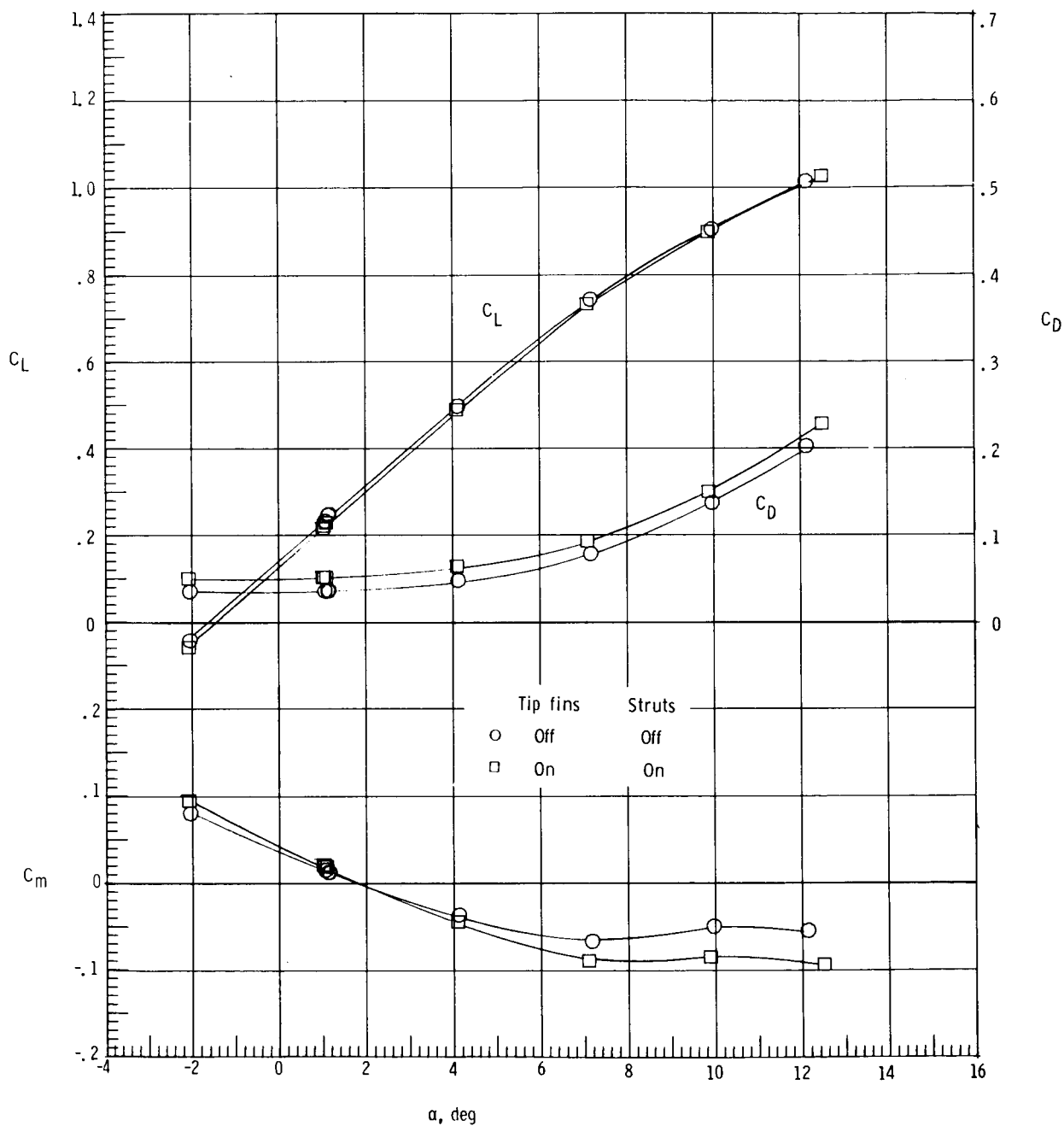
(c) M = 0.5.

Figure 4.- Concluded.
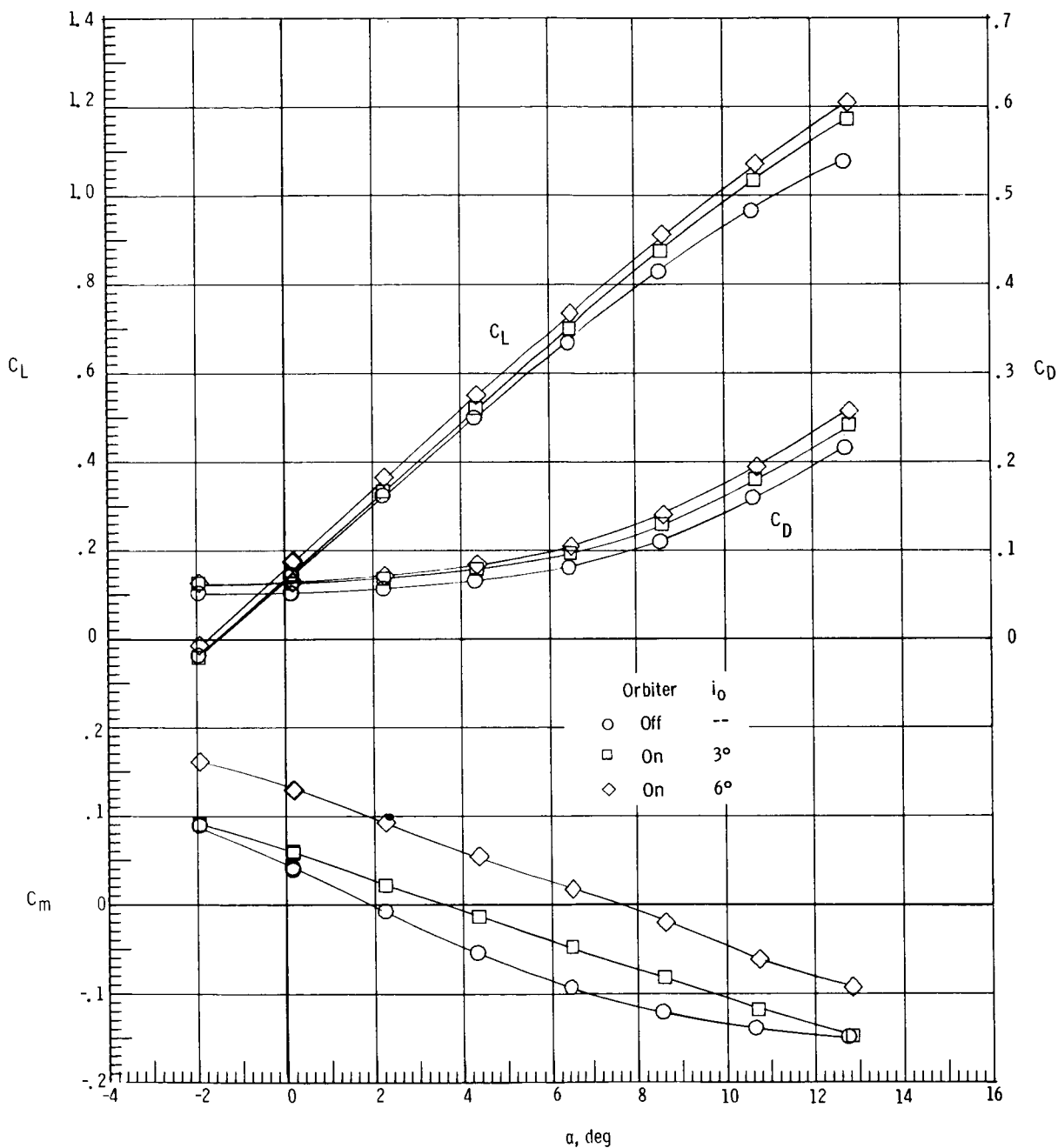
(a) M = 0.2.

Figure 5.- Effect of orbiter and orbiter incidence on static longitudinal
characteristics of modified 747. Faired struts; tail cone on.
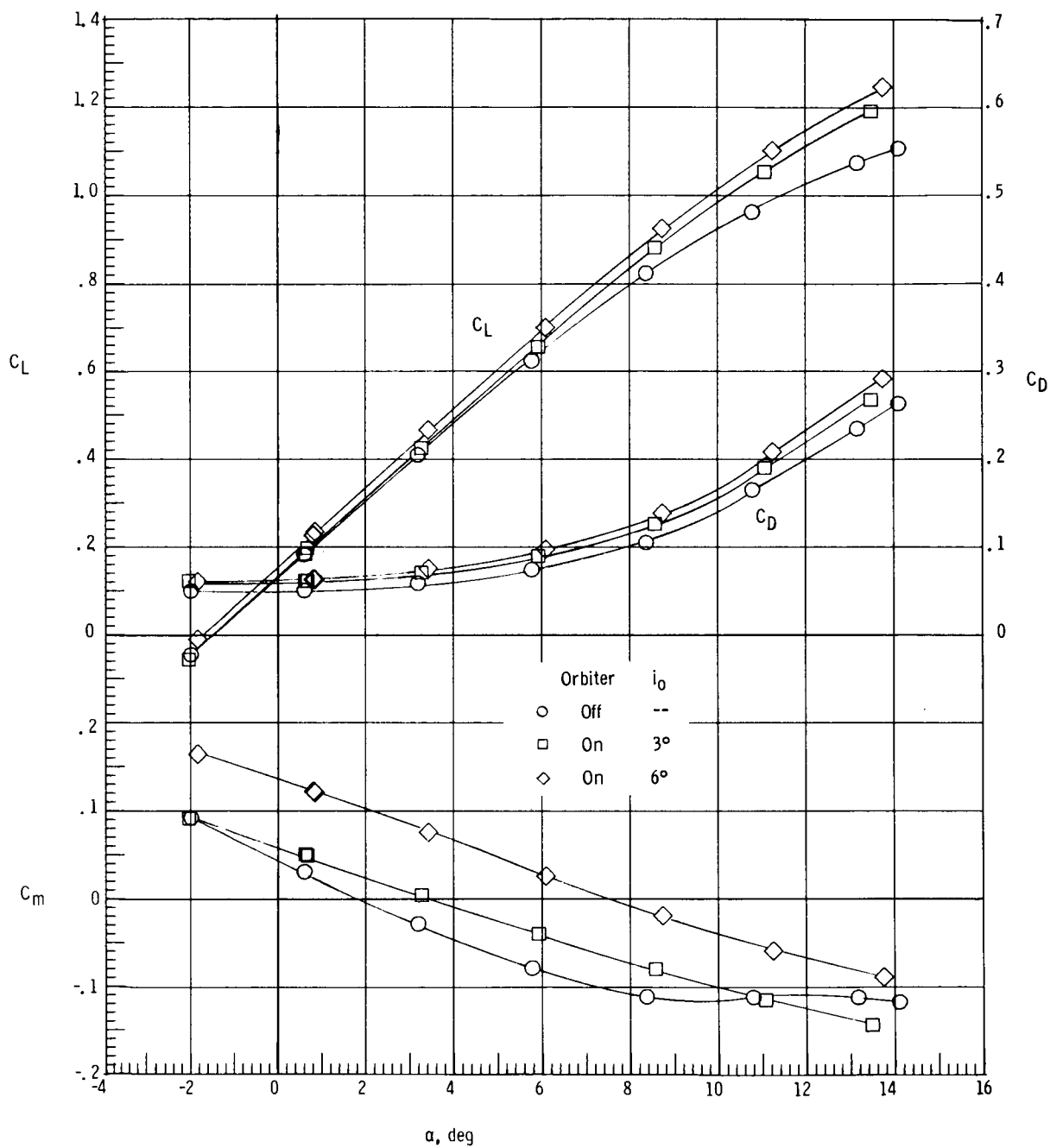
(b) M = 0.4.

Figure 5.- Continued.
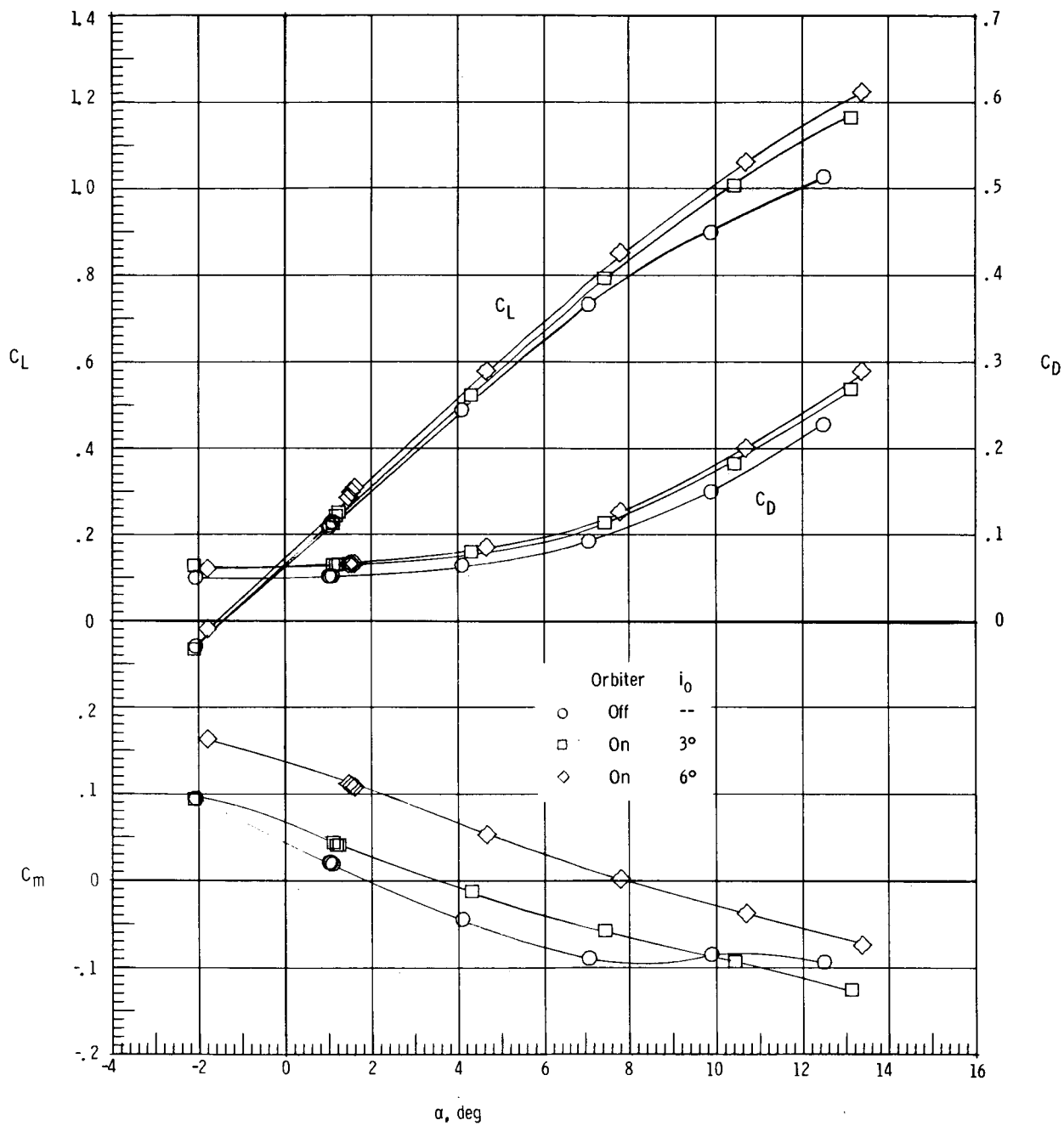
(c)   M = 0.5.

Figure 5.- Concluded.
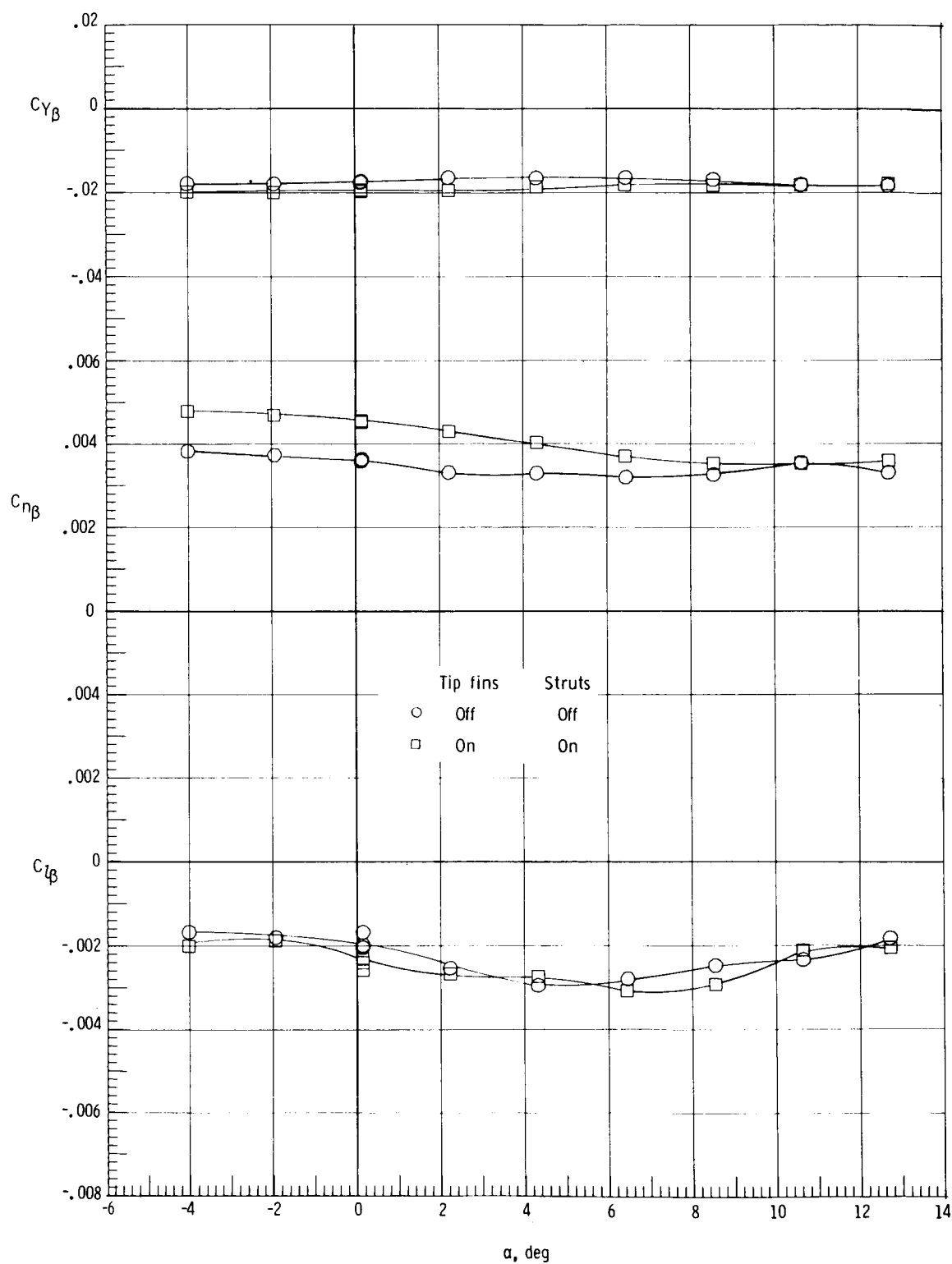
(a) M = 0.2.

Figure 6.- Effect of tip fins and struts on static lateral
characteristics of basic 747. Unfaired struts.
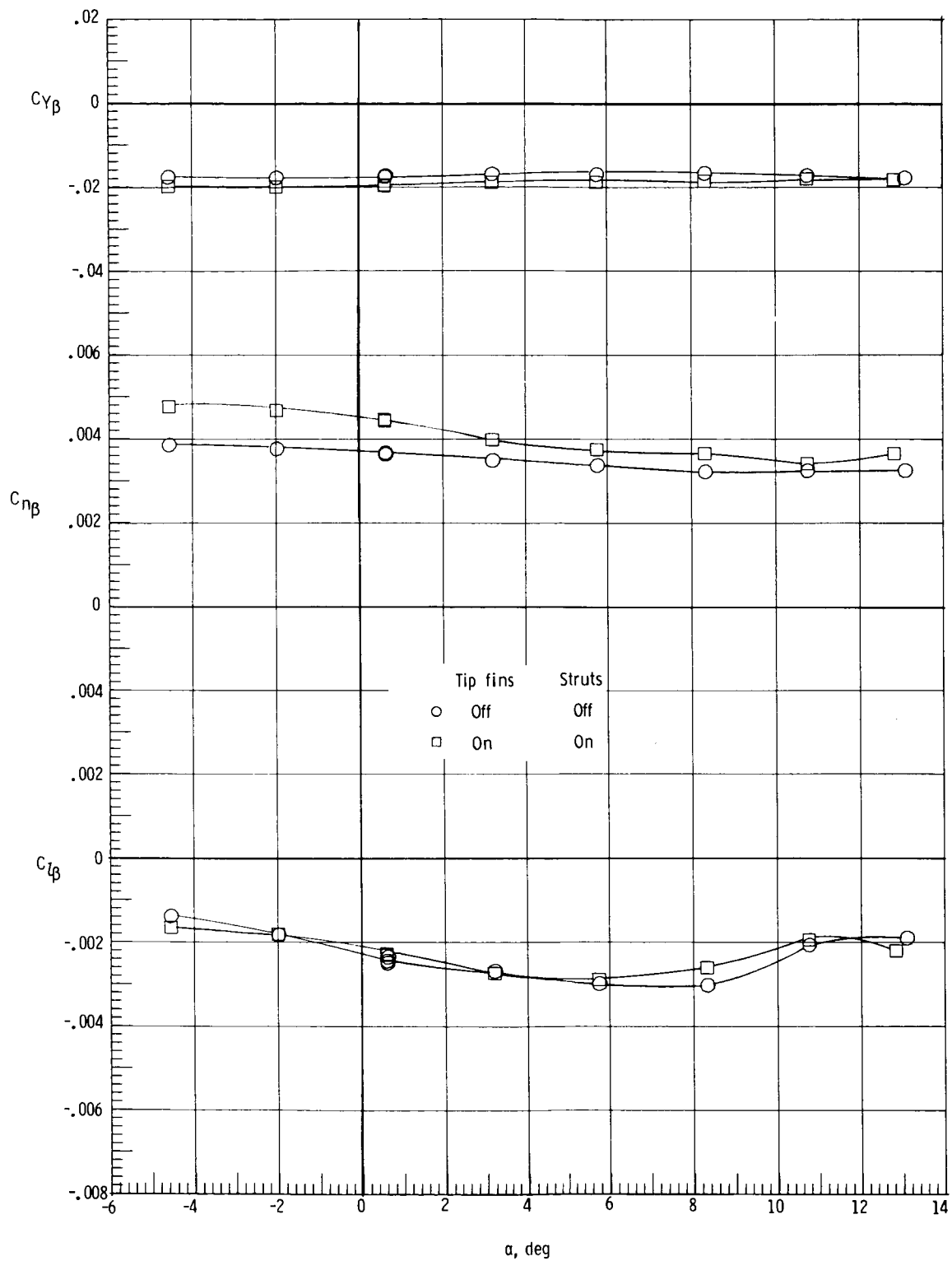
(b) M = 0.4.

Figure 6.- Continued.
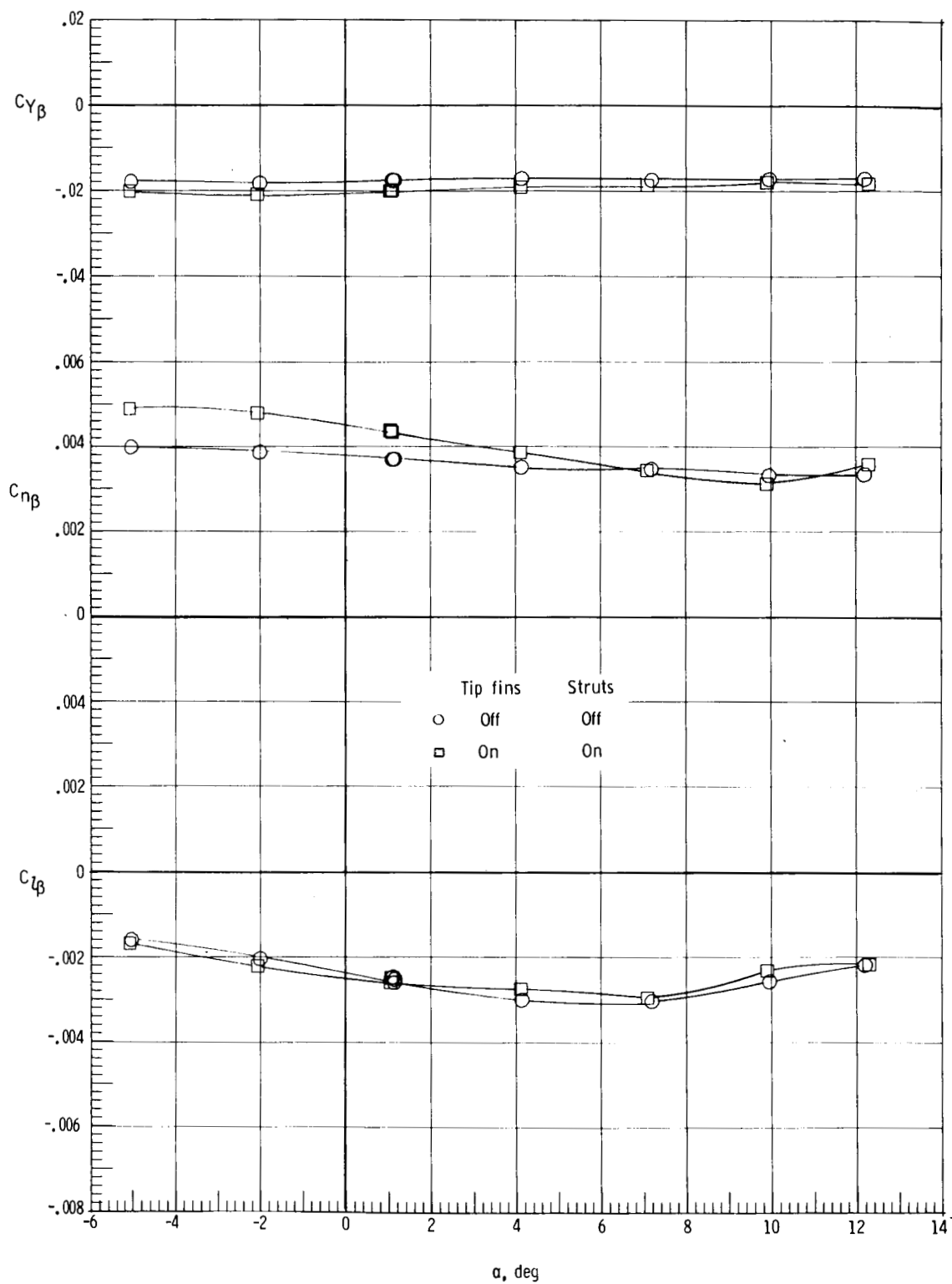
(c) M = 0.5.

Figure 6.- Concluded.
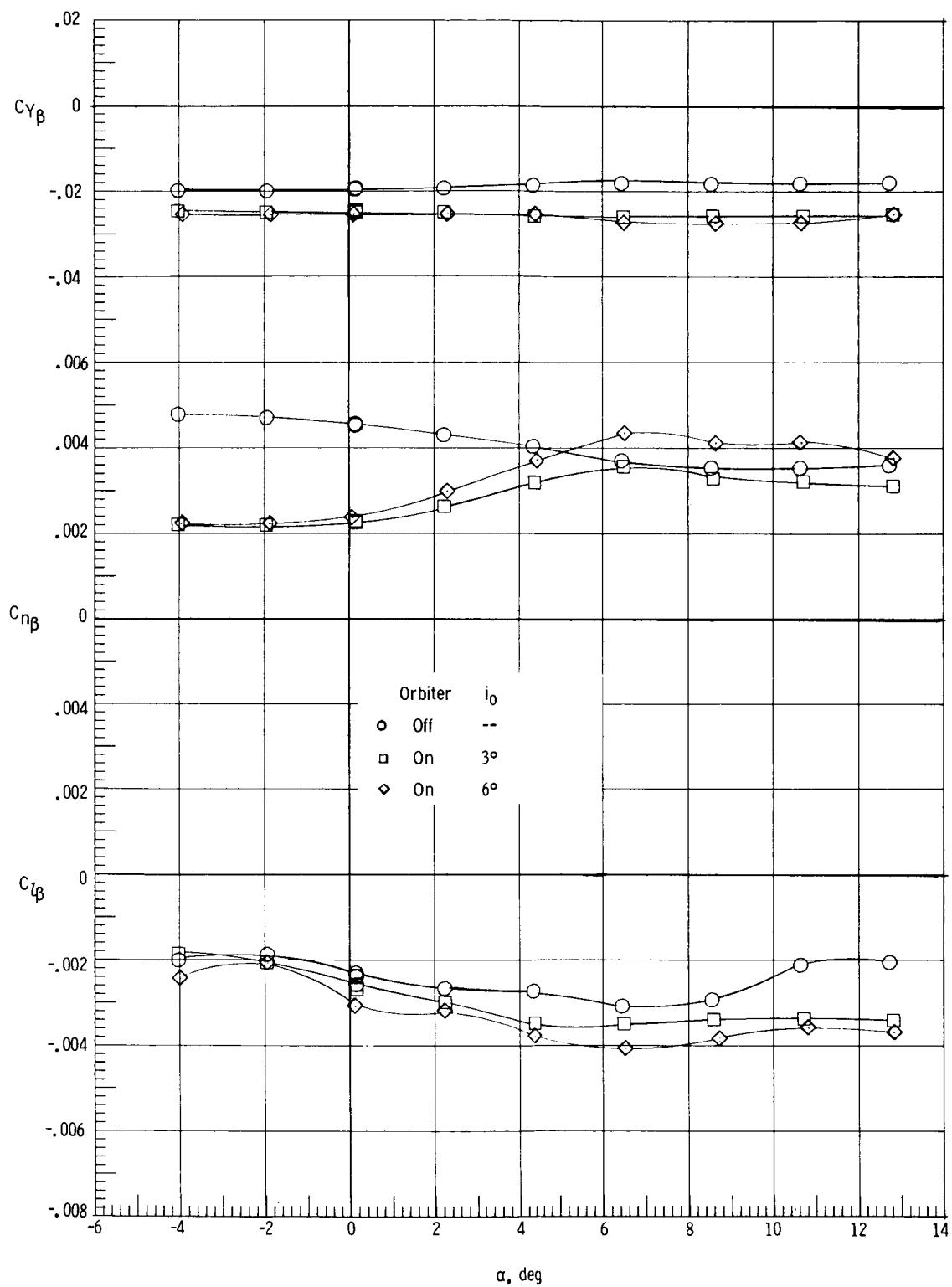
(a) M = 0.2.

Figure 7.- Effect of orbiter and orbiter incidence on static lateral
characteristics of modified 747. Unfaired struts; tail cone on.
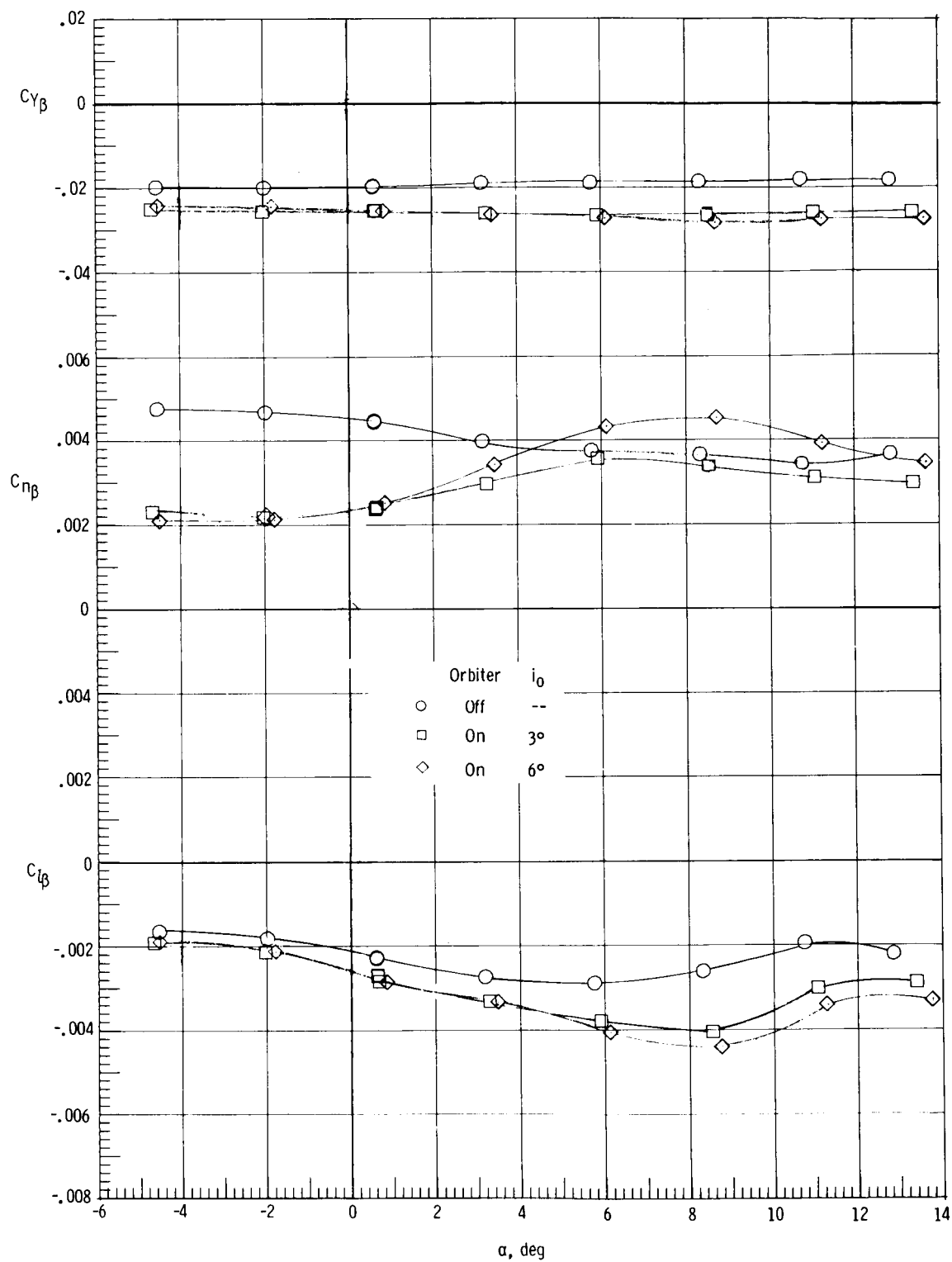
(b) M = 0.4.

Figure 7.- Continued.
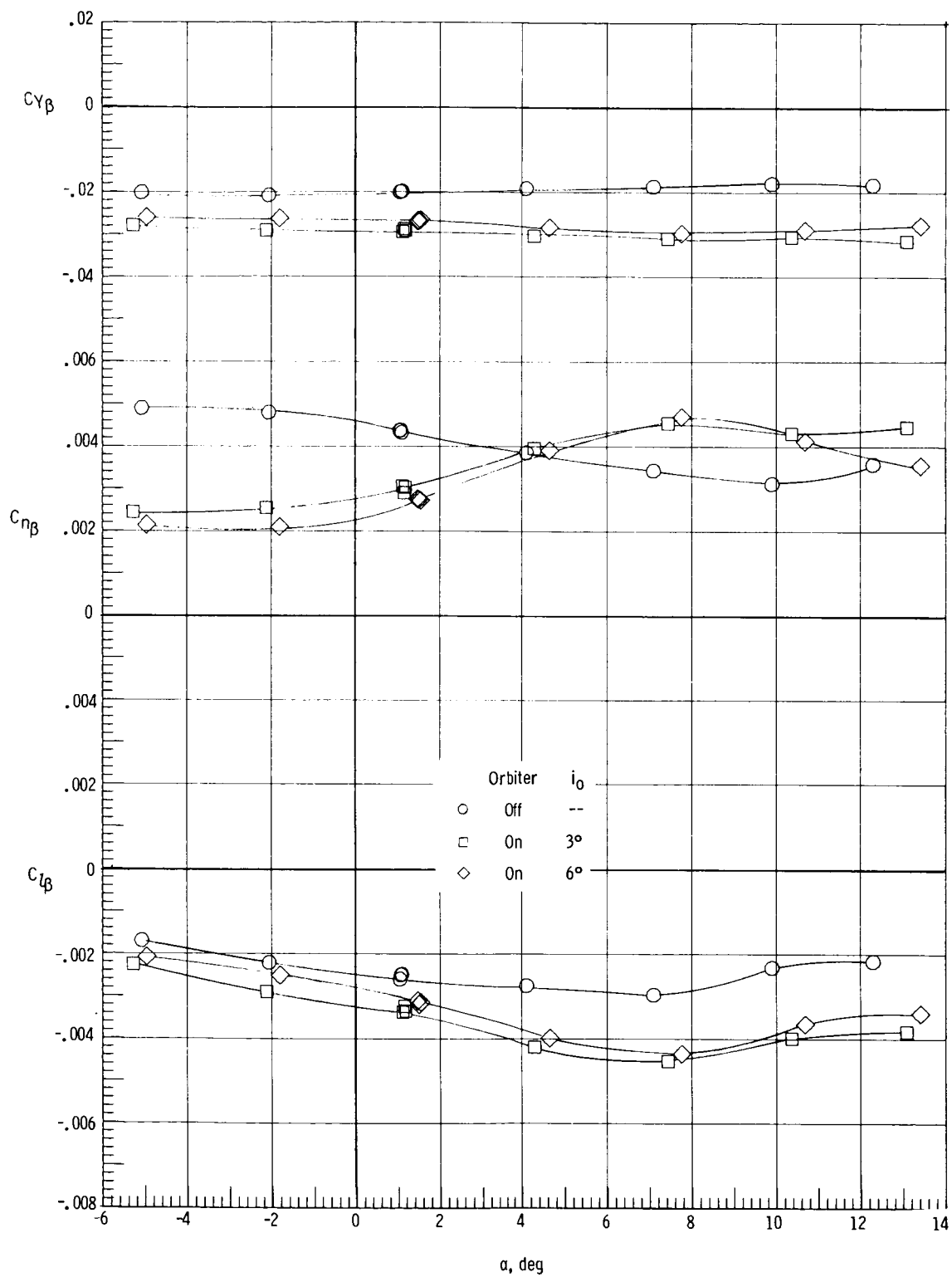
(c) M = 0.5.

Figure 7.- Concluded.
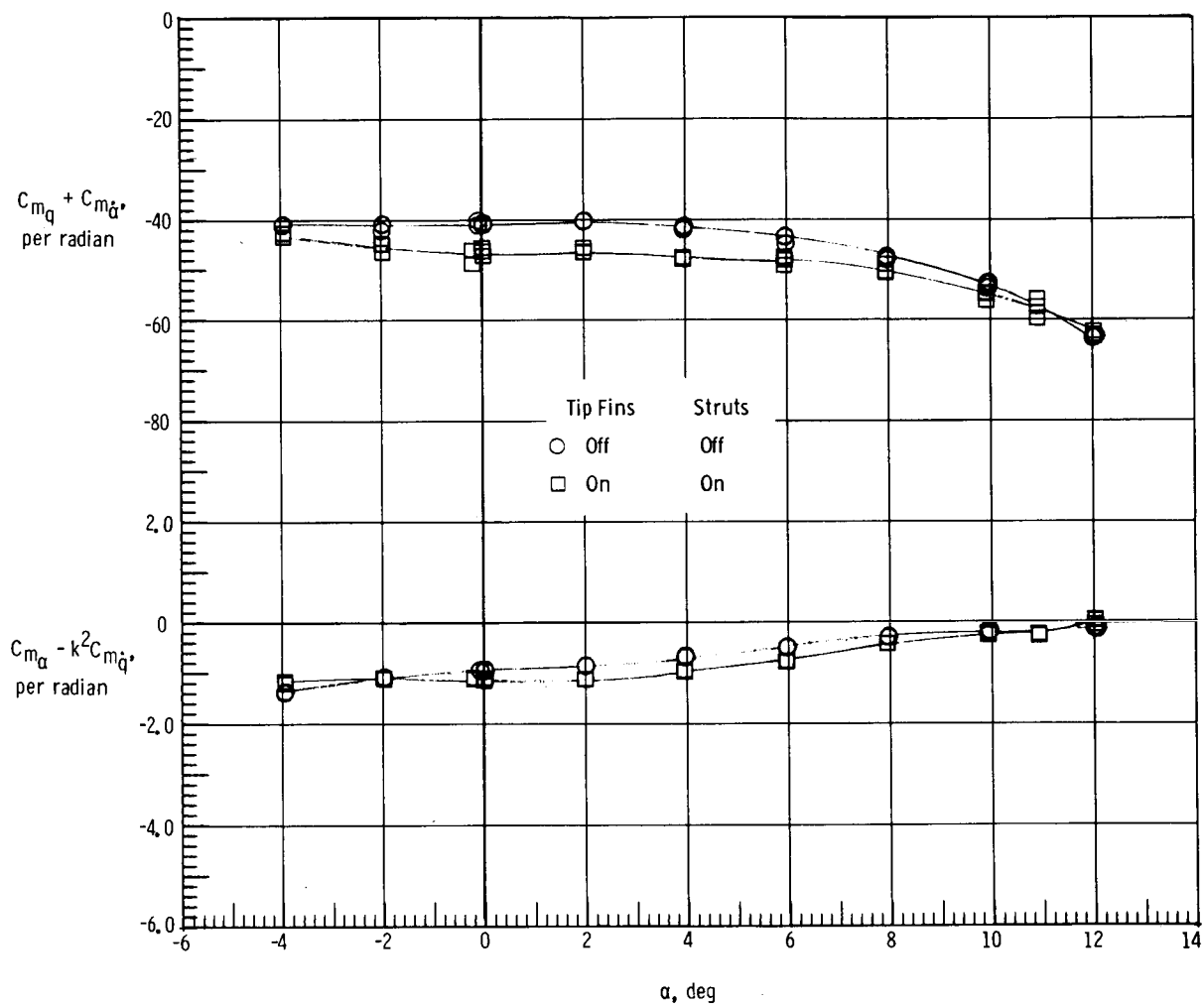
(a) M = 0.2.

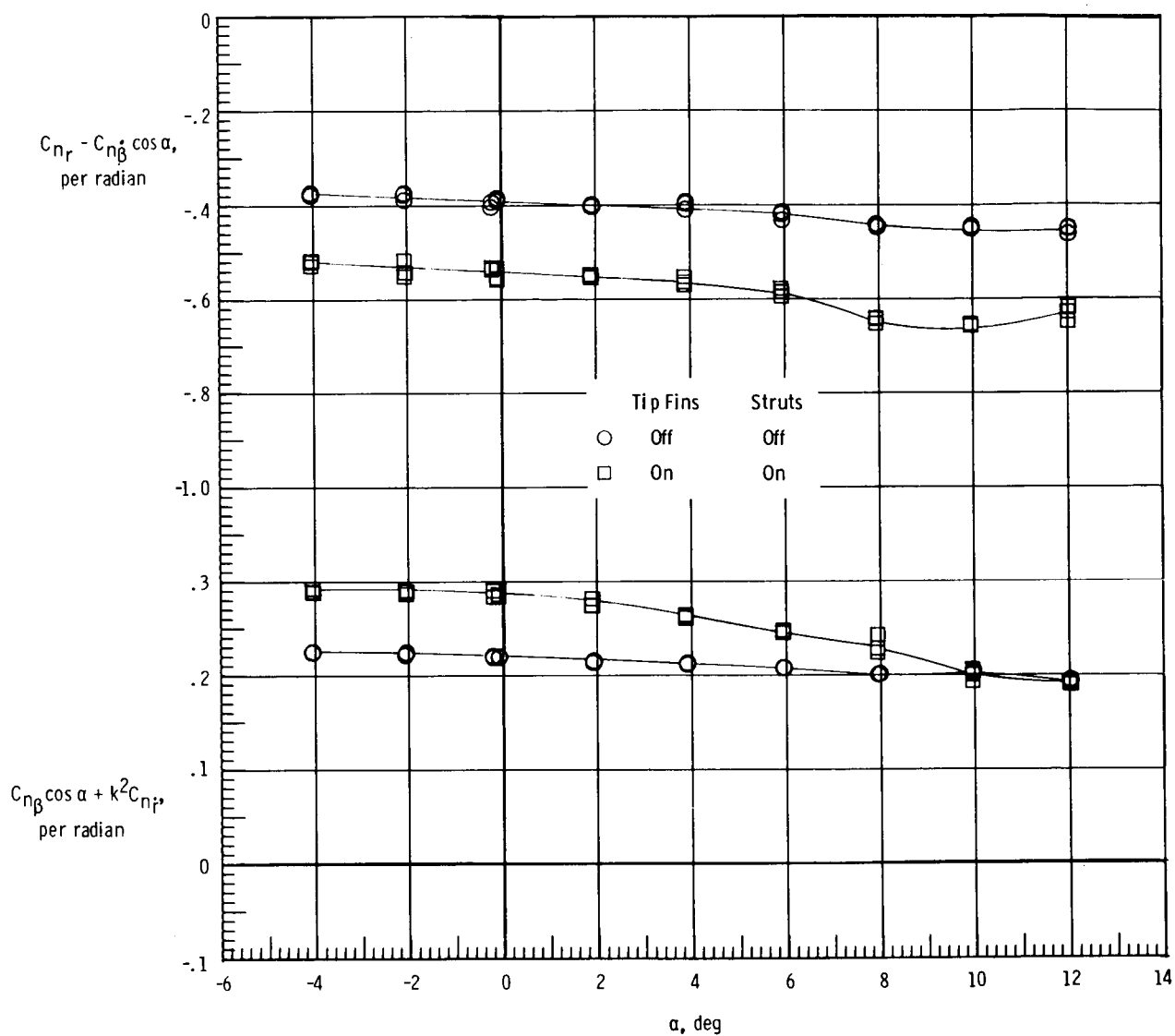Figure 8.- Effect of tip fins and struts on damping-in-pitch parameter and on oscillatory stability-in-pitch parameter of basic 747. Faired struts.
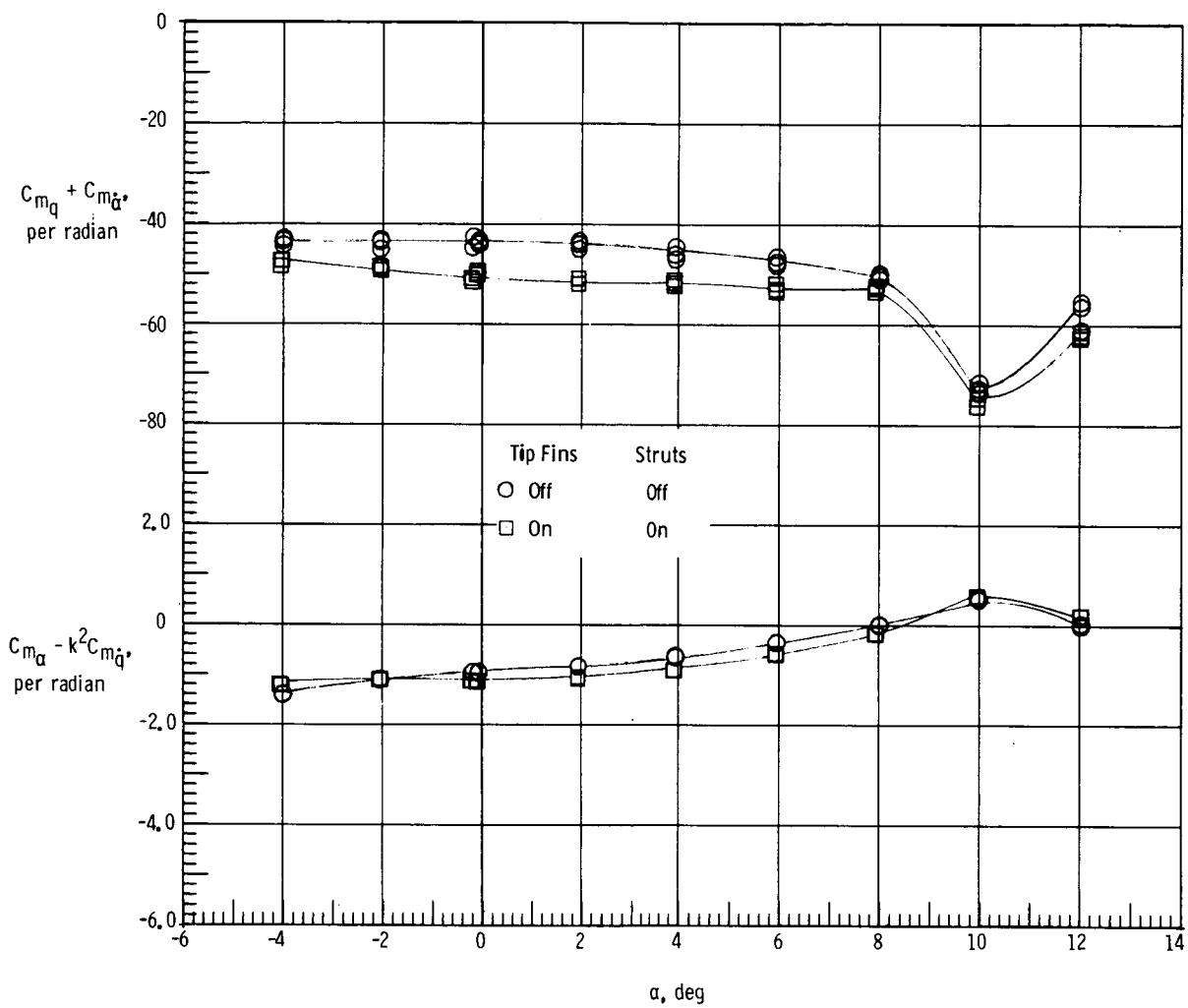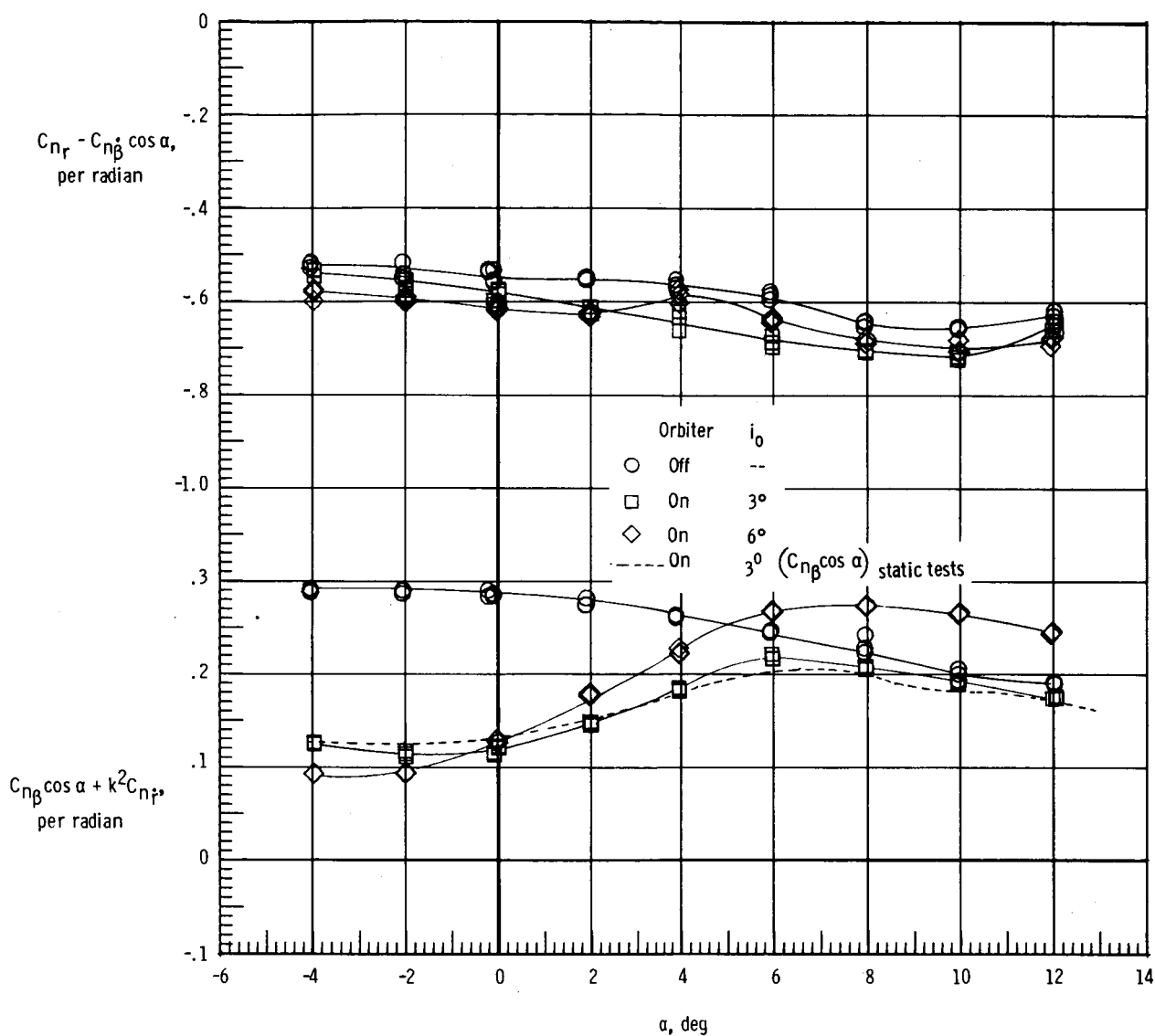
(b) M = 0.4.

Figure 8.- Continued.
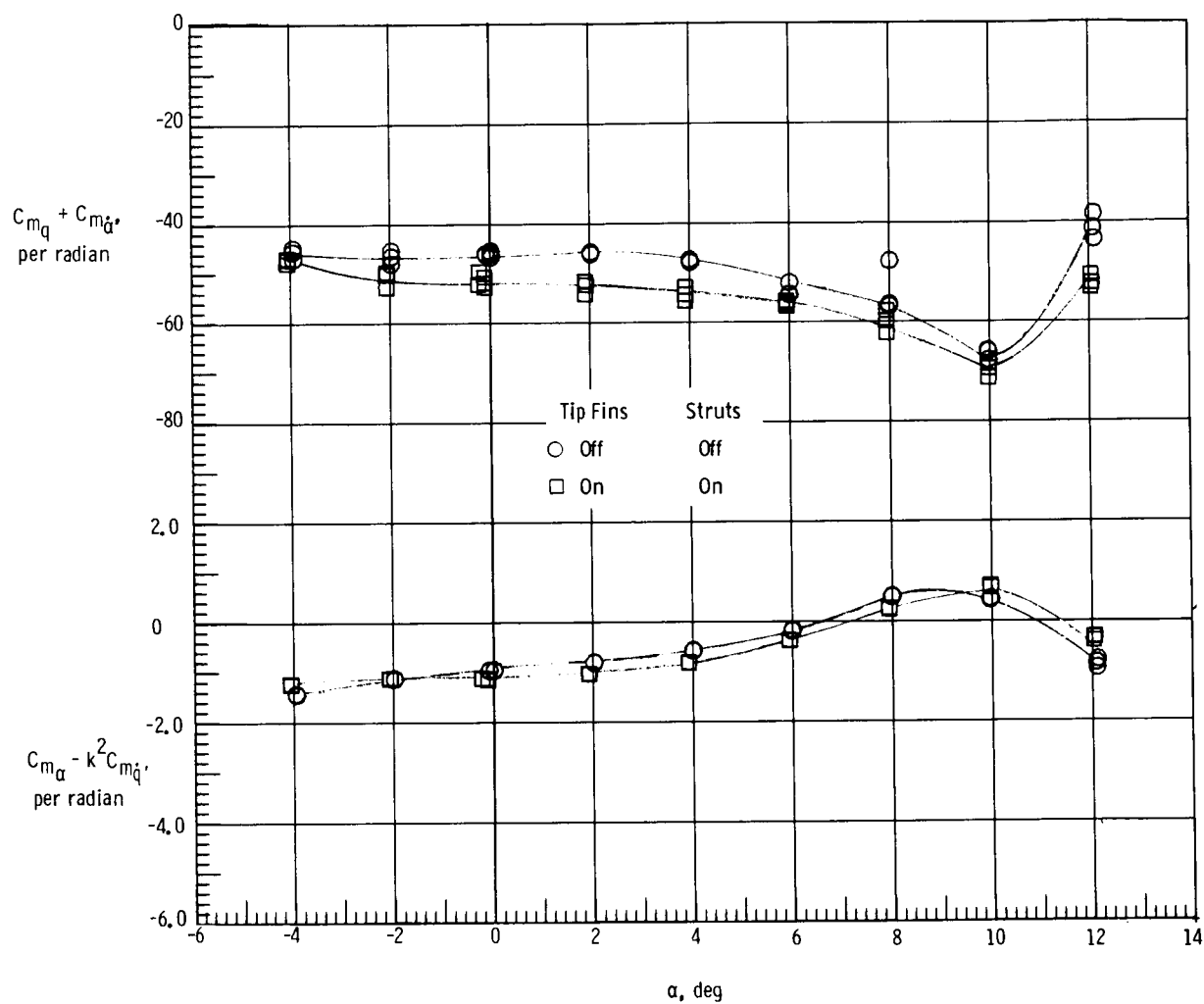
(c)   M = 0.5.

Figure 8.- Concluded.
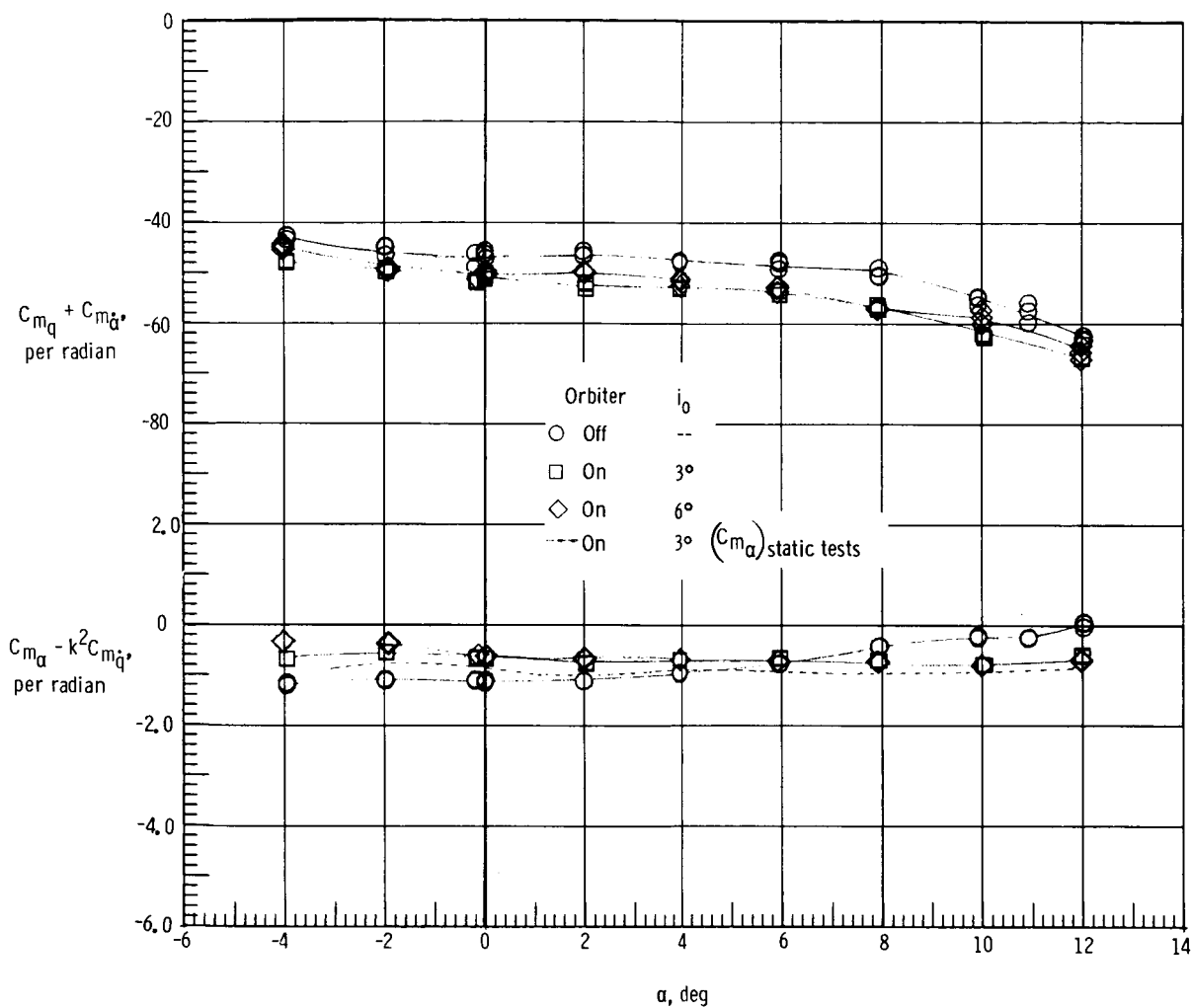
(a) M = 0.2.

Figure 9.- Effect of orbiter and orbiter incidence on damping-in-pitch parameter and on oscillatory stability-in-pitch parameter of modified 747. Faired struts; tail cone on.
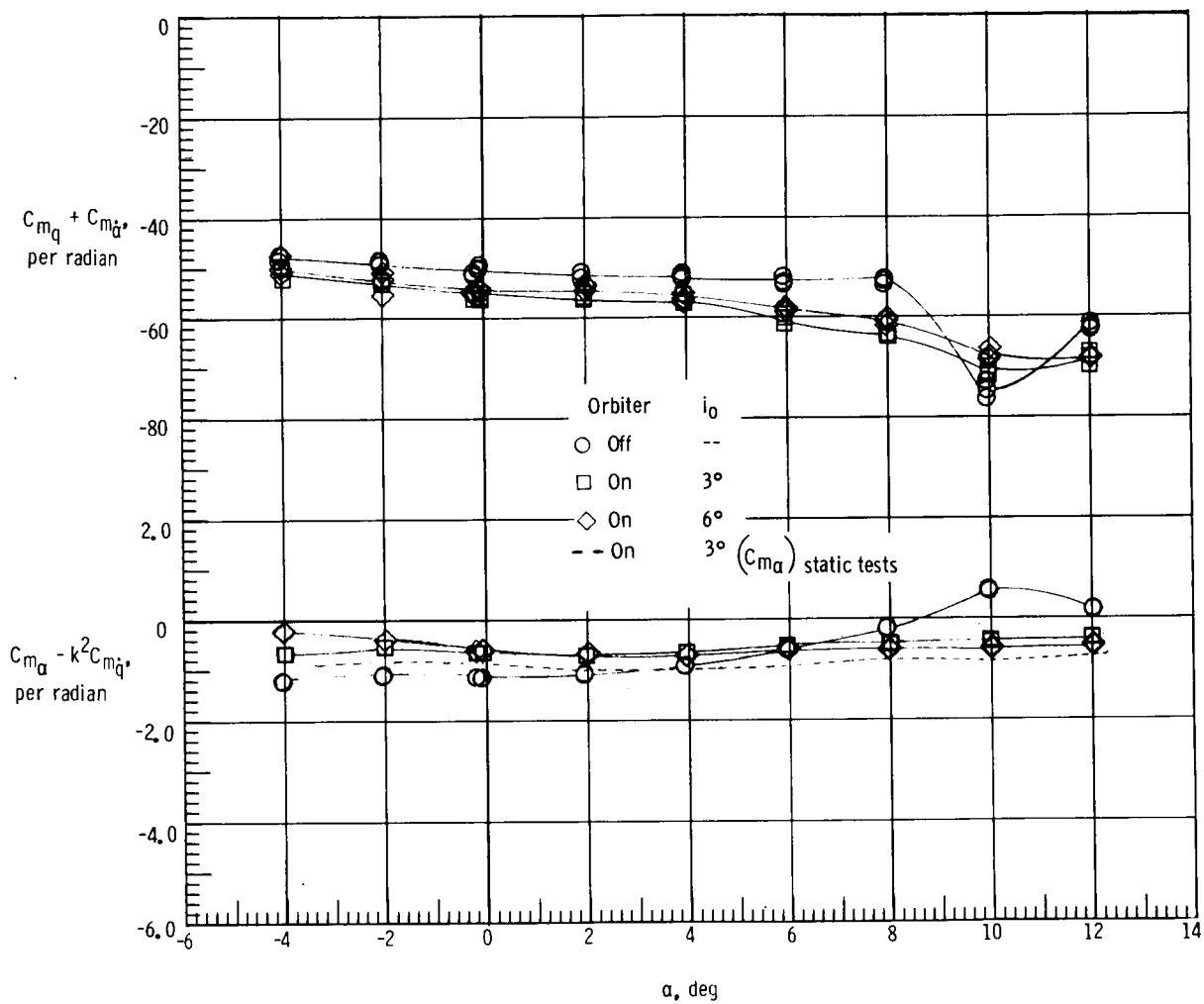
(b)   M = 0.4.

Figure 9.- Continued.
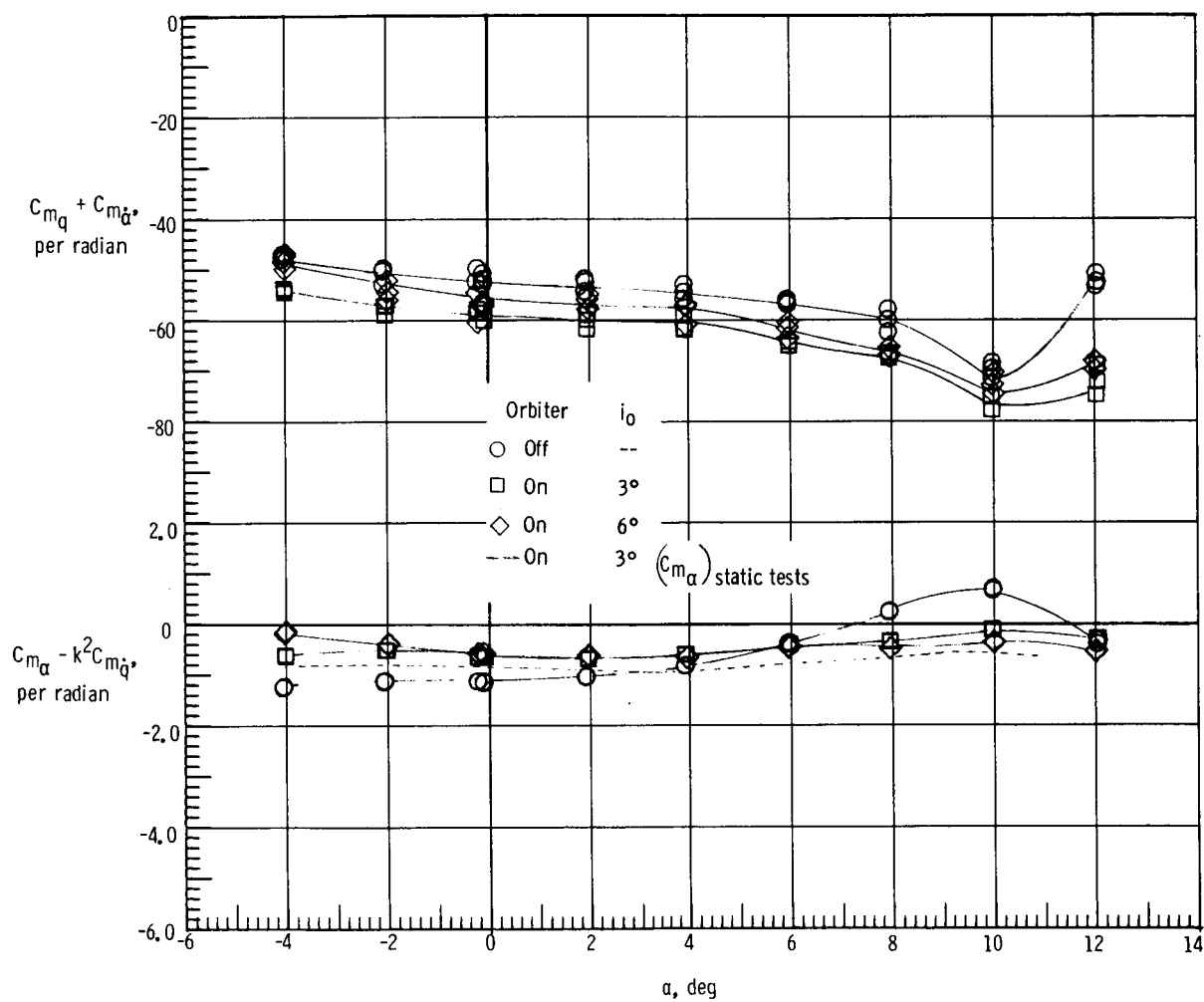
(c)   M = 0.5.

Figure 9.- Concluded.
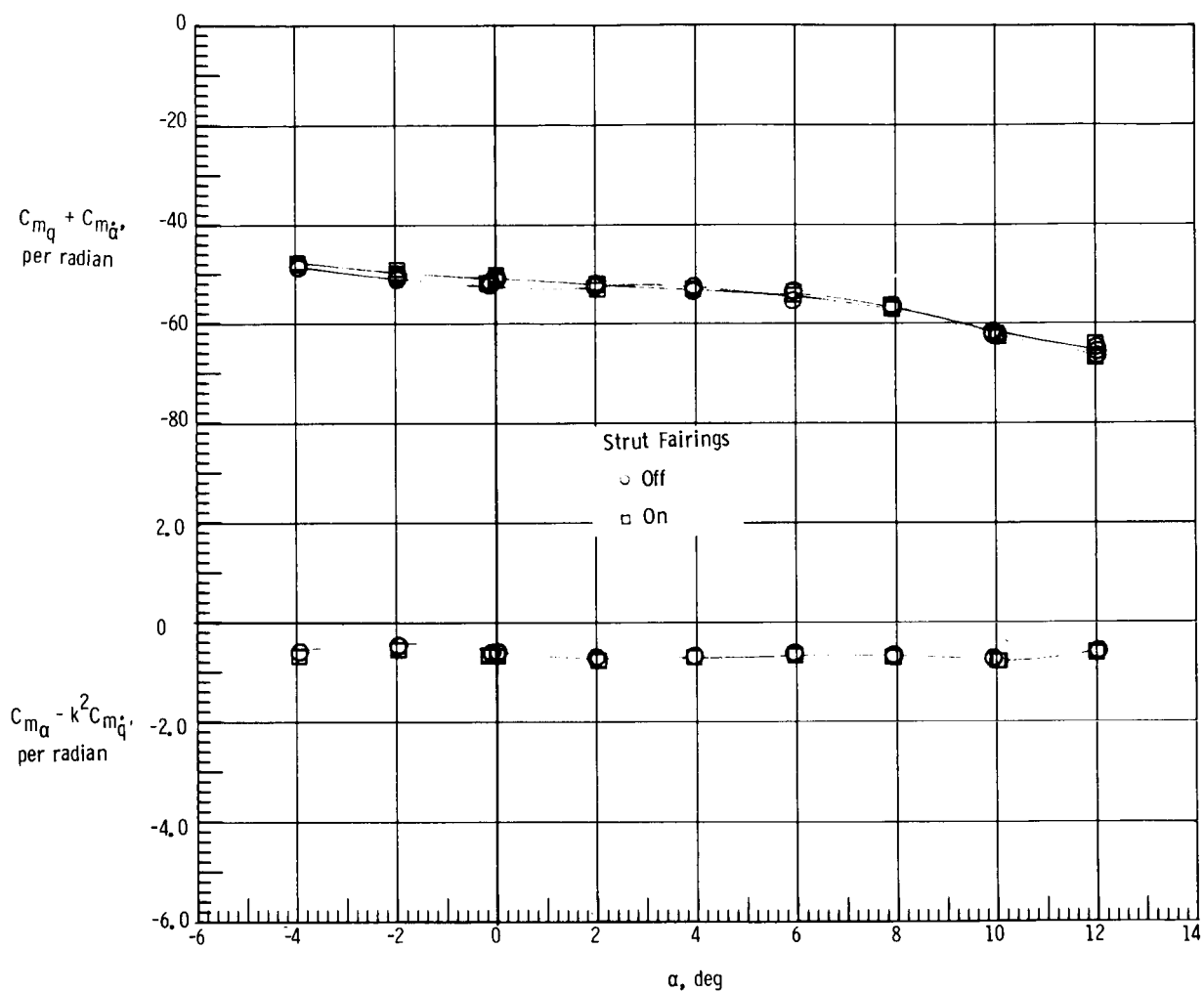
(a)   M = 0.2.

Figure 10.- Effect of strut fairings on damping-in-pitch parameter and
on oscillatory stability-in-pitch parameter of ferry configuration.
$i_O = 3^o$; tail cone on.
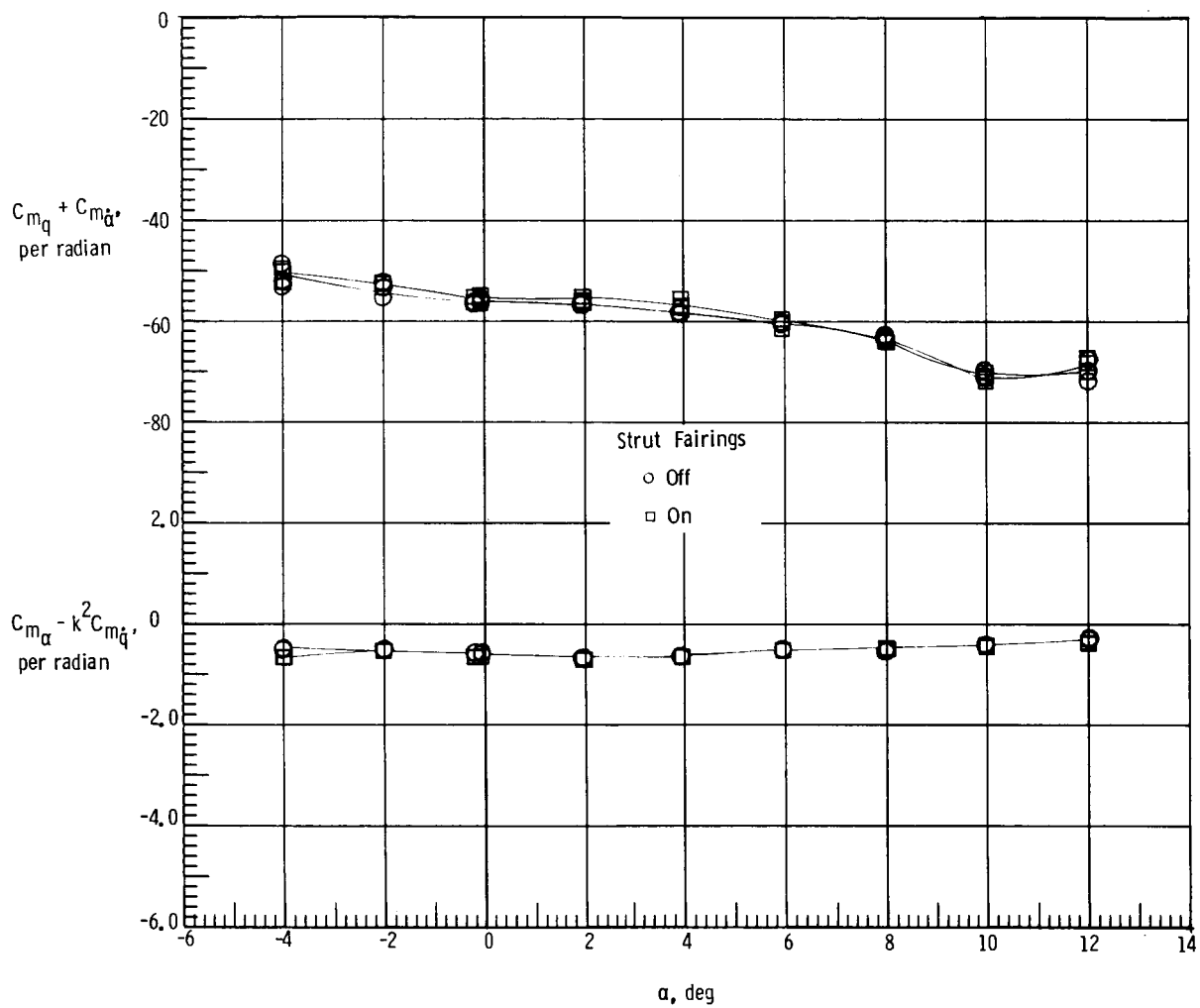
(b) M = 0.4.

Figure 10.- Continued.
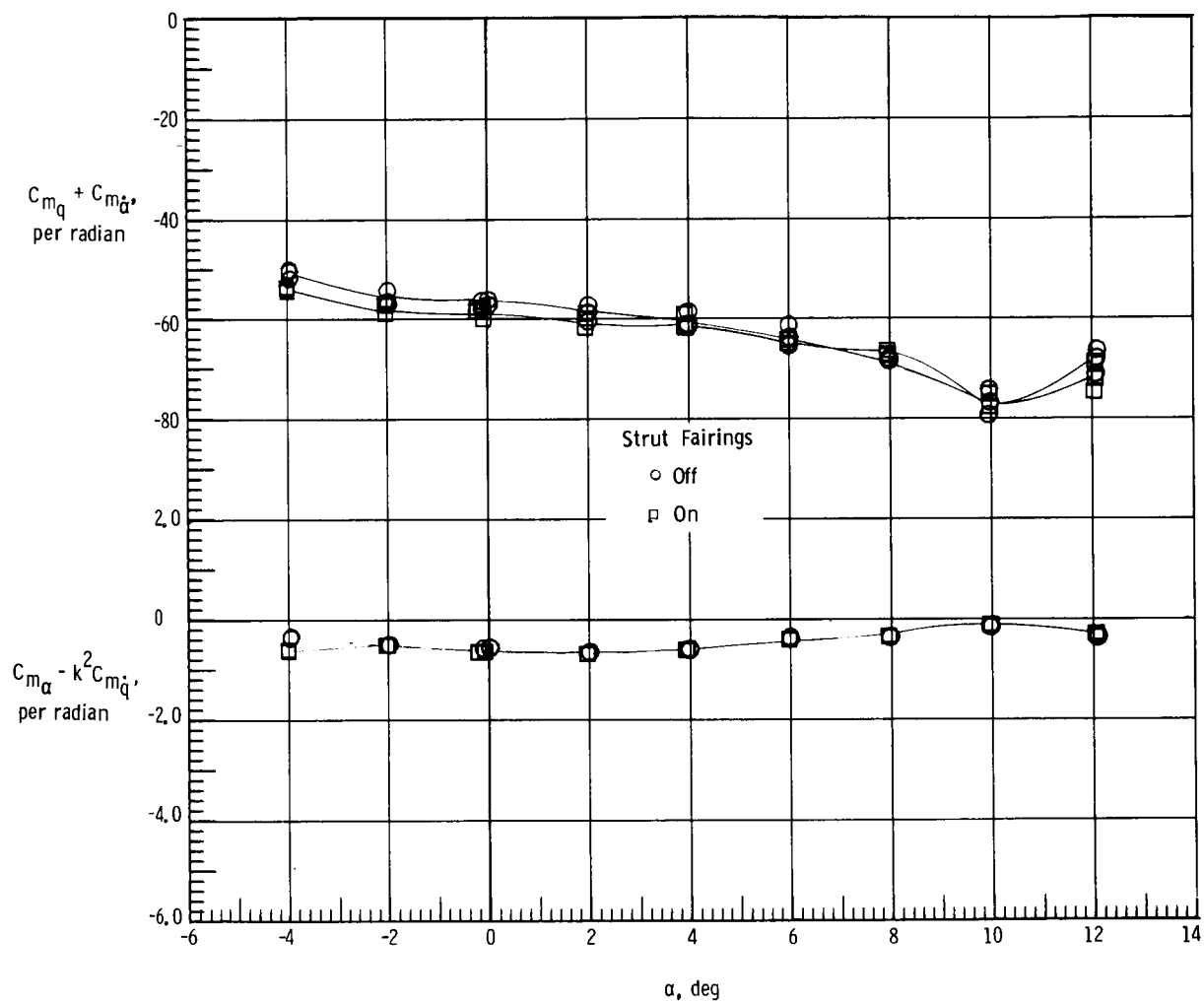
(c) M = 0.5.

Figure 10.- Concluded.
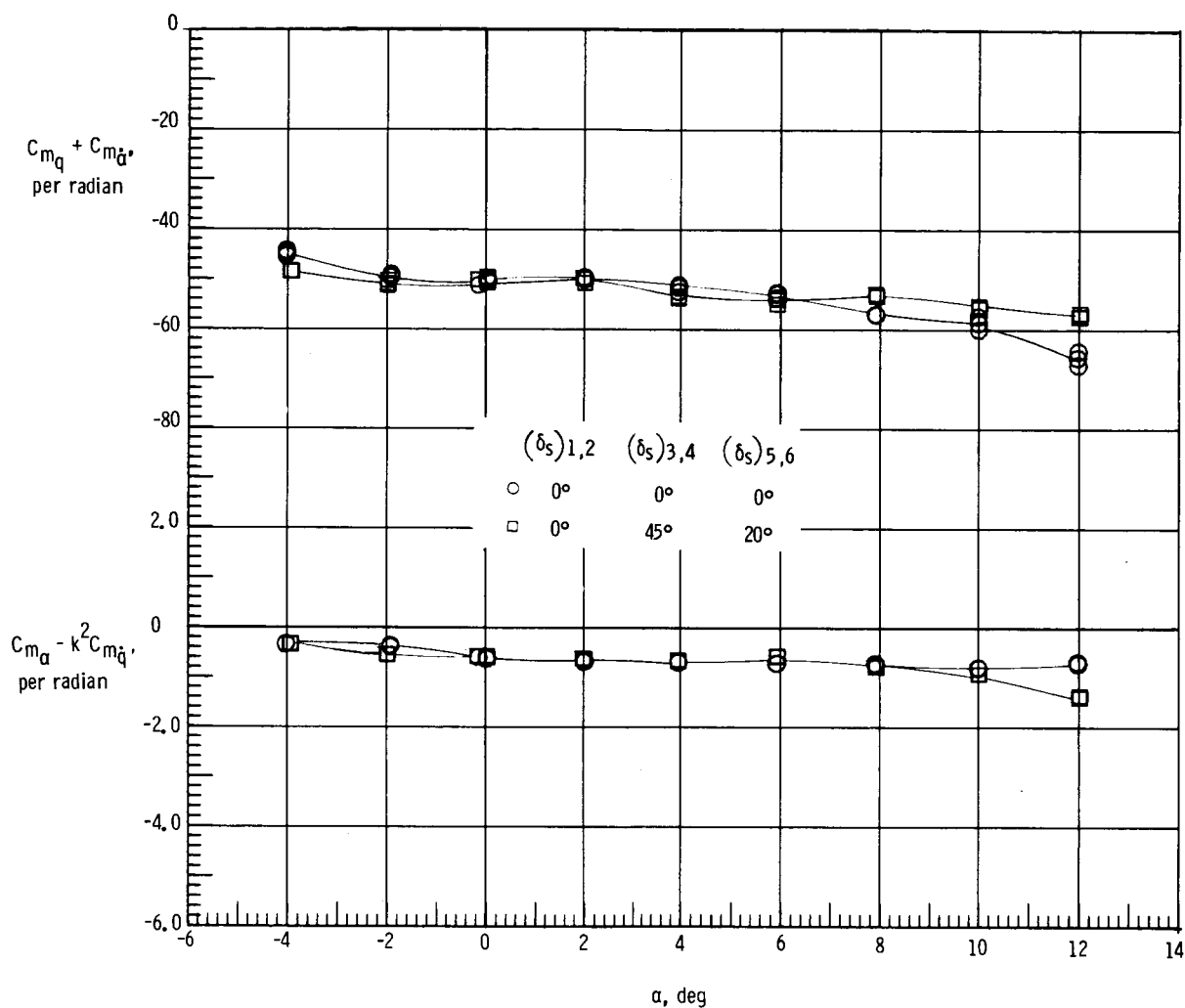
(a) M = 0.2.

Figure 11.- Effect of spoiler deployment on damping-in-pitch parameter
and on oscillatory stability-in-pitch parameter of ALT configuration.
$i_o = 6°$; faired struts; tail cone on.
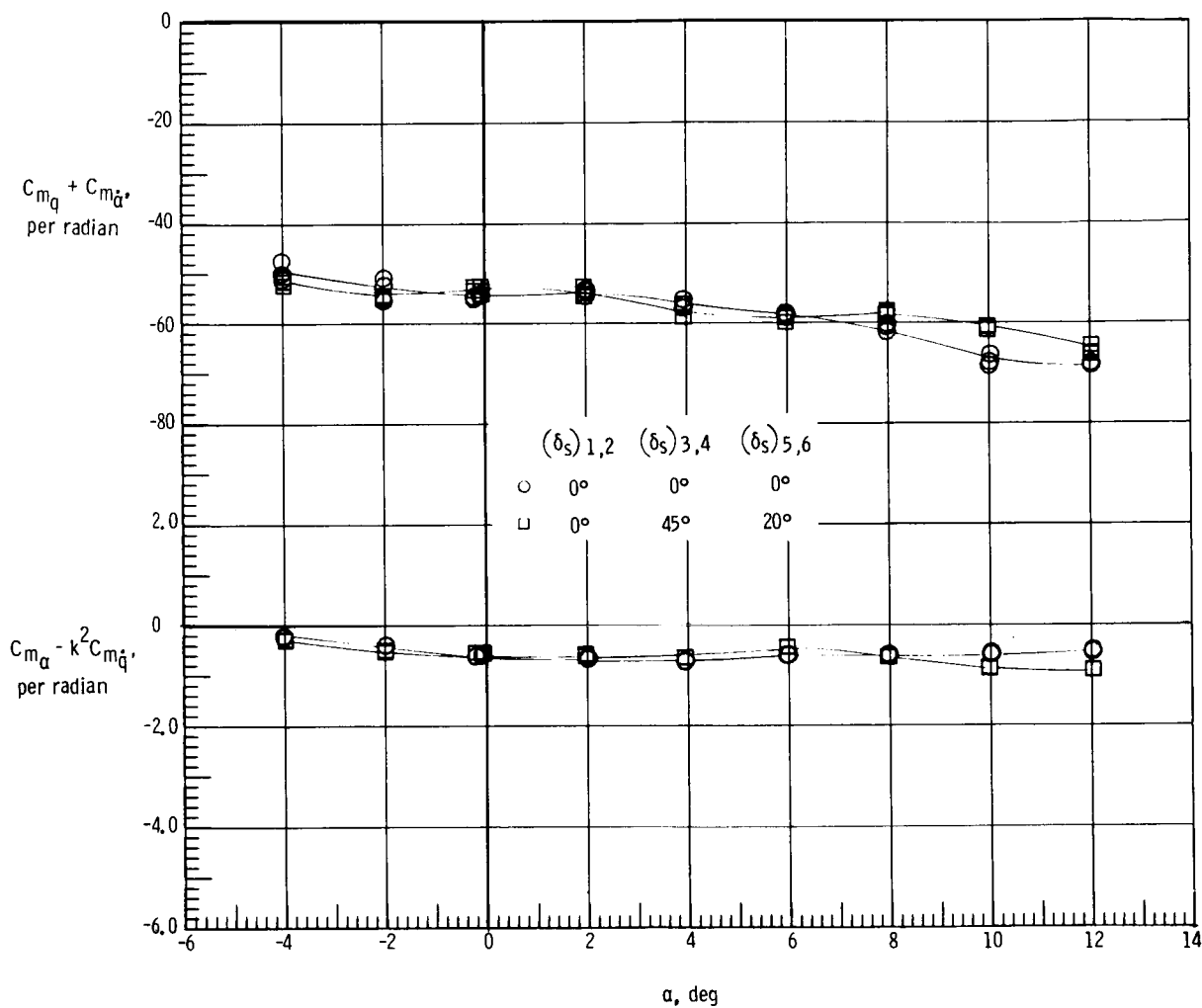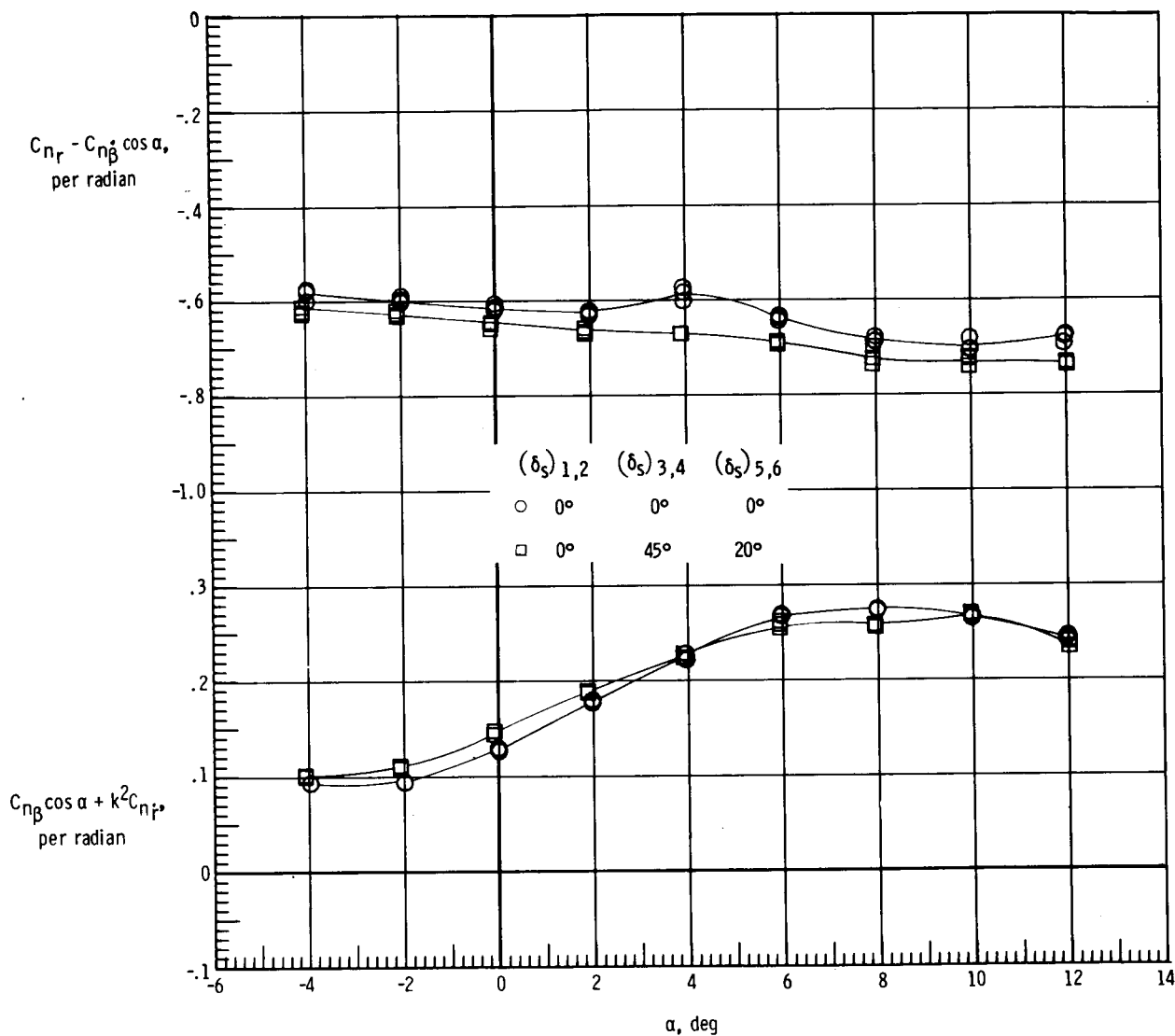
(b) M = 0.4.

Figure 11.- Continued.
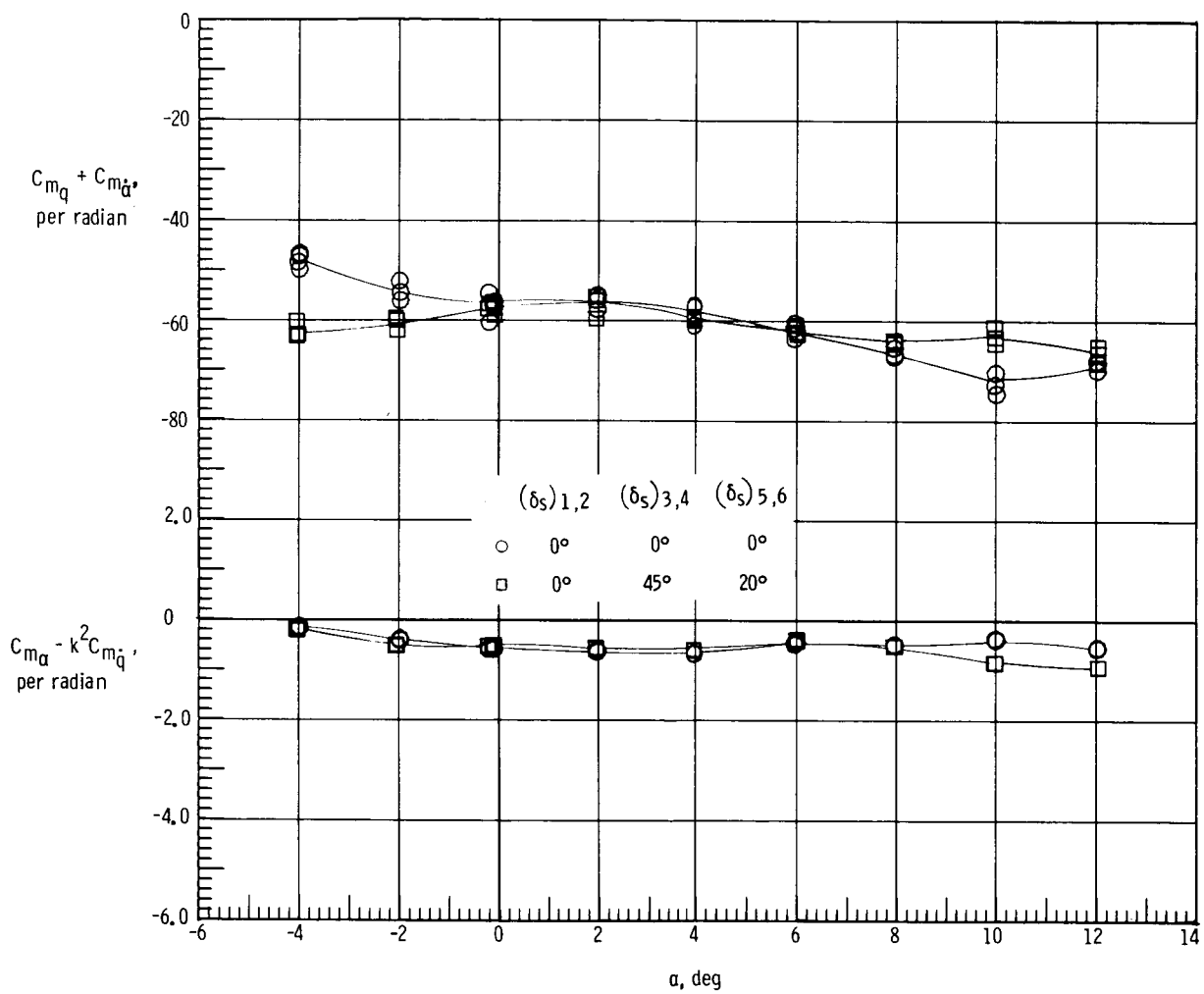
(c) M = 0.5.

Figure 11.- Concluded.
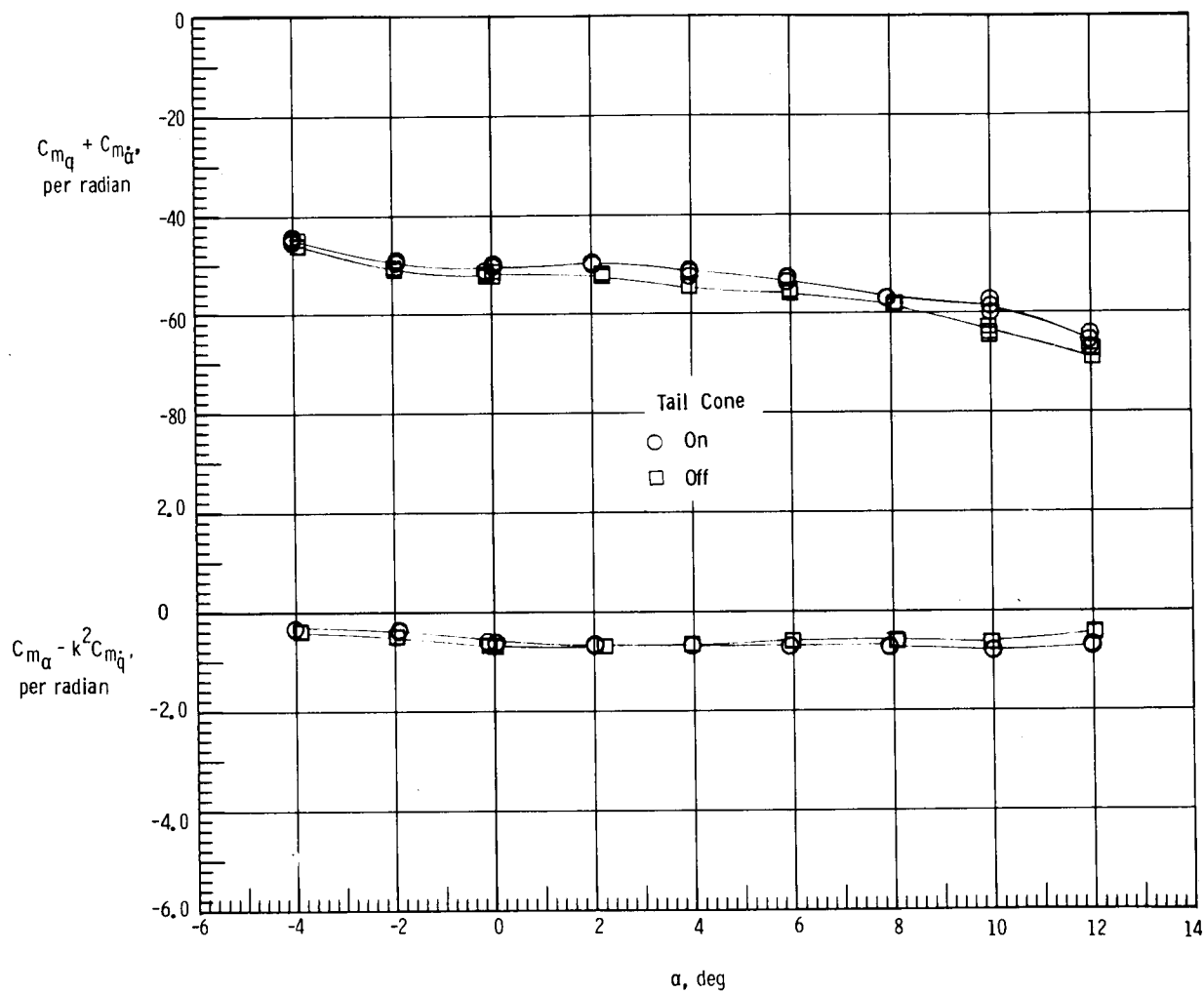
(a)   M = 0.2.

Figure 12.— Effect of tail cone on damping-in-pitch parameter and on oscillatory
stability-in-pitch parameter of ALT configuration. $i_o = 6°$; faired struts.
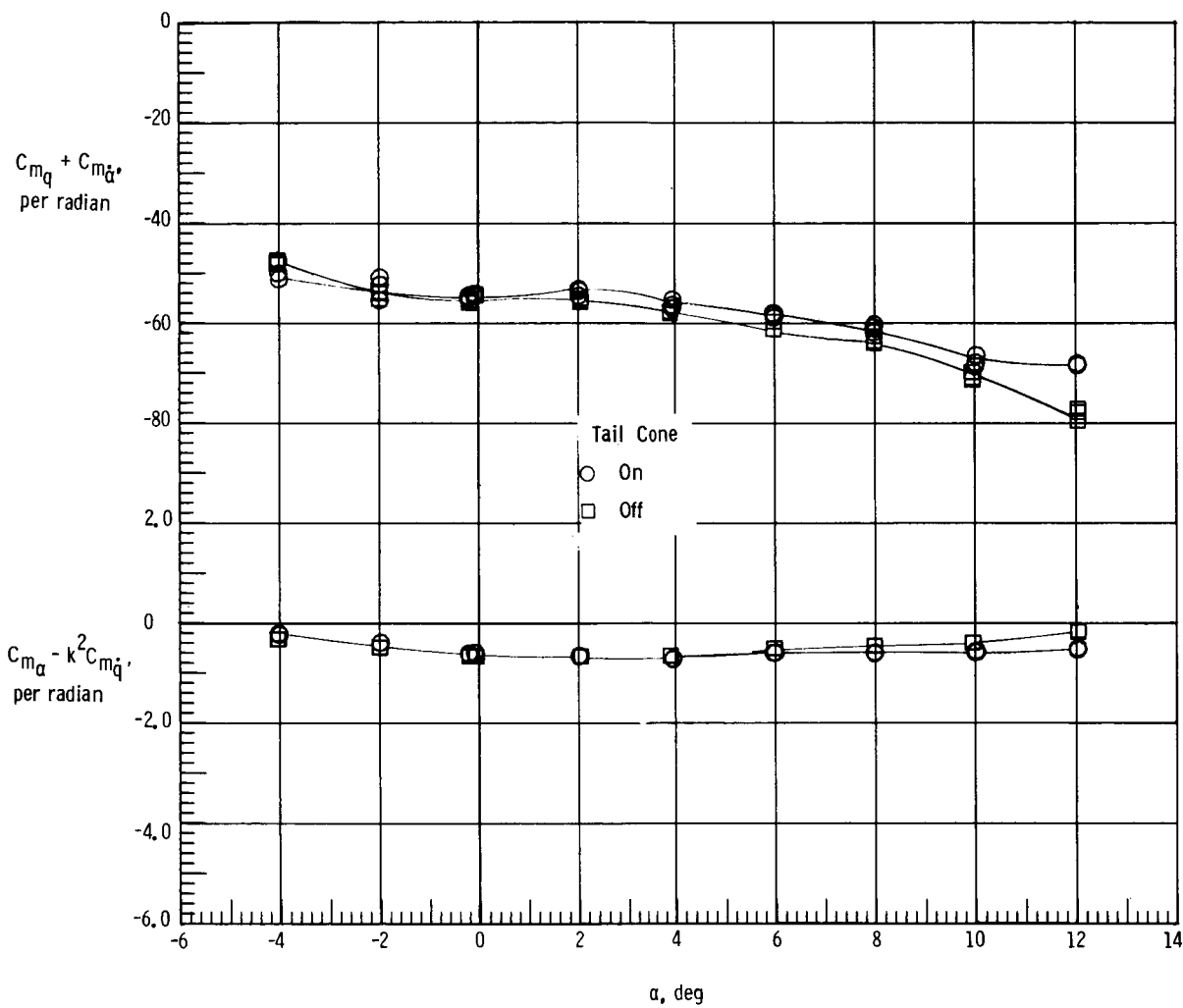
(b) M = 0.4.

Figure 12.- Continued.
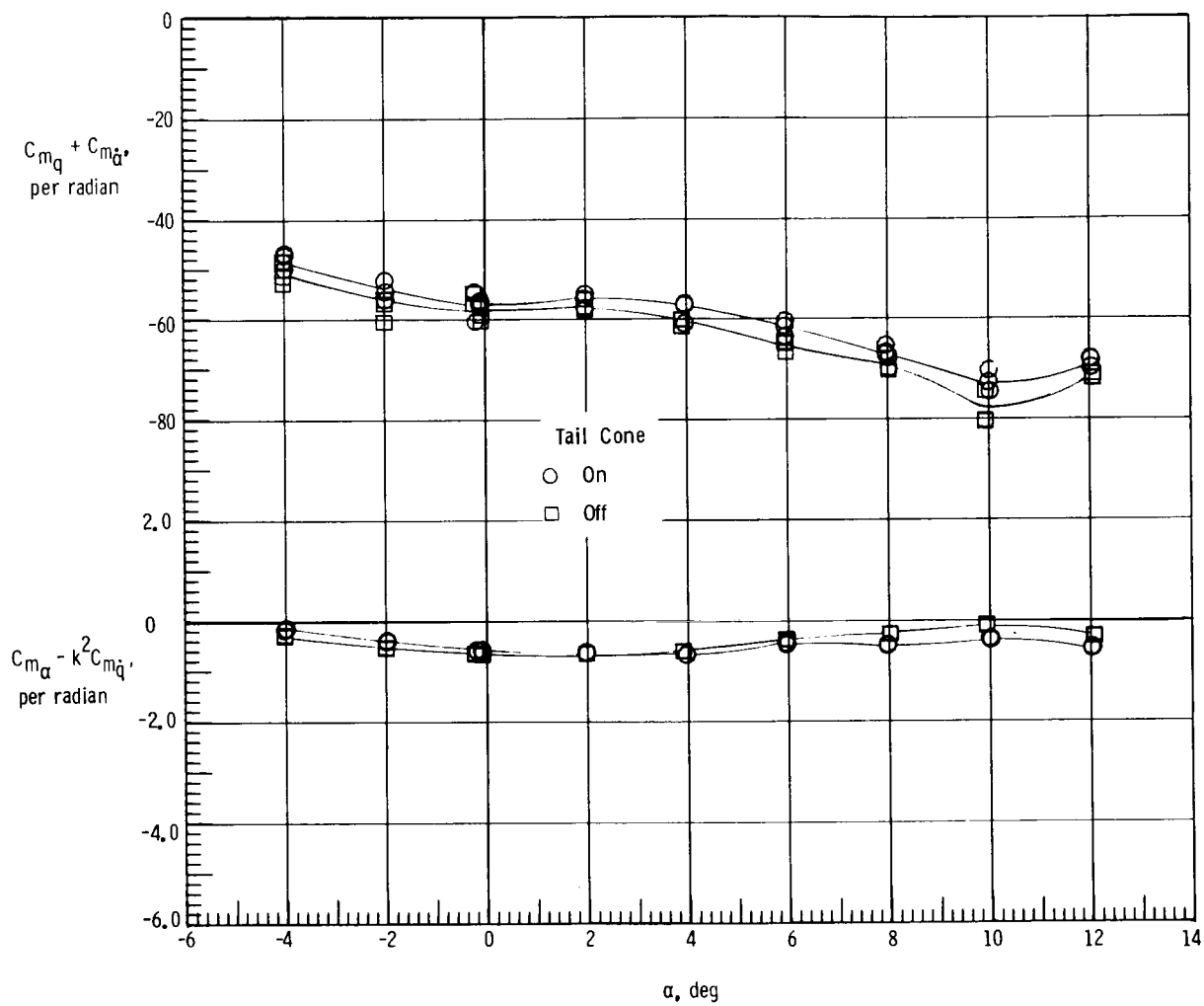
(c) M = 0.5.

Figure 12.- Concluded.
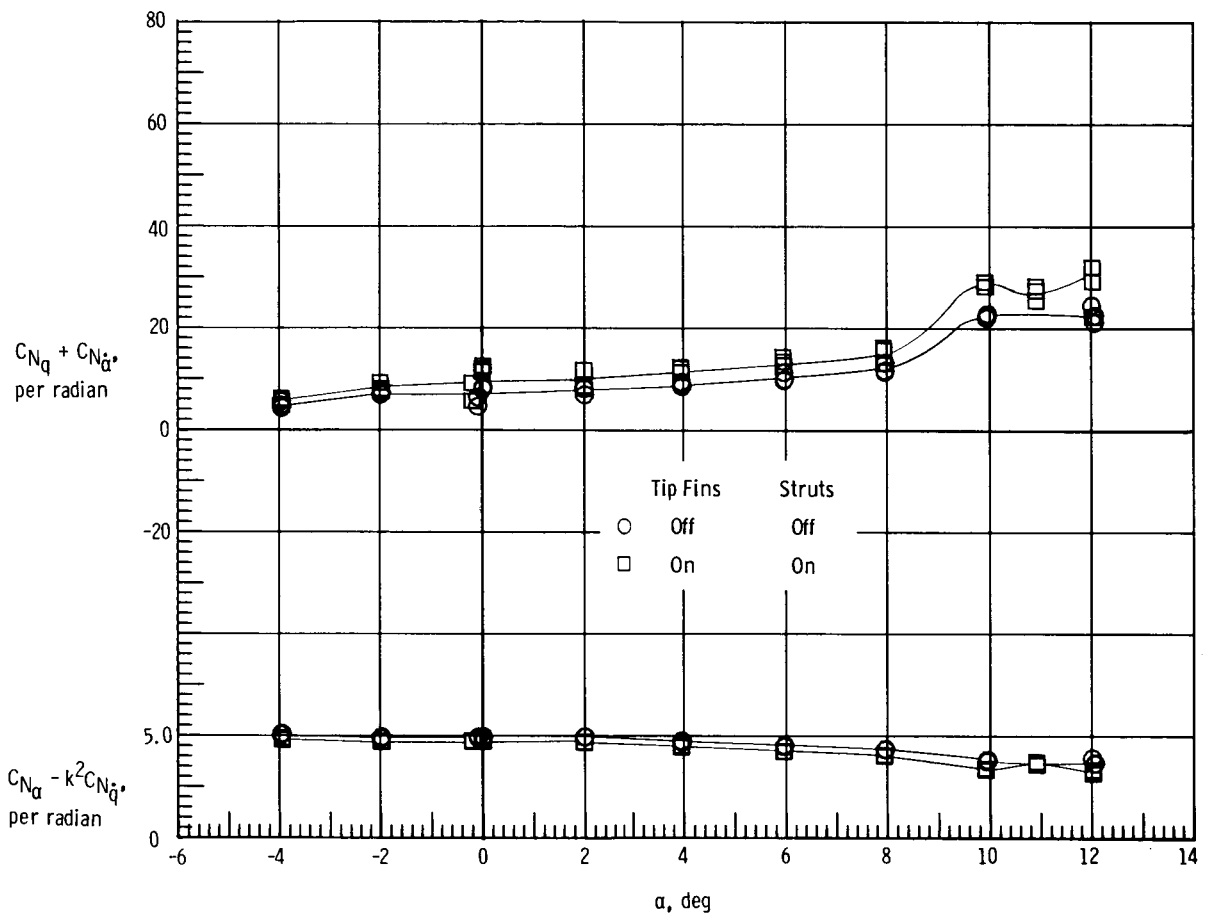
(a) M = 0.2.

Figure 13.- Effect of tip fins and struts on normal force due to pitch-rate
    parameter and normal force due to pitch-displacement parameter of basic
    747. Faired struts.
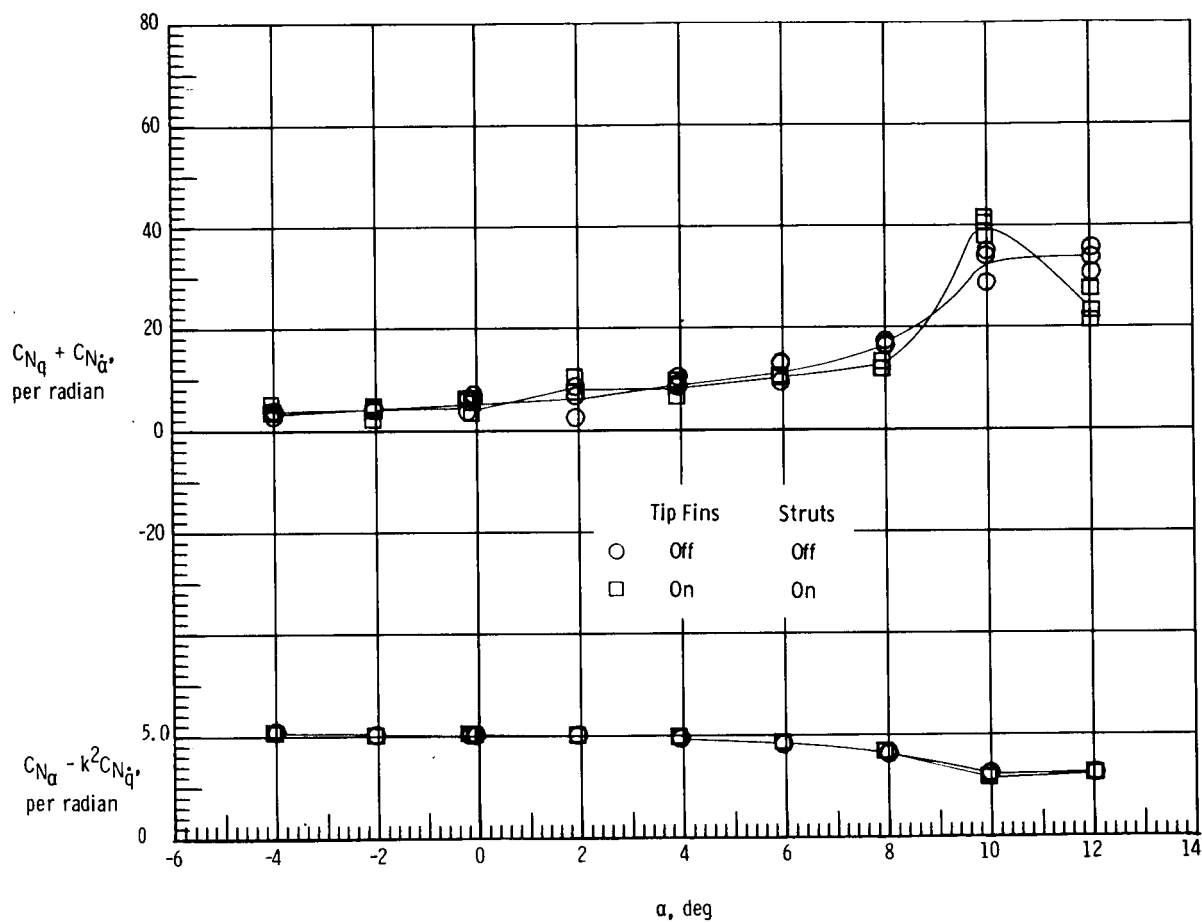
(b) M = 0.4.

Figure 13.- Continued.

52
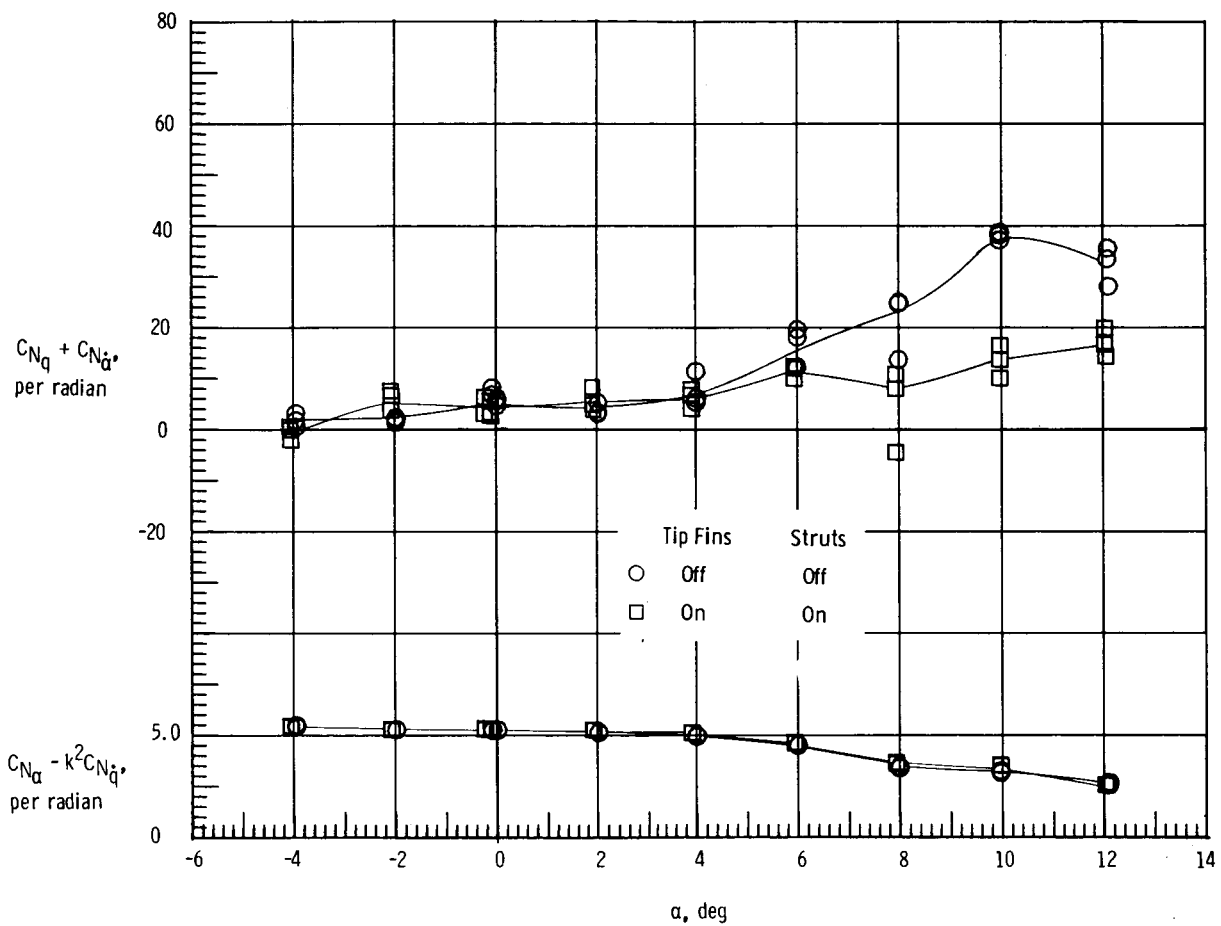
(c) M = 0.5.

Figure 13.- Concluded.
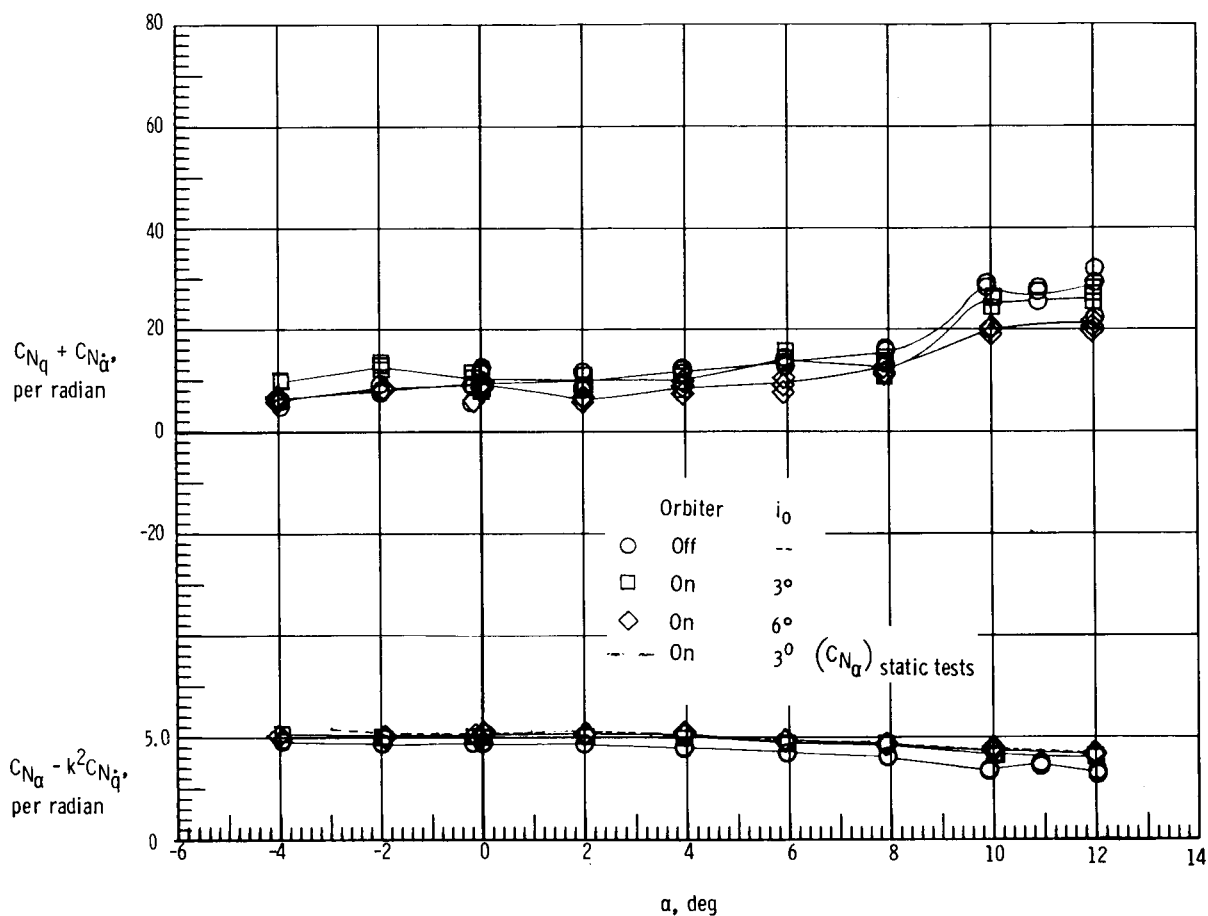
(a) M = 0.2.

Figure 14.- Effect of orbiter and orbiter incidence on normal force due to pitch-rate parameter and normal force due to pitch-displacement parameter of modified 747. Faired struts; tail cone on.

80

60

40

20

$C_{N_q} + C_{N_{\dot{\alpha}}}$,
per radian

0

-20

	Orbiter	i_0
○	Off	--
□	On	3°
◇	On	6°
-----	On	3° $\left(C_{N_\alpha}\right)$static tests

5.0

$C_{N_\alpha} - k^2 C_{N_{\dot{q}}}$,
per radian

0

-6   -4   -2   0   2   4   6   8   10   12   14

α, deg
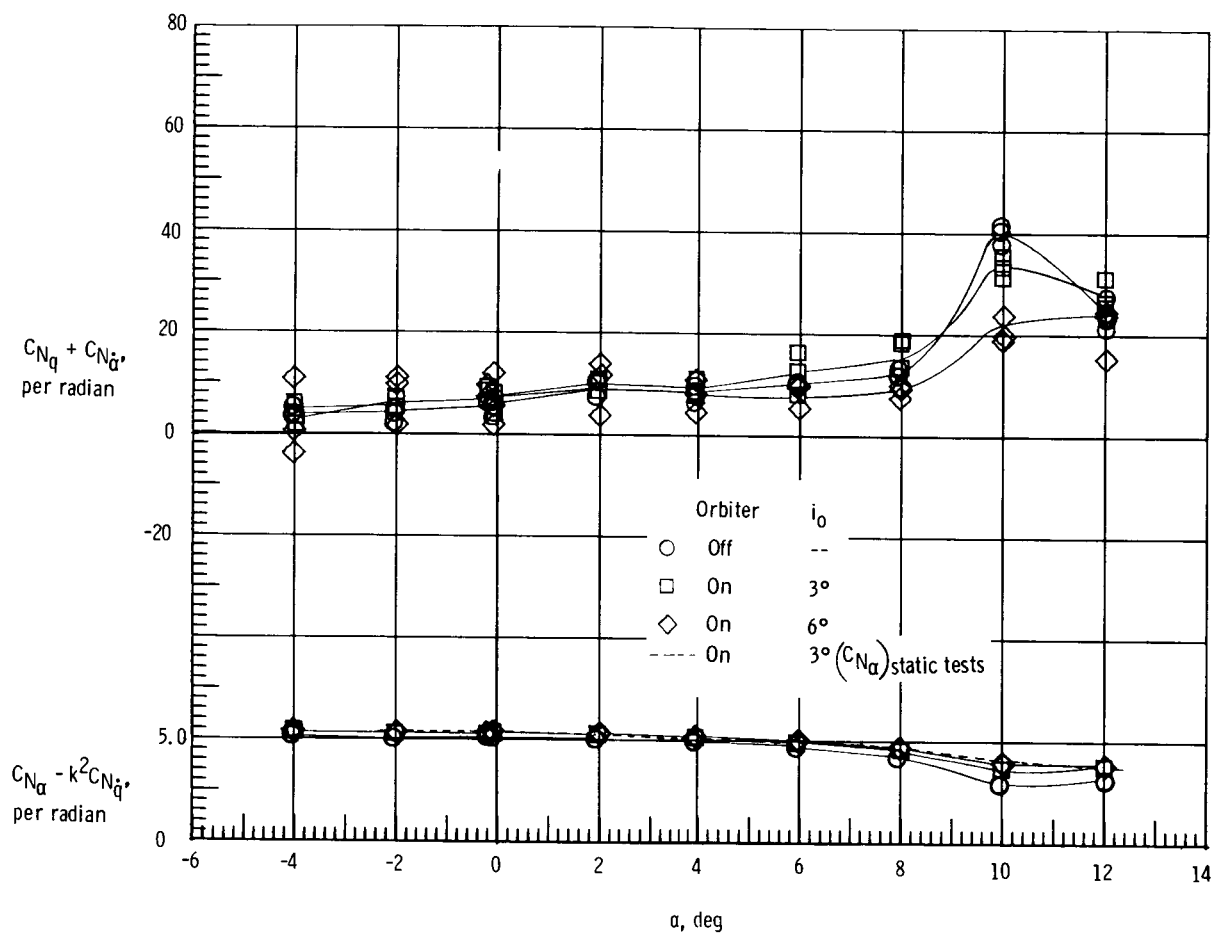
(b)   M ◻ 0.4.

Figure 14.- Continued.
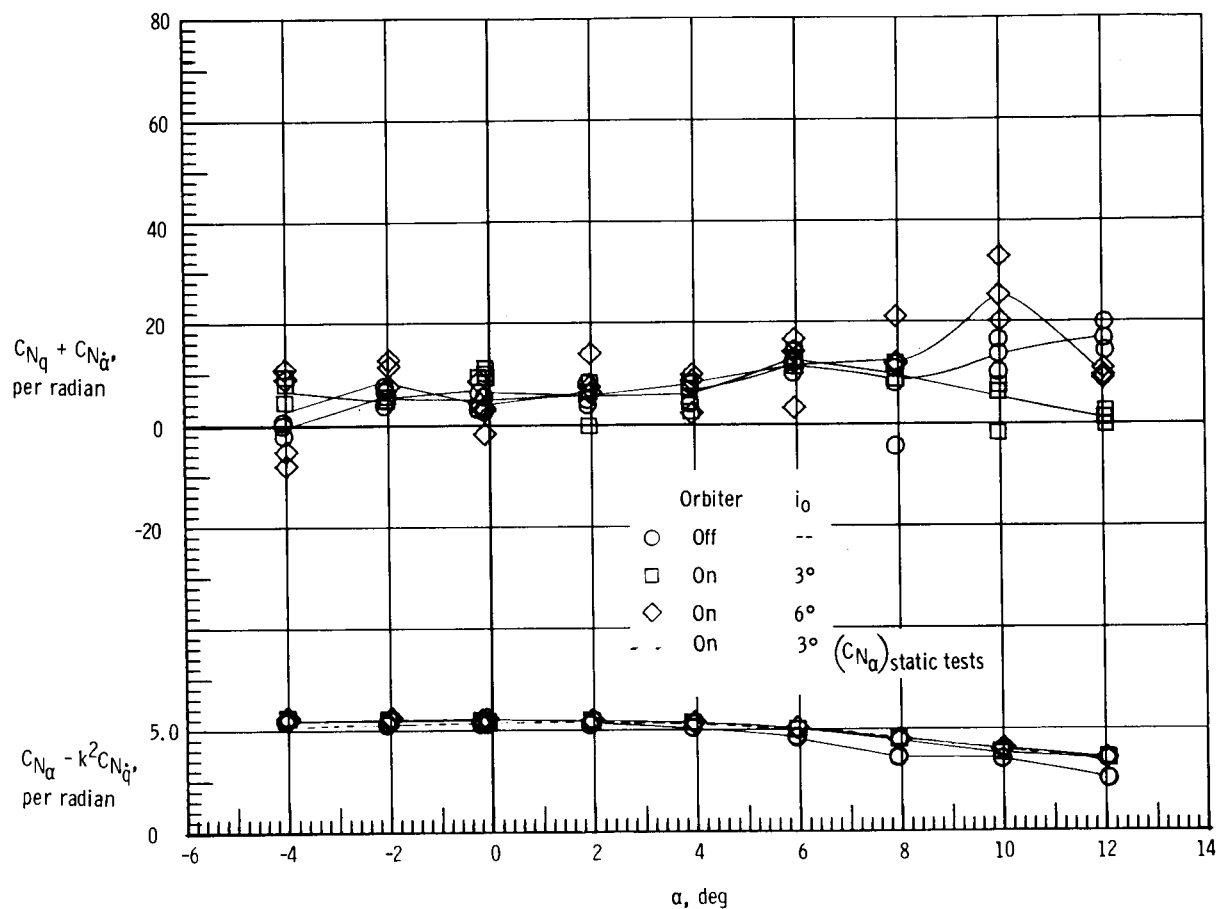
(c) M = 0.5.

Figure 14.- Concluded.
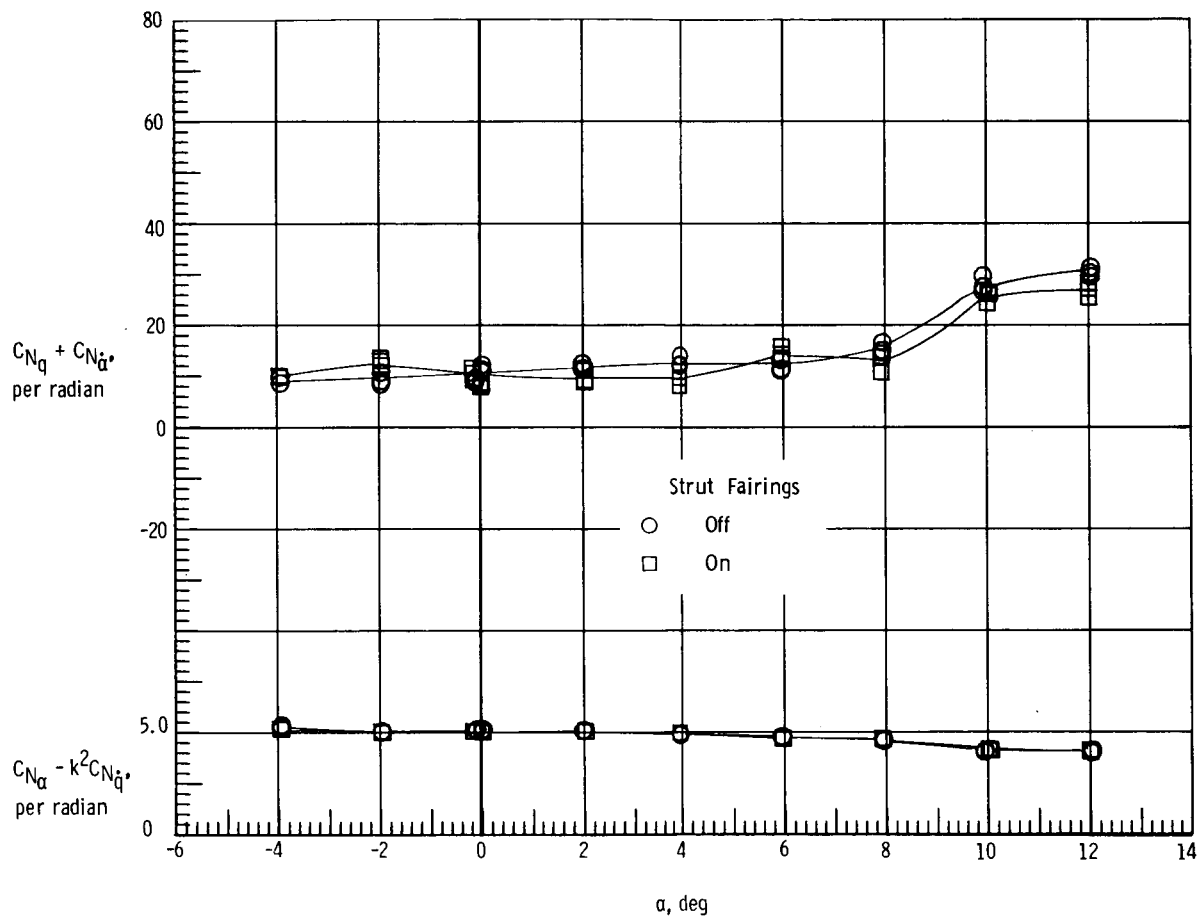
(a)   M = 0.2.

Figure 15.- Effect of strut fairings on normal force due to pitch-rate parameter
and normal force due to pitch-displacement parameter of ferry configuration.
$i_O = 3^O$; tail cone on.
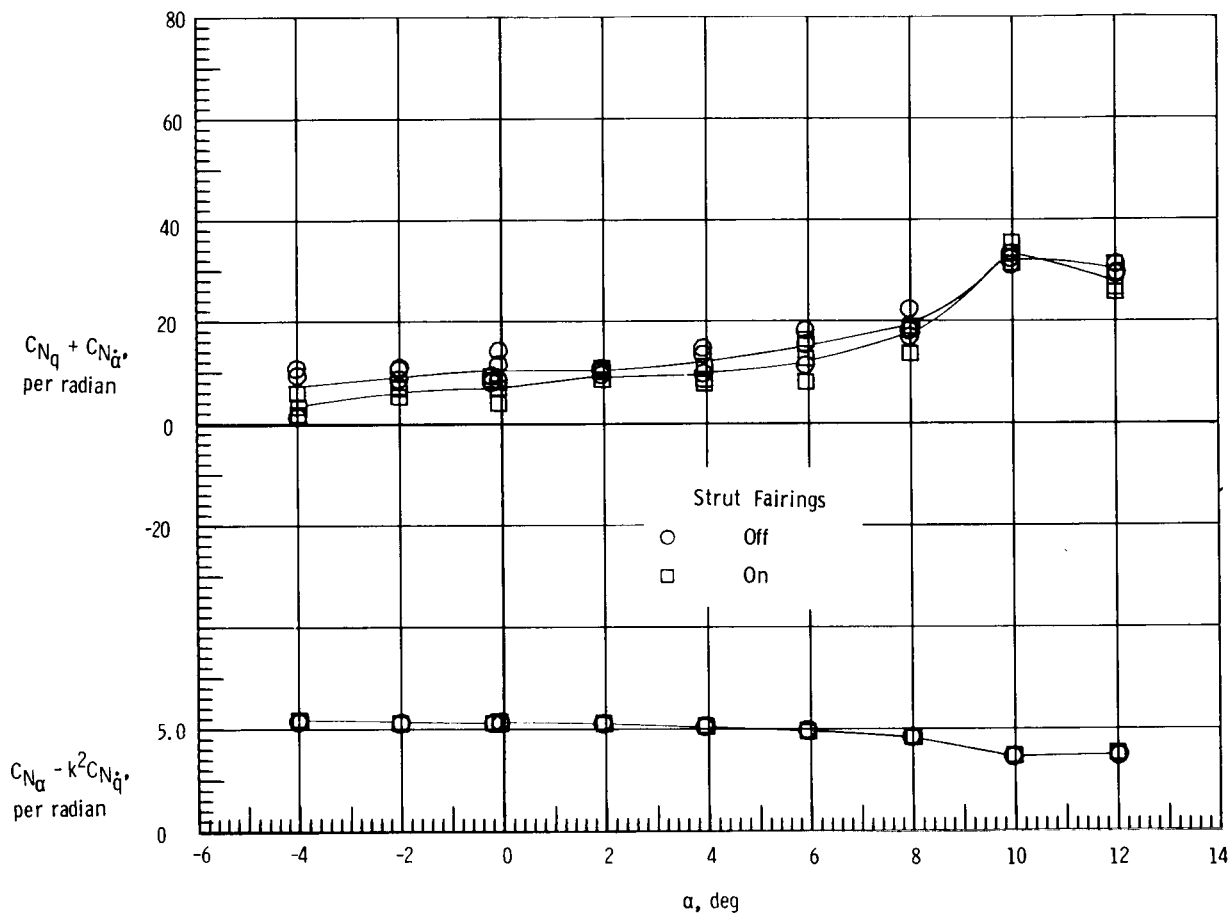
(b)   M = 0.4.

Figure 15.- Continued.

58
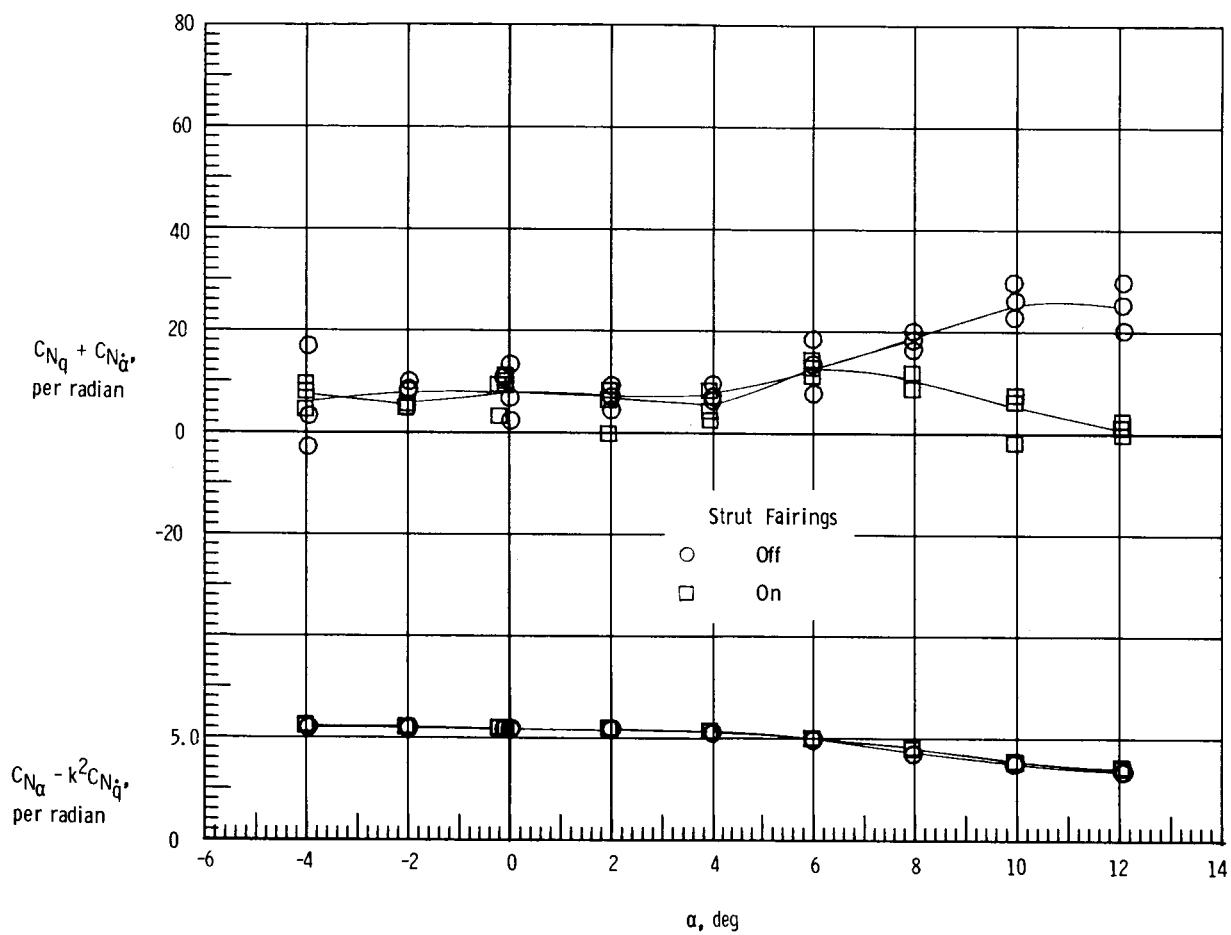
(c) M = 0.5.

Figure 15.- Concluded.
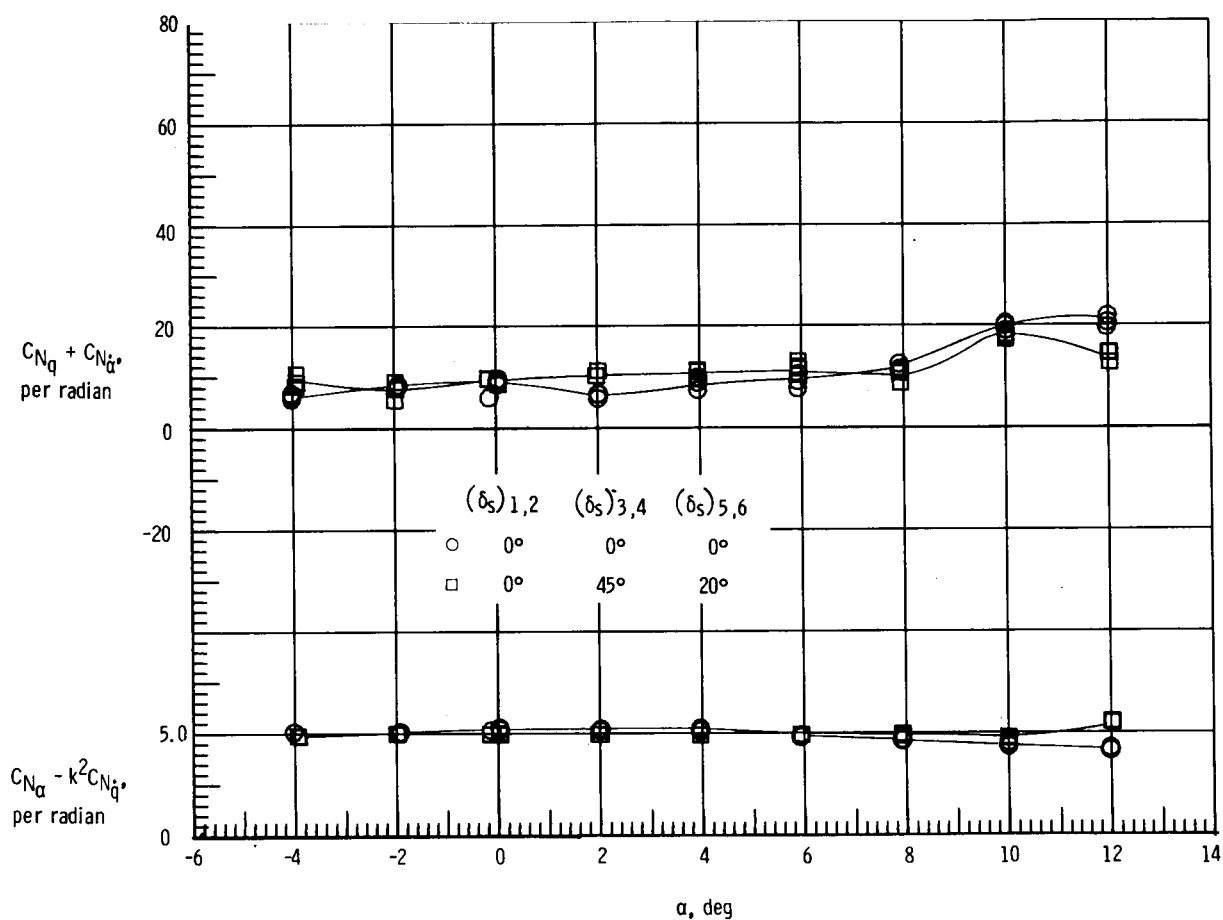
(a) M = 0.2.

Figure 16.- Effect of spoiler deployment on normal force due to pitch-rate
parameter and normal force due to pitch-displacement parameter of ALT
configuration. $i_O = 6^O$; faired struts; tail cone on.

60
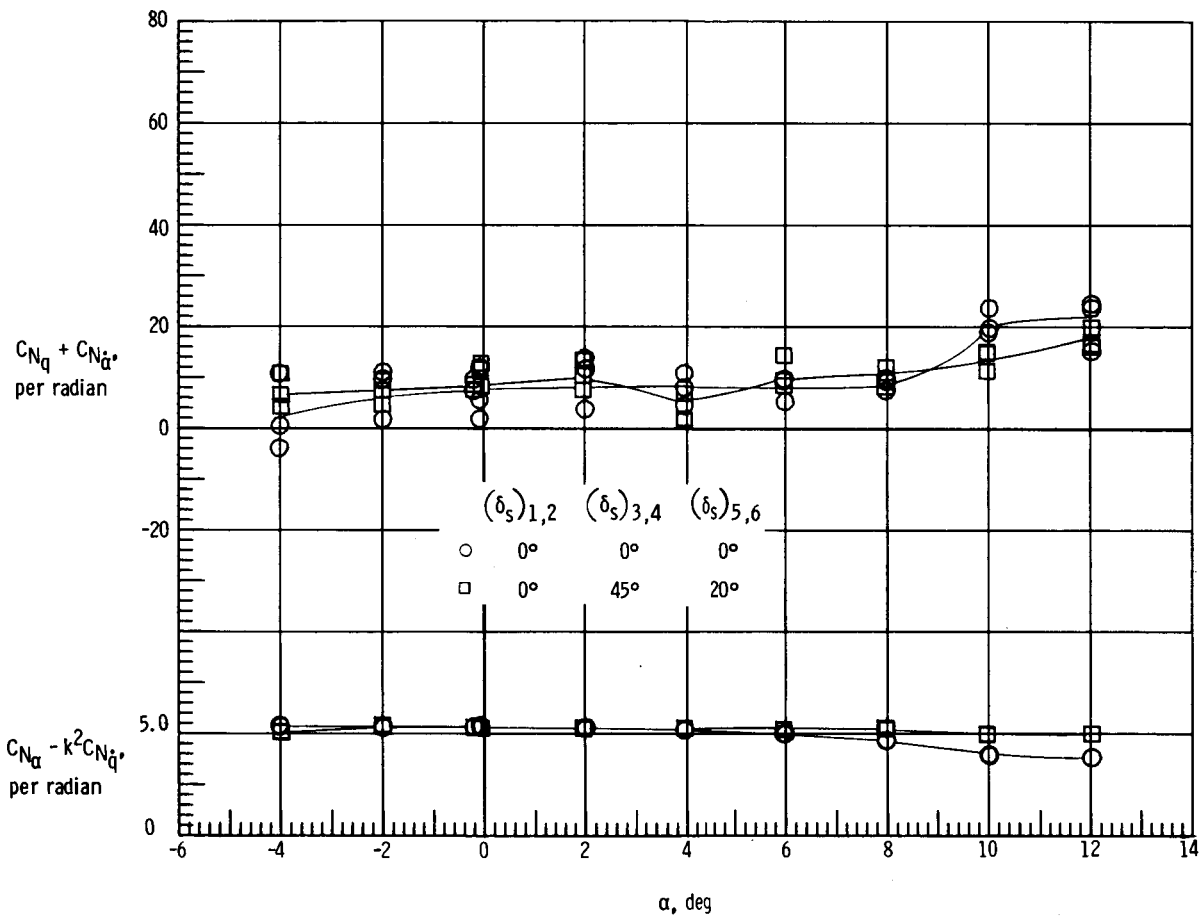
(b) M = 0.4.

Figure 16.- Continued.

80

60

40

$C_{N_q} + C_{N_{\dot\alpha}}$, per radian

20

0

-20

$(\delta_s)_{1,2}$ $(\delta_s)_{3,4}$ $(\delta_s)_{5,6}$

○   0°   0°   0°

□   0°   45°   20°

5.0

$C_{N_\alpha} - k^2 C_{N_{\dot q}}$, per radian

0

-6   -4   -2   0   2   4   6   8   10   12   14

α, deg
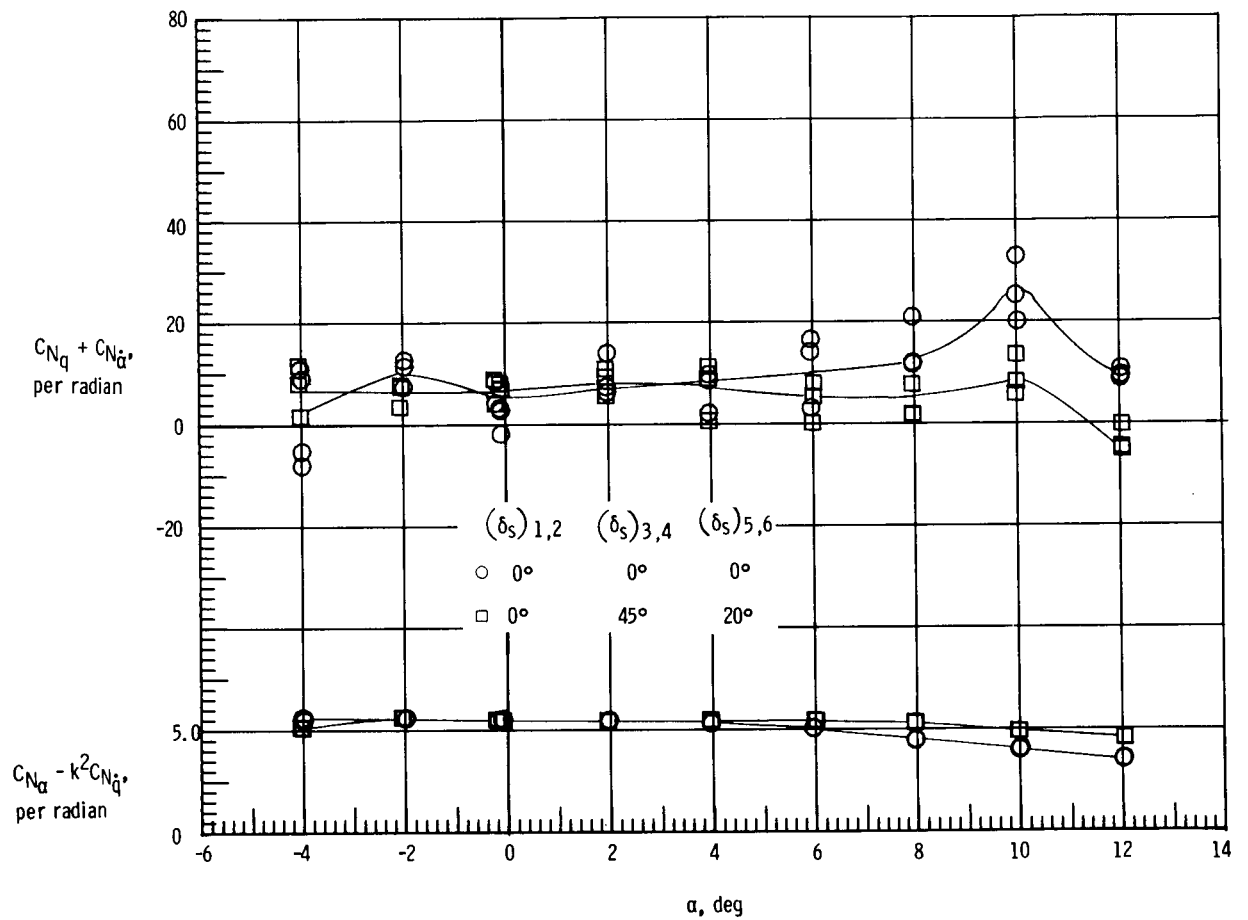
(c)   M = 0.5.

Figure 16.- Concluded.
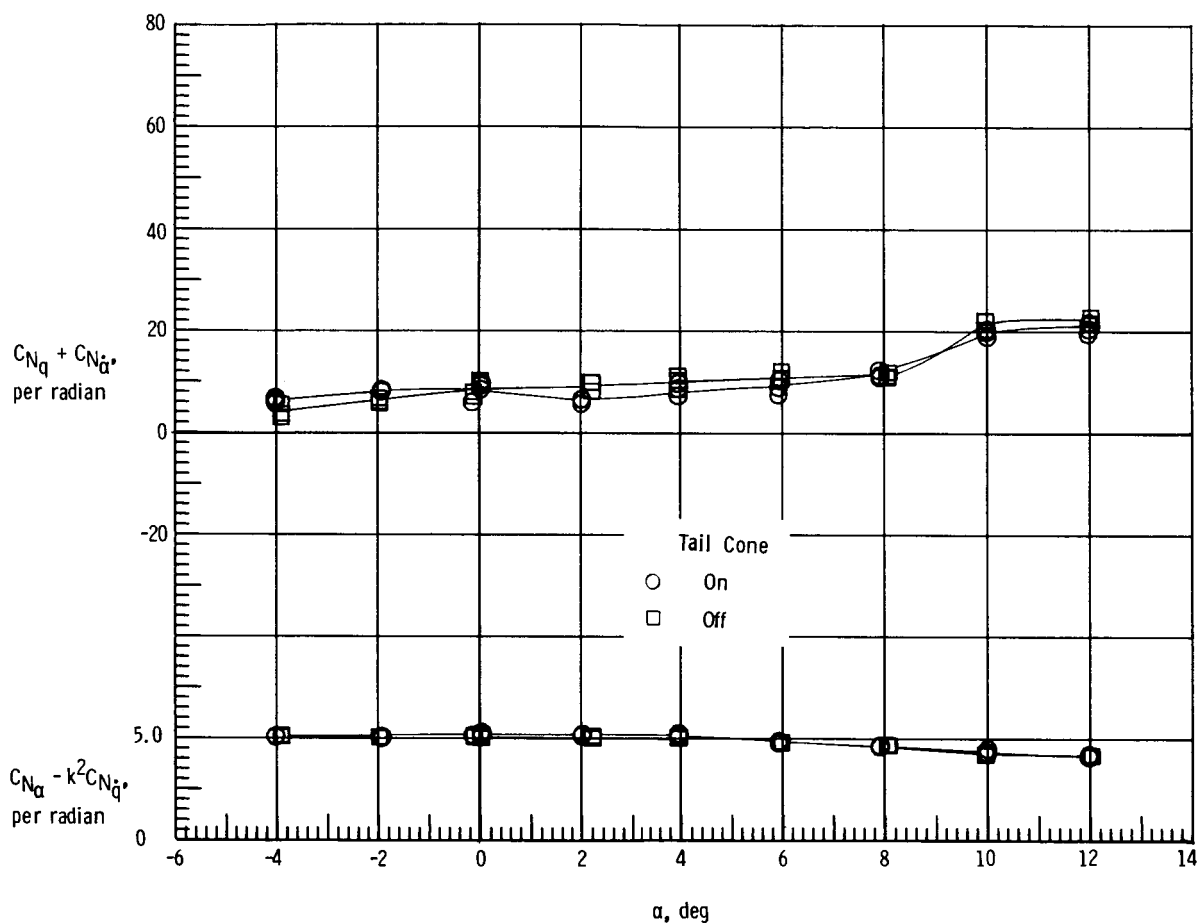
(a) M = 0.2.

Figure 17.- Effect of tail cone on normal force due to pitch-rate parameter
   and normal force due to pitch-displacement parameter of ALT configuration.
   $i_O = 6^O$; faired struts.
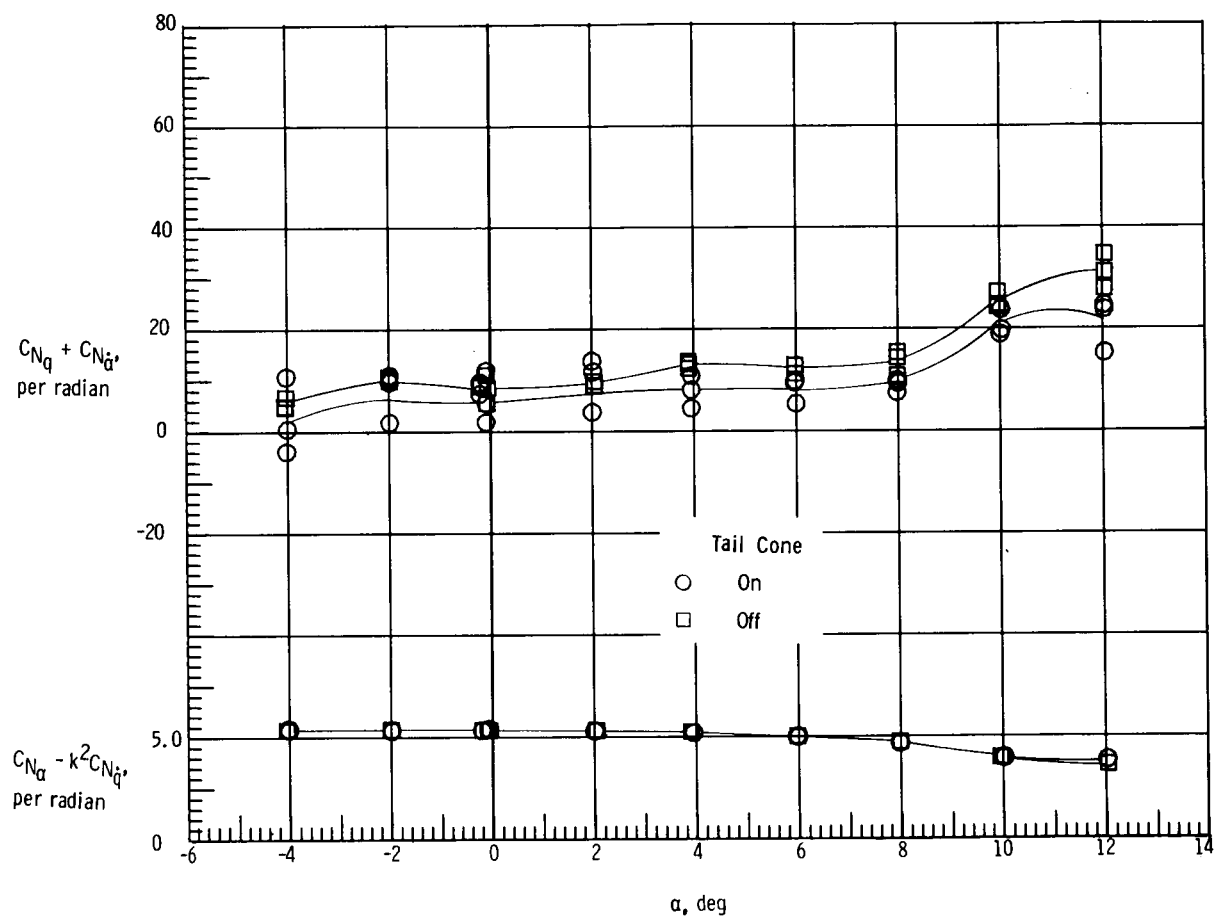
(b) M = 0.4.

Figure 17.- Continued.
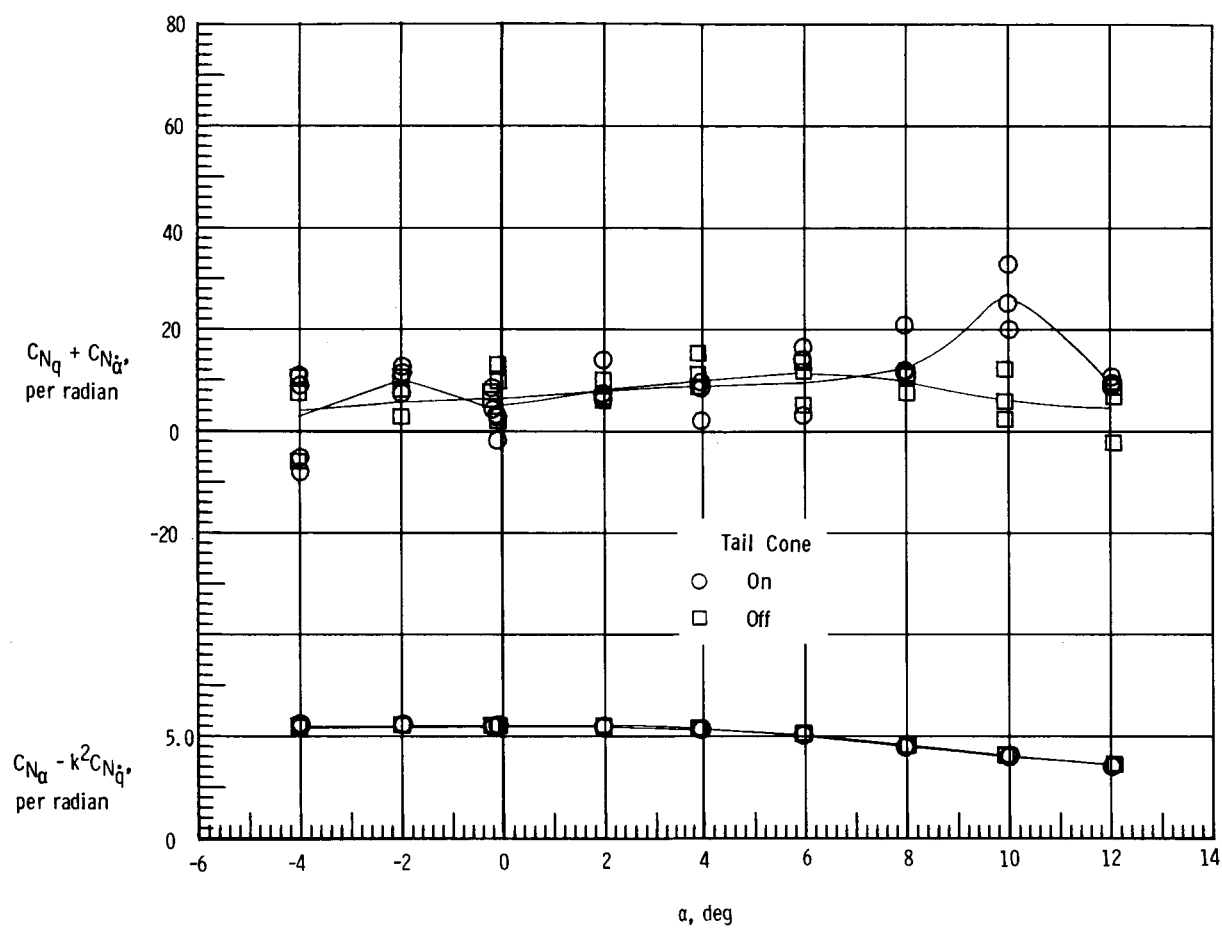
(c) M = 0.5.

Figure 17.- Concluded.

(a)   M = 0.2.

Figure 18.- Effect of tip fins and struts on damping-in-yaw parameter and on oscillatory directional-stability parameter of basic 747.   Unfaired struts.
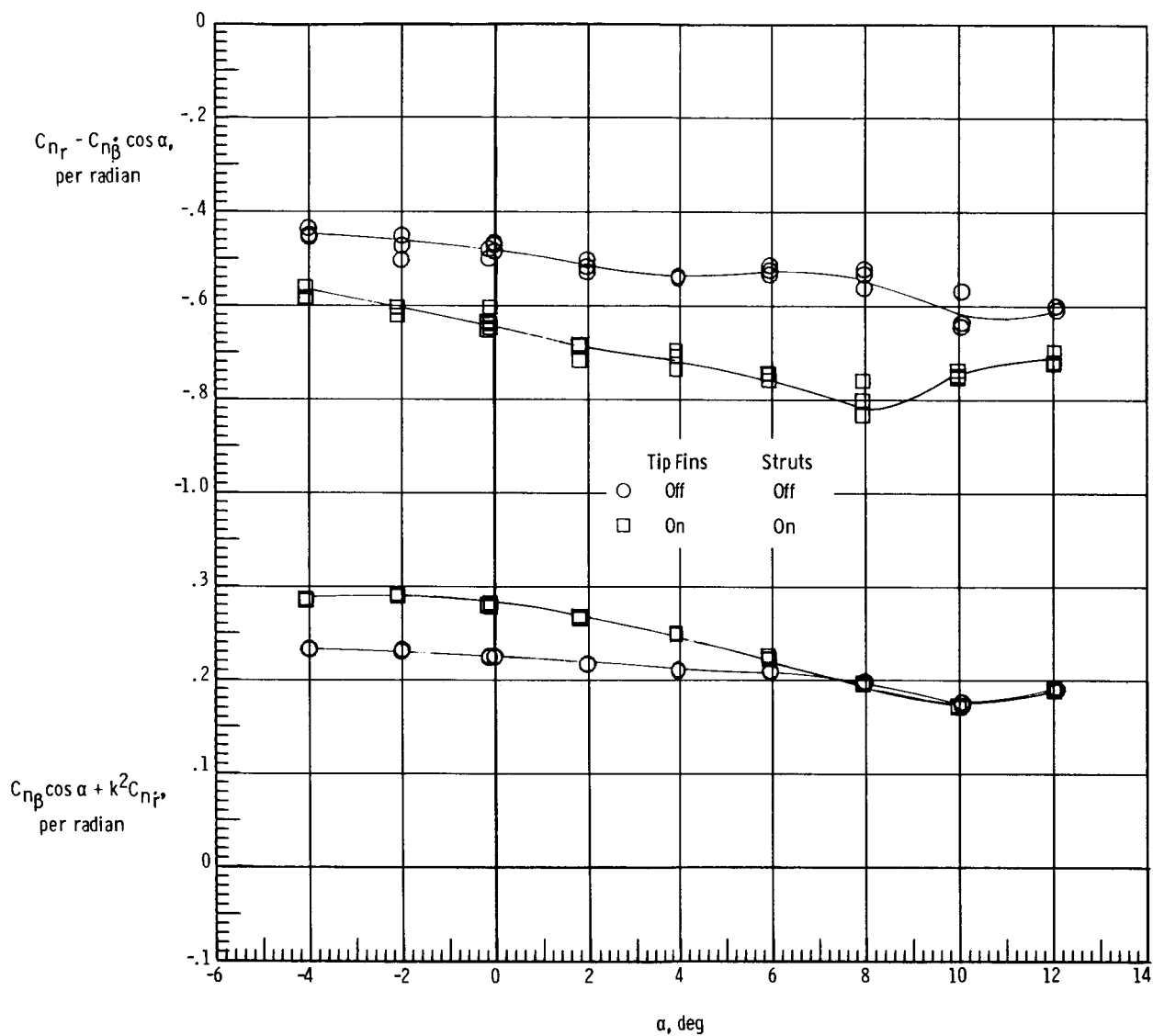
(b) M = 0.4.

Figure 18.- Continued.
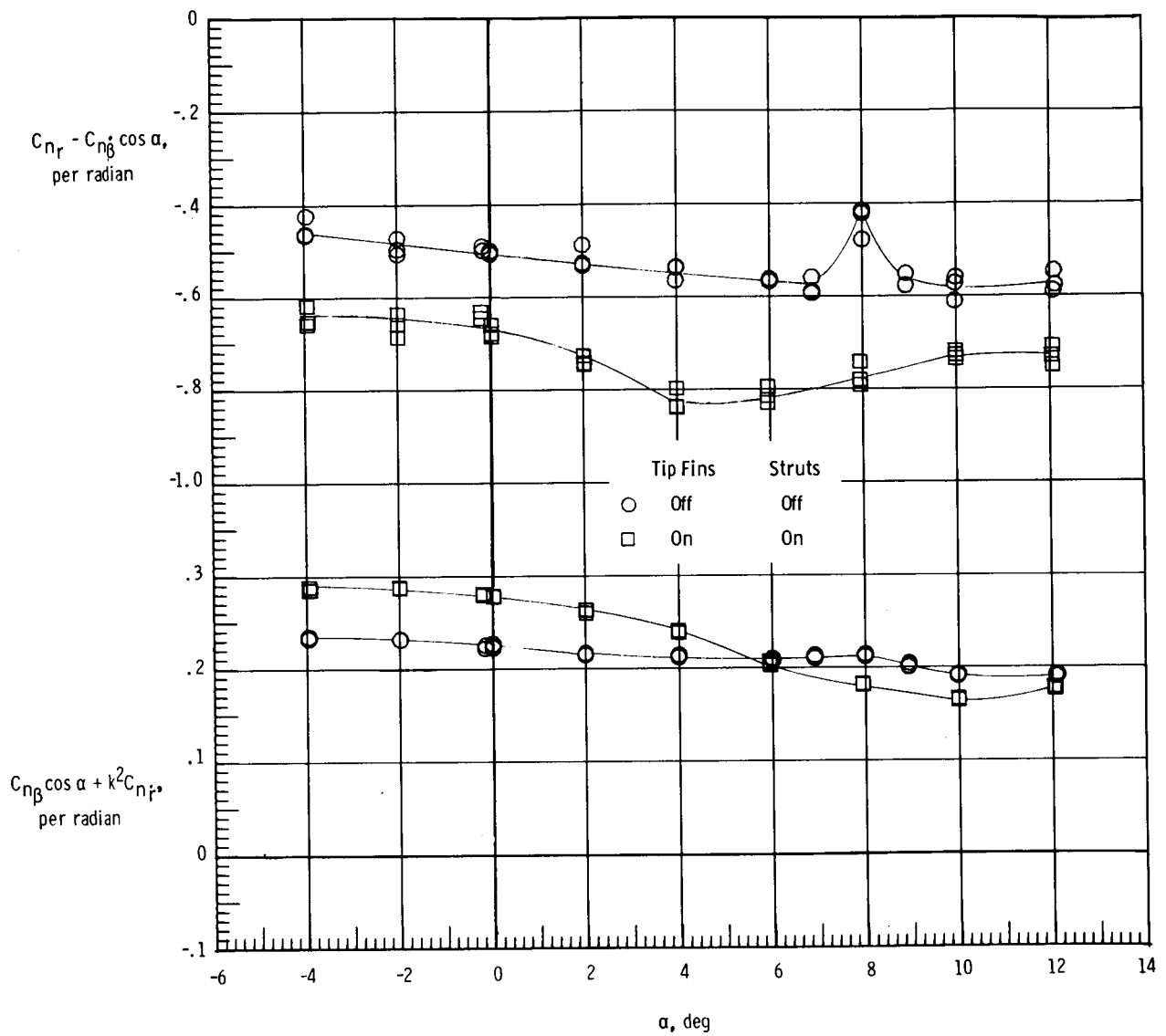
(c)   M = 0.5.

Figure 18.- Concluded.

(a) M = 0.2.

Figure 19.- Effect of orbiter and orbiter incidence on damping-in-yaw parameter
and on oscillatory directional-stability parameter of modified 747. Unfaired
struts; tail cone on.

$C_{n_r} - C_{n_{\dot{\beta}}} \cos \alpha,$
per radian

$C_{n_\beta} \cos \alpha + k^2 C_{n_{\dot{r}}},$
per radian

Orbiter	i_0
○ Off	--
□ On	3°
◇ On	6°
---- On	3° $\left(C_{n_\beta} \cos \alpha\right)$ static tests
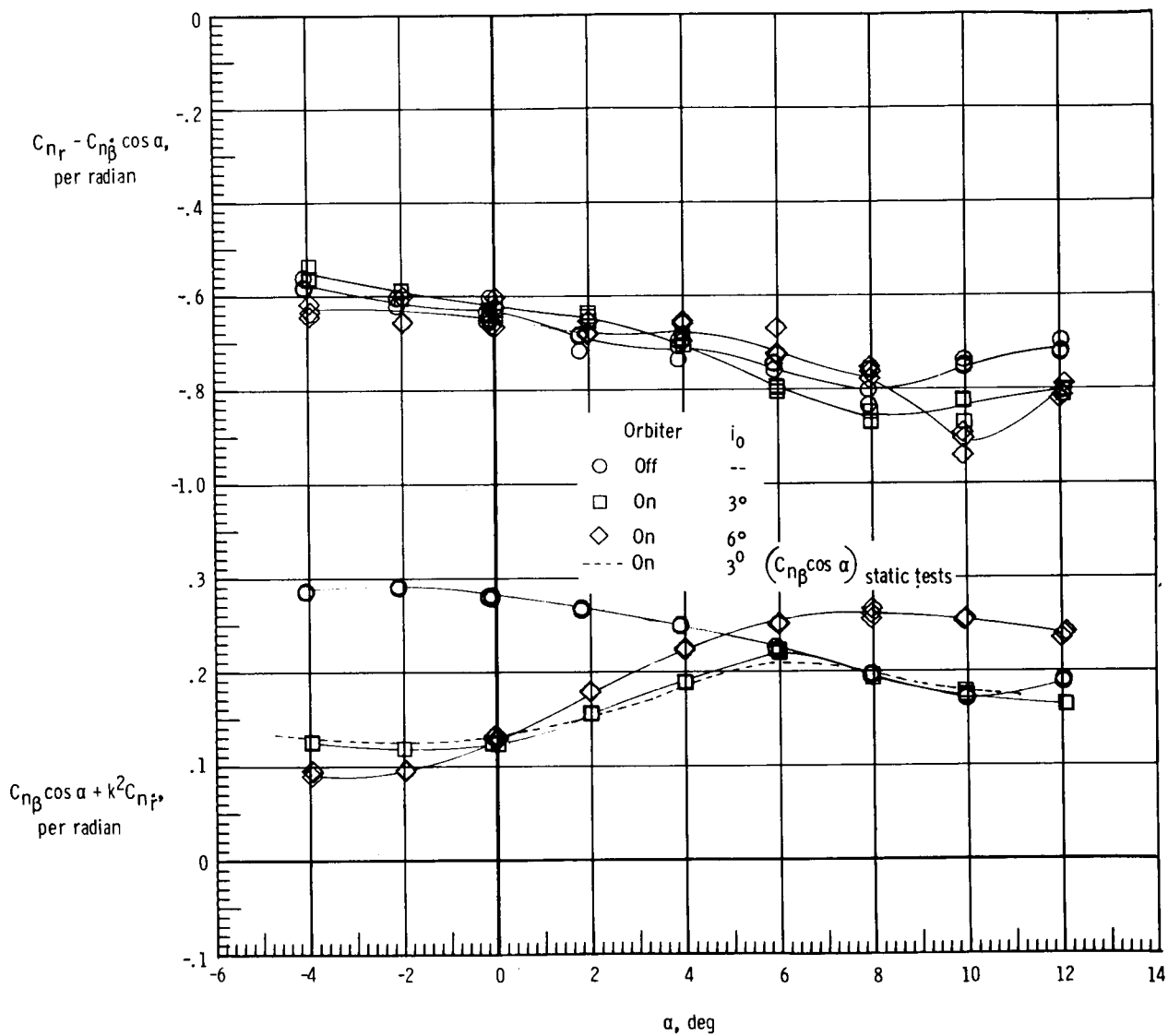
(b)   M = 0.4.

Figure 19.- Continued.
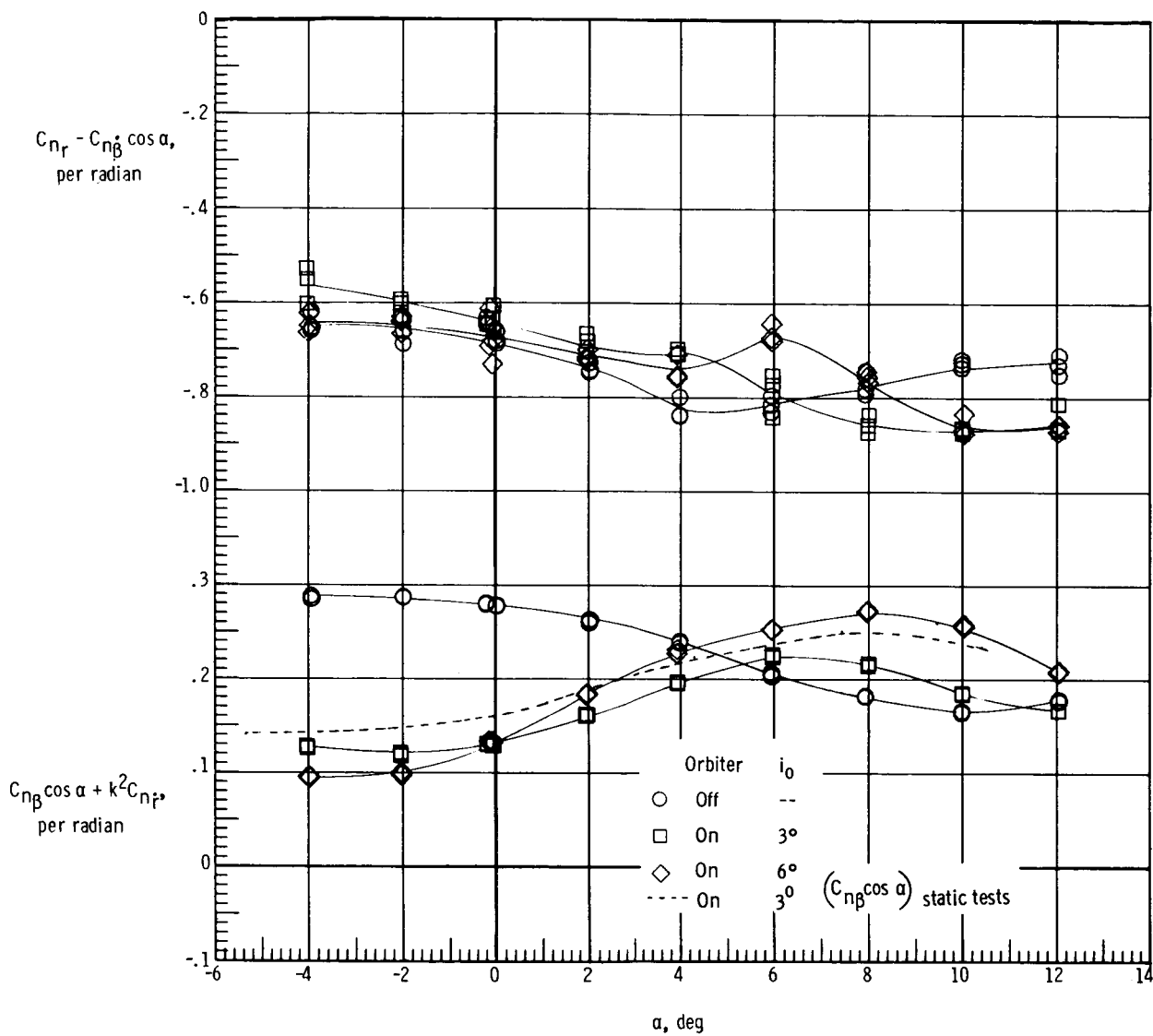
(c) M = 0.5.

Figure 19.- Concluded.

(a) M = 0.2.

Figure 20.- Effect of spoiler deployment on damping-in-yaw parameter and oscillatory directional-stability parameter of ALT configuration. $i_O = 6^O$; unfaired struts; tail cone on.

(b) M = 0.4.

Figure 20.- Continued.
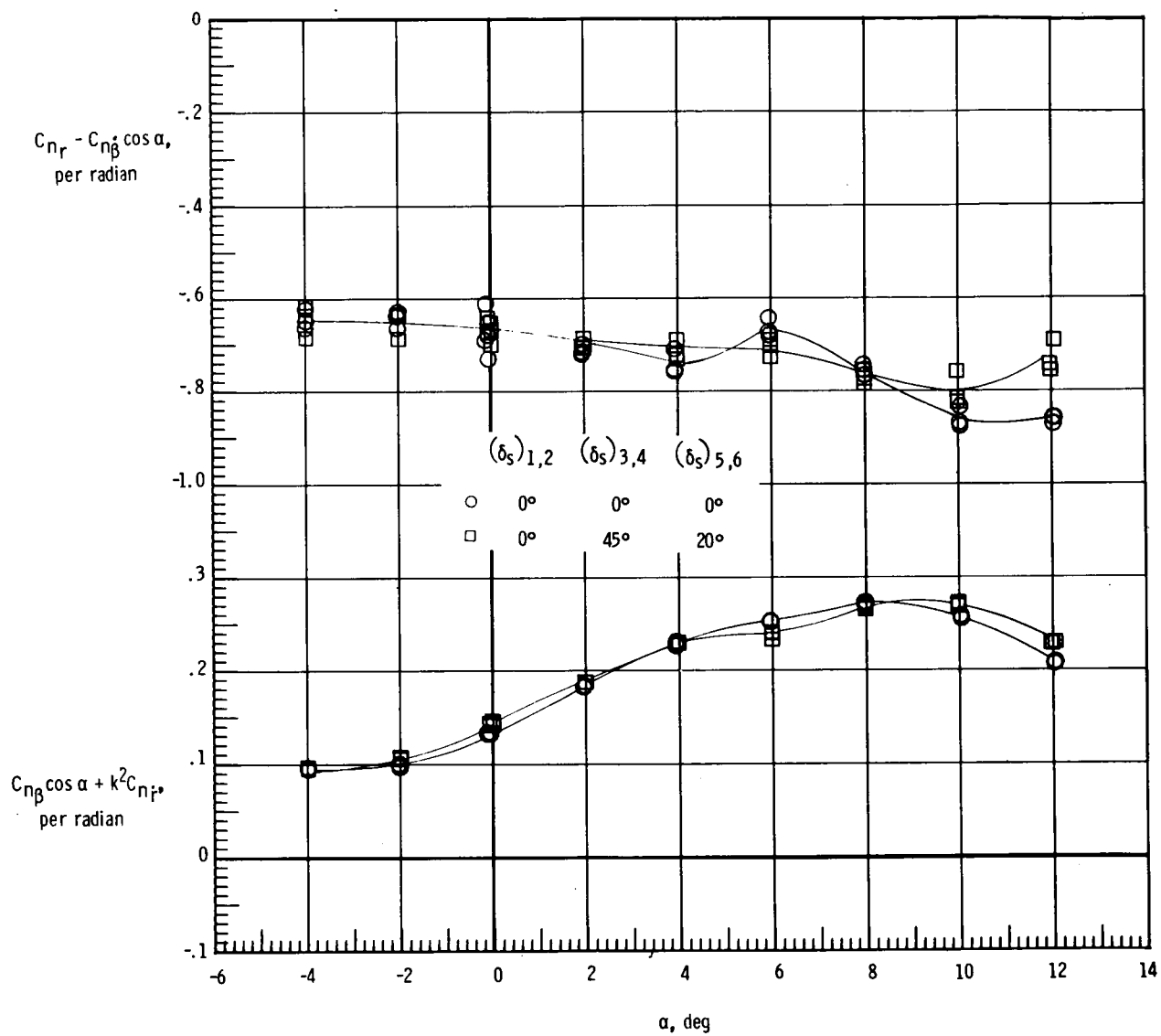
(c) M = 0.5.

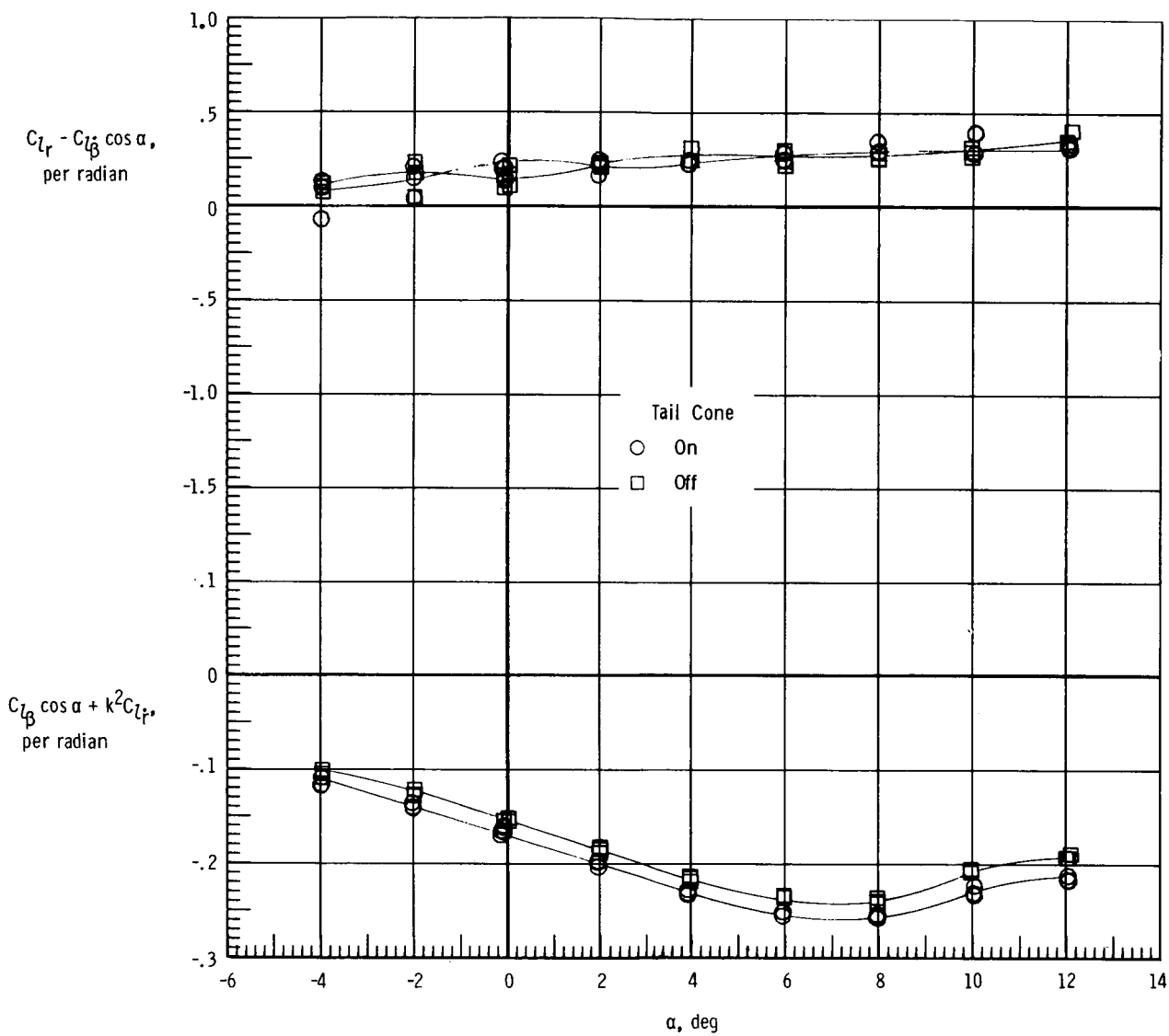Figure 20.- Concluded.

$C_{n_r} - C_{n_{\dot{\beta}}} \cos \alpha,$ per radian

$C_{n_\beta} \cos \alpha + k^2 C_{n_{\dot{r}}},$ per radian

Tail Cone

○   On

□   Off

α, deg
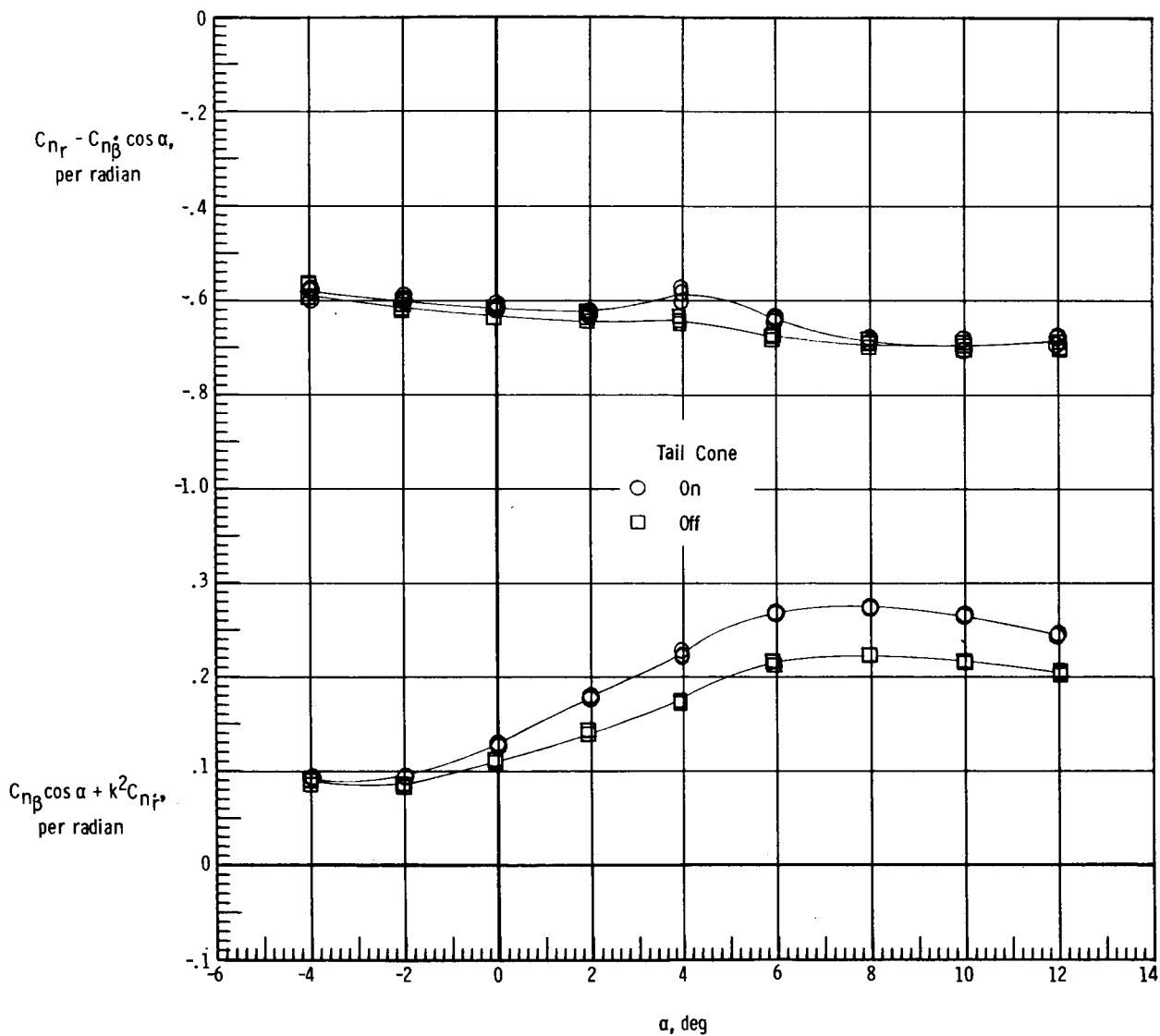
(a)   M = 0.2.

Figure 21.- Effect of tail cone on damping-in-yaw parameter and on oscillatory directional-stability parameter of ALT configuration. i_o = 6°; unfaired struts.

(b)   M = 0.4.

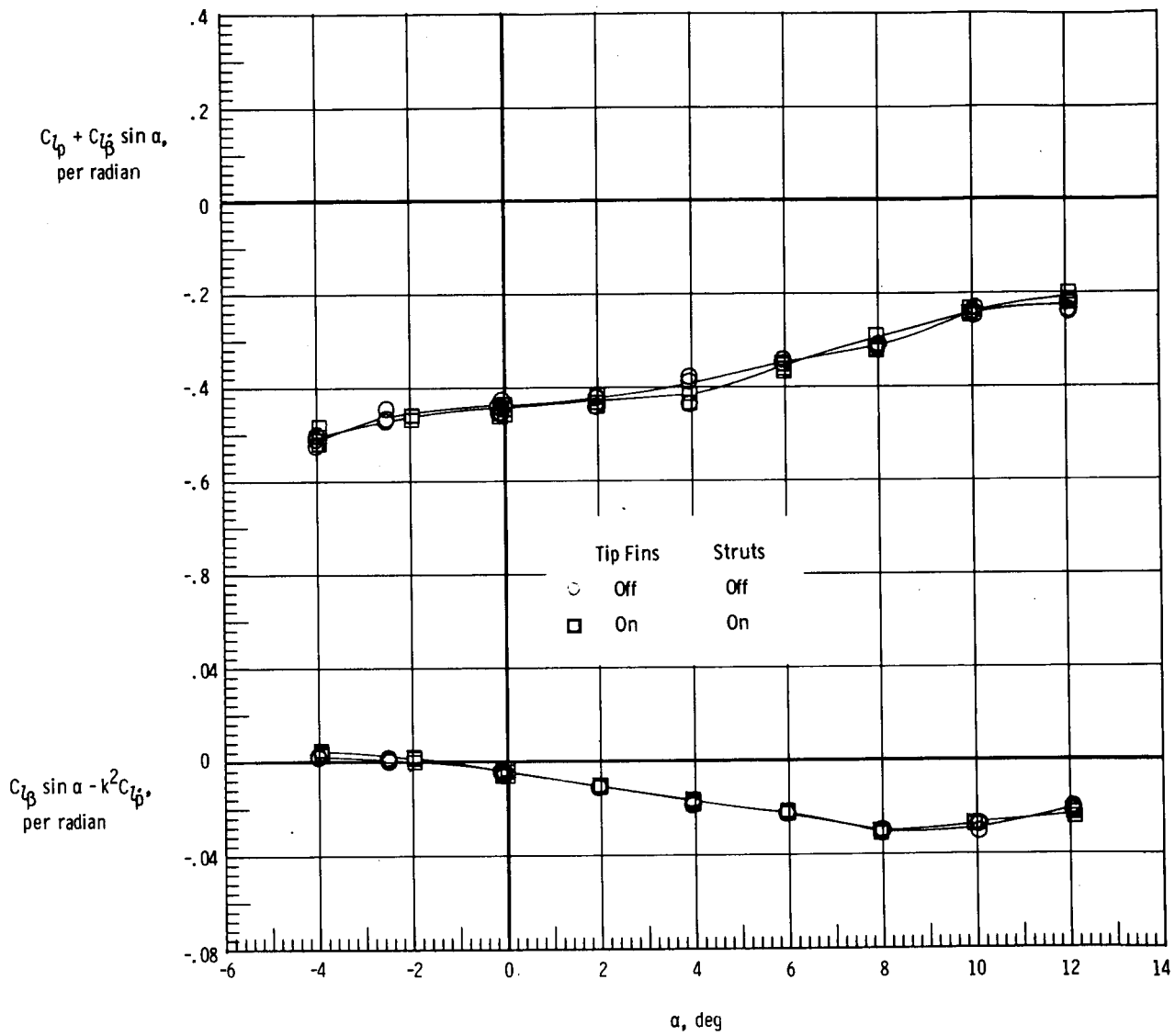Figure 21.- Continued.
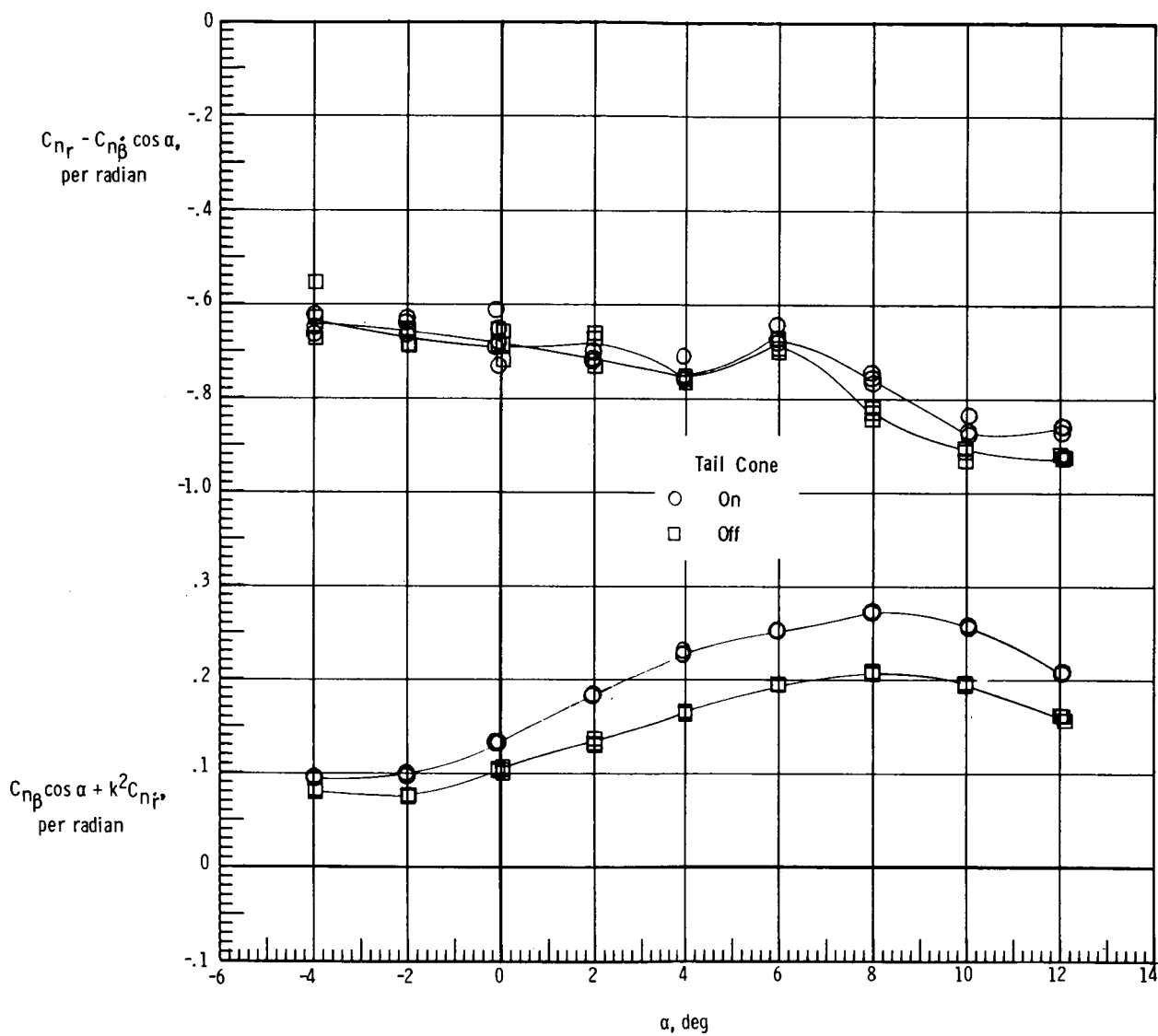
(c) M = 0.5.

Figure 21.- Concluded.
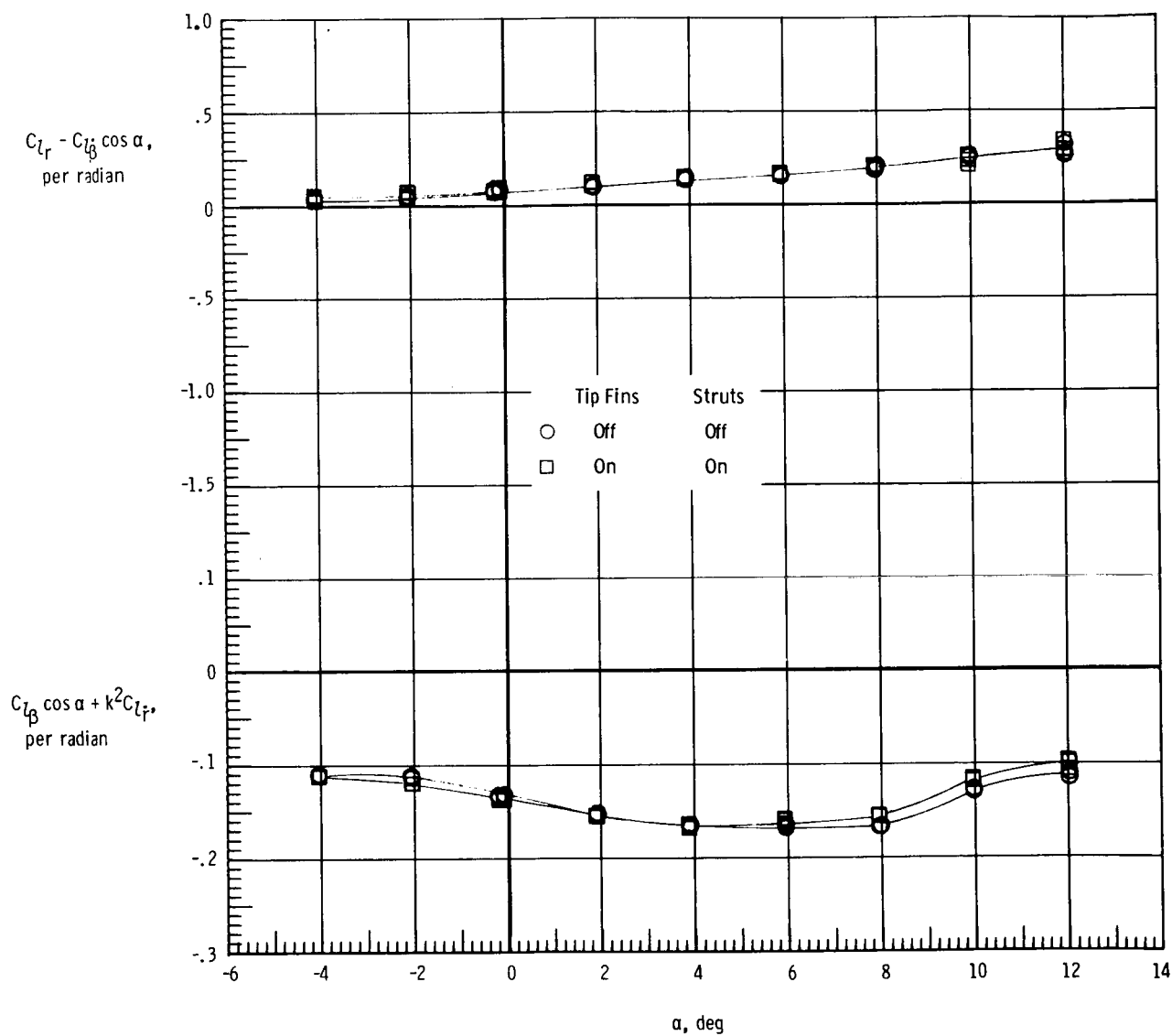
(a) M = 0.2.

Figure 22.- Effect of tip fins and struts on rolling moment due to yaw-rate parameter and on effective dihedral parameter of basic 747. Unfaired struts.
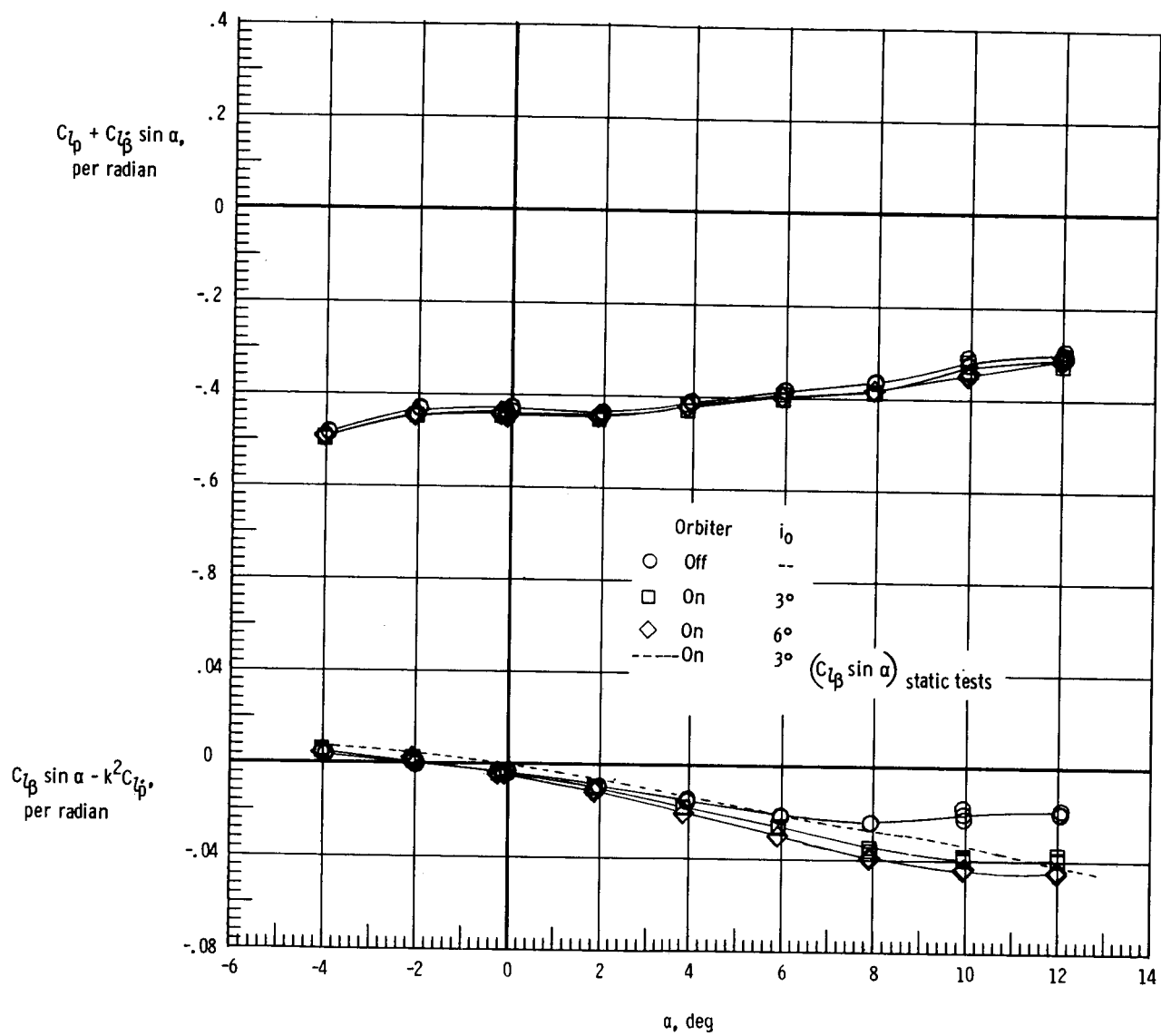
78
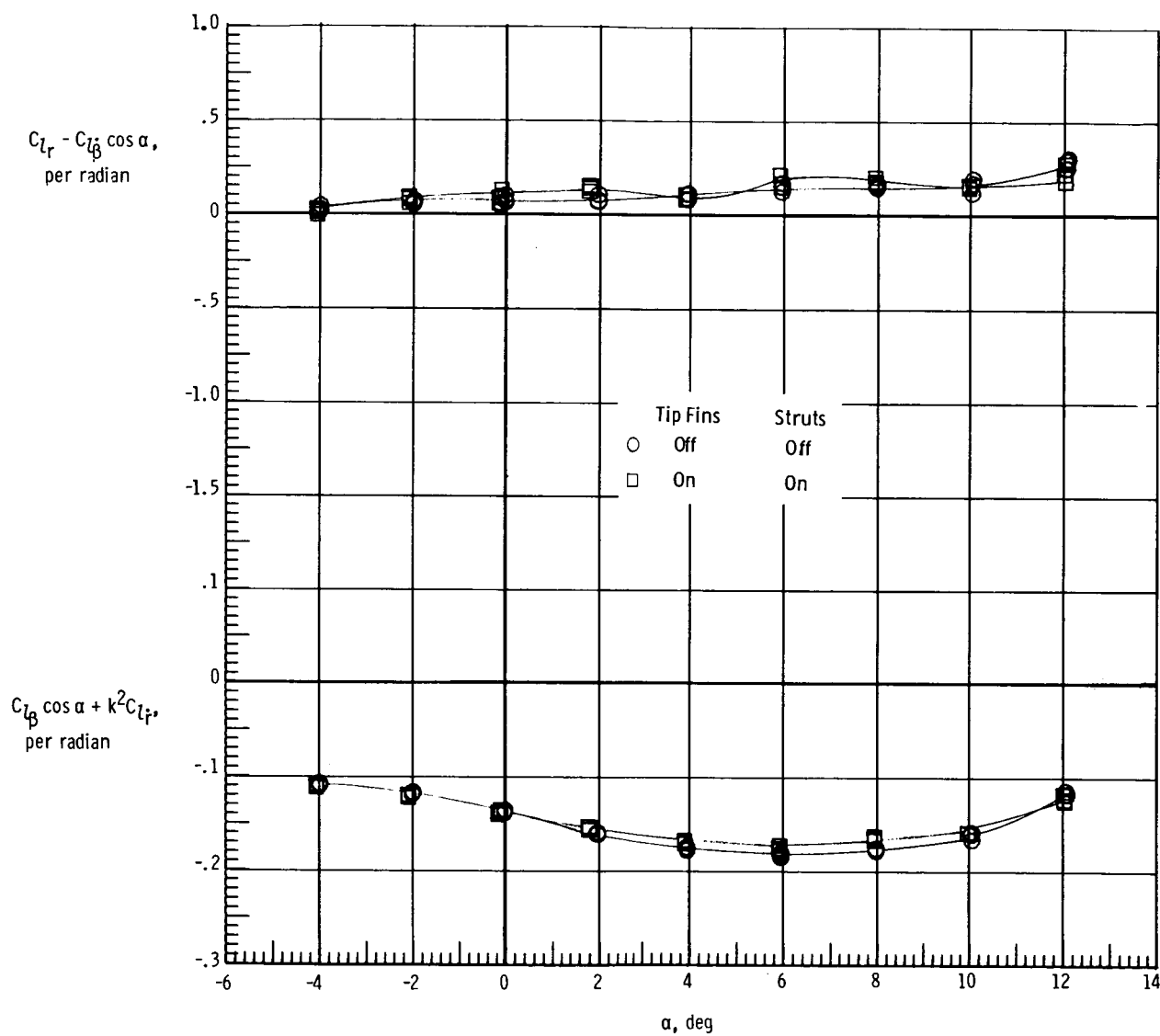
(b) M = 0.4.

Figure 22.- Continued.
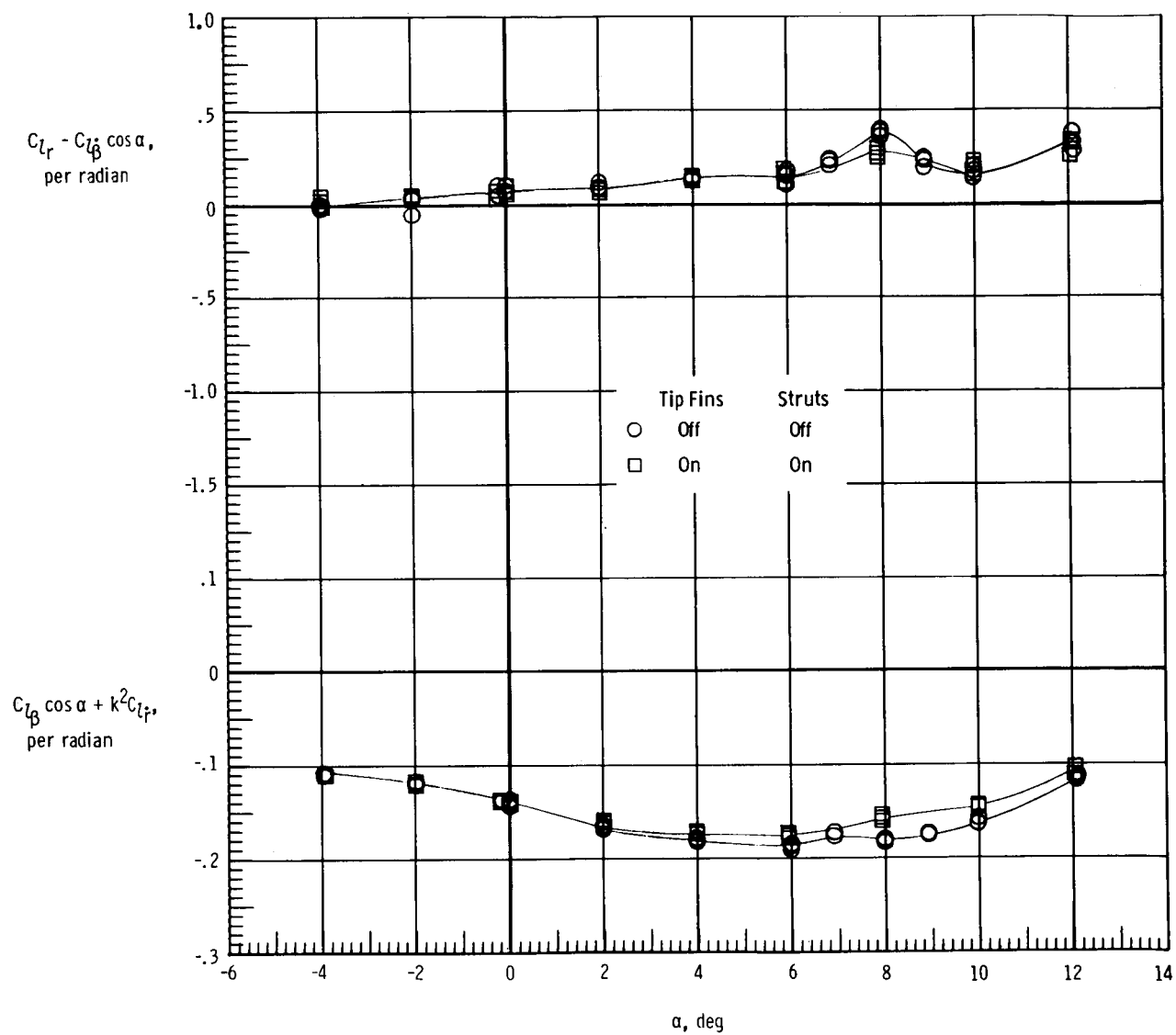
(c) M = 0.5.

Figure 22.- Concluded.
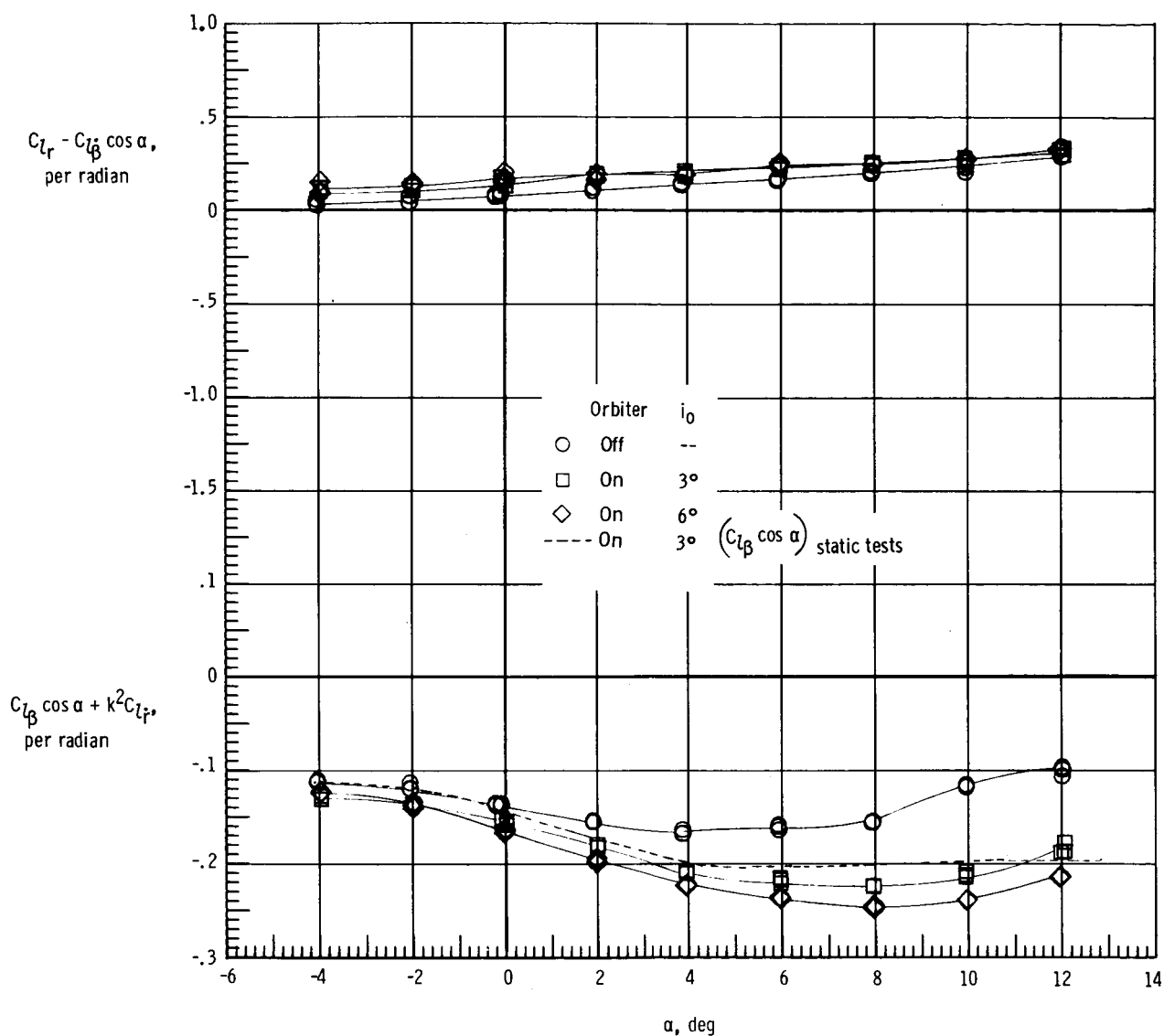
(a) M = 0.2.

Figure 23.- Effect of orbiter and orbiter incidence on rolling moment due to
yaw-rate parameter and on effective dihedral parameter of modified 747.
Unfaired struts; tail cone on.
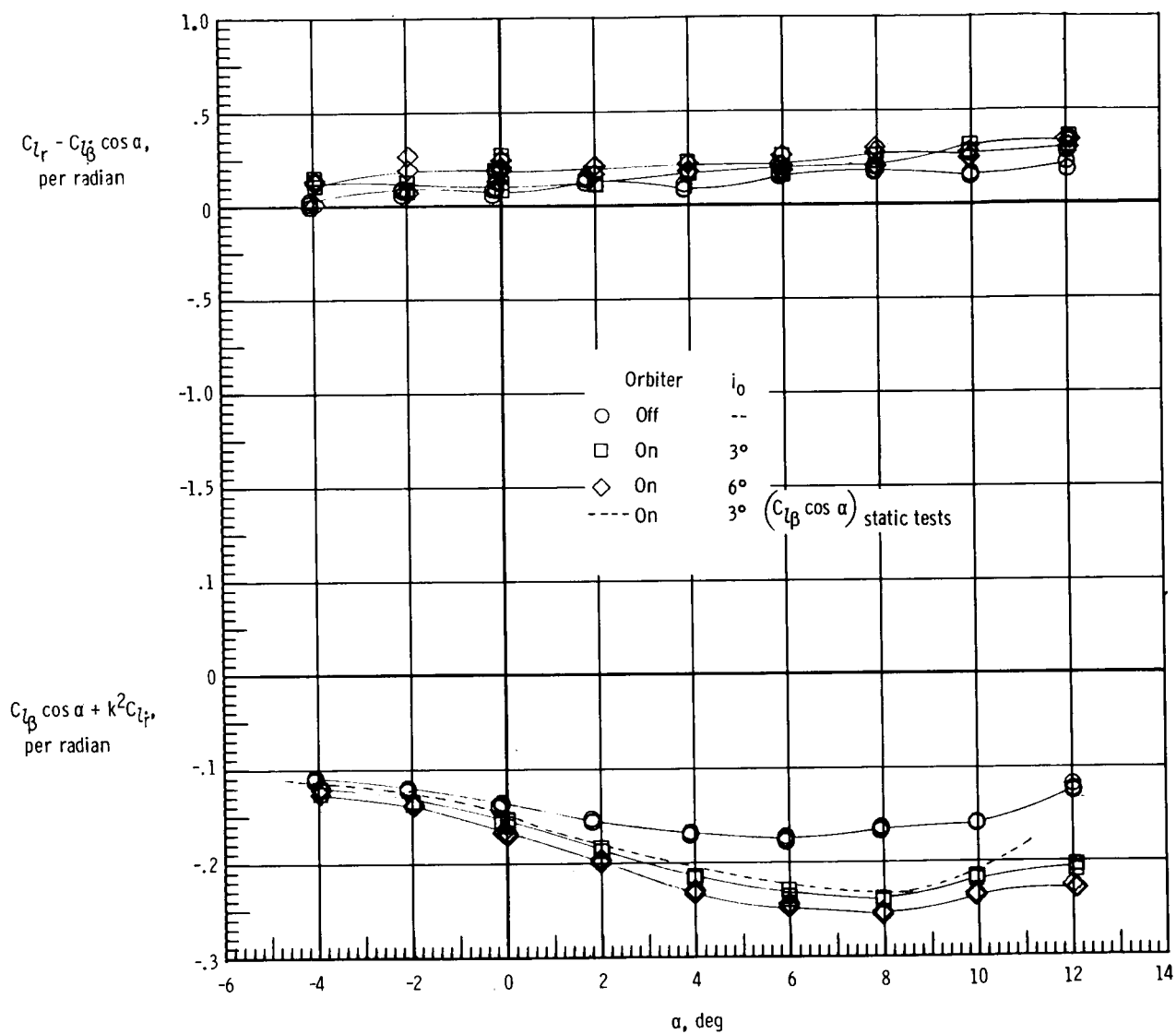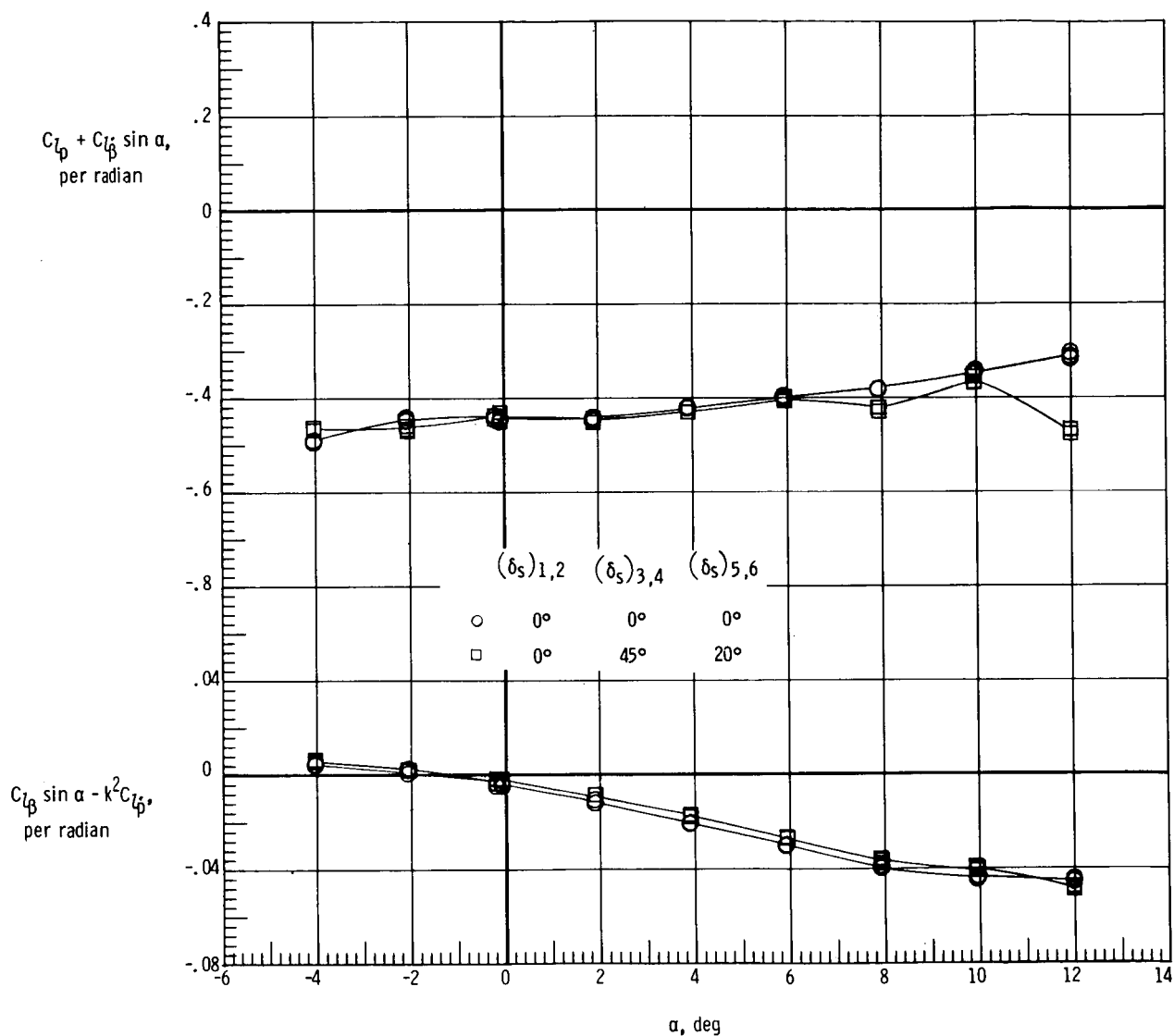
(b) M = 0.4.

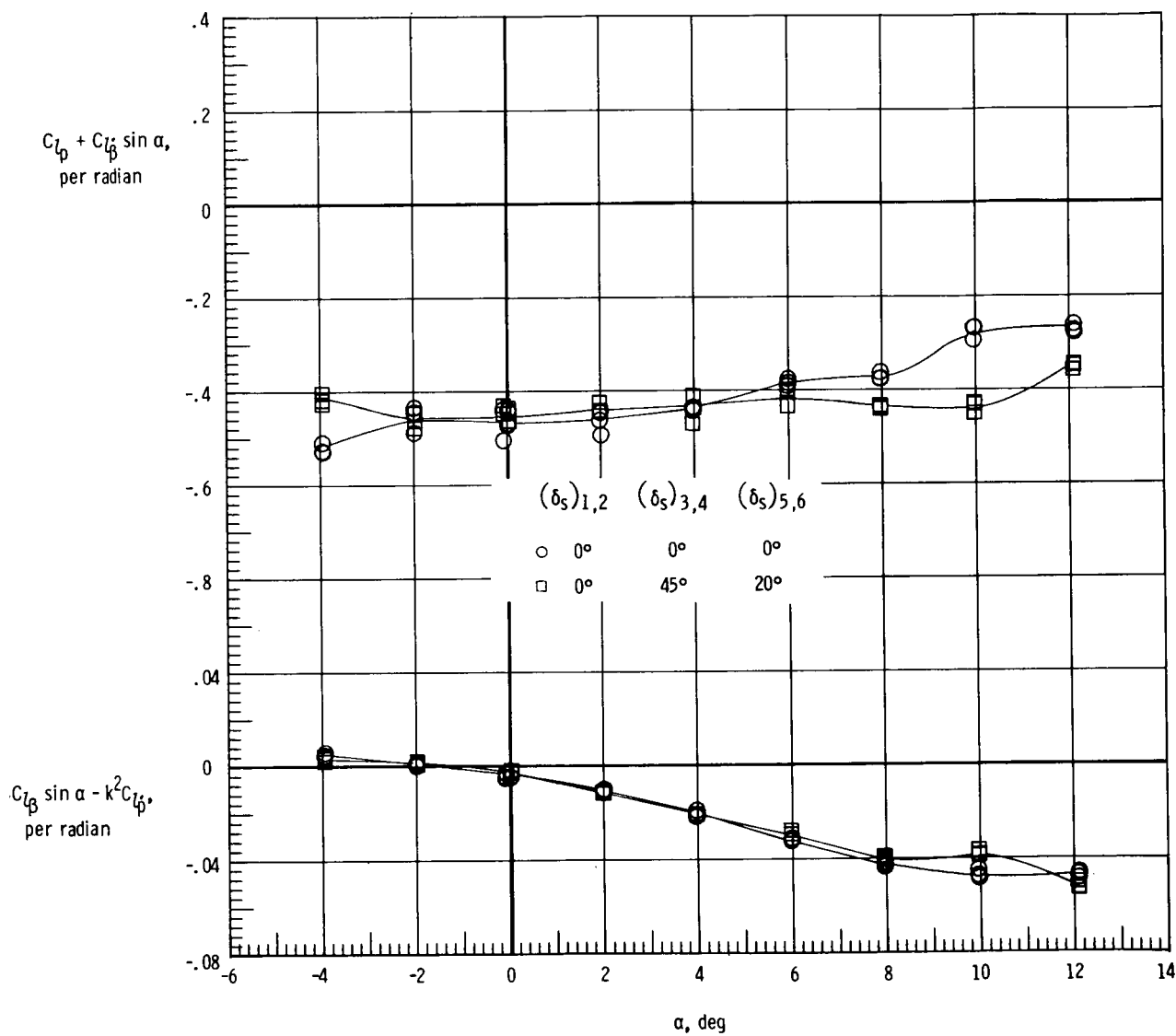Figure 23.- Continued.
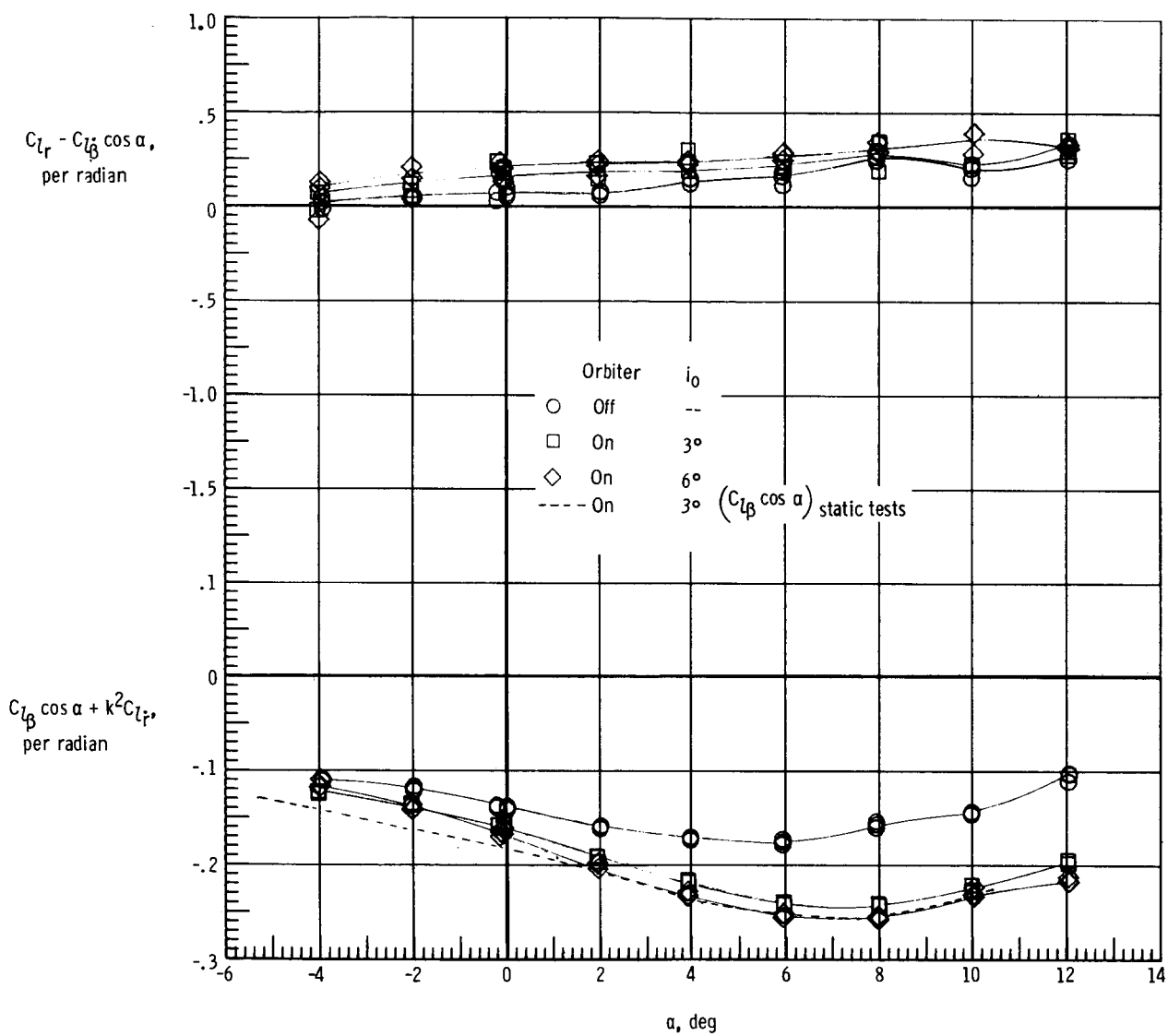
(c)   M = 0.5.

Figure 23.- Concluded.
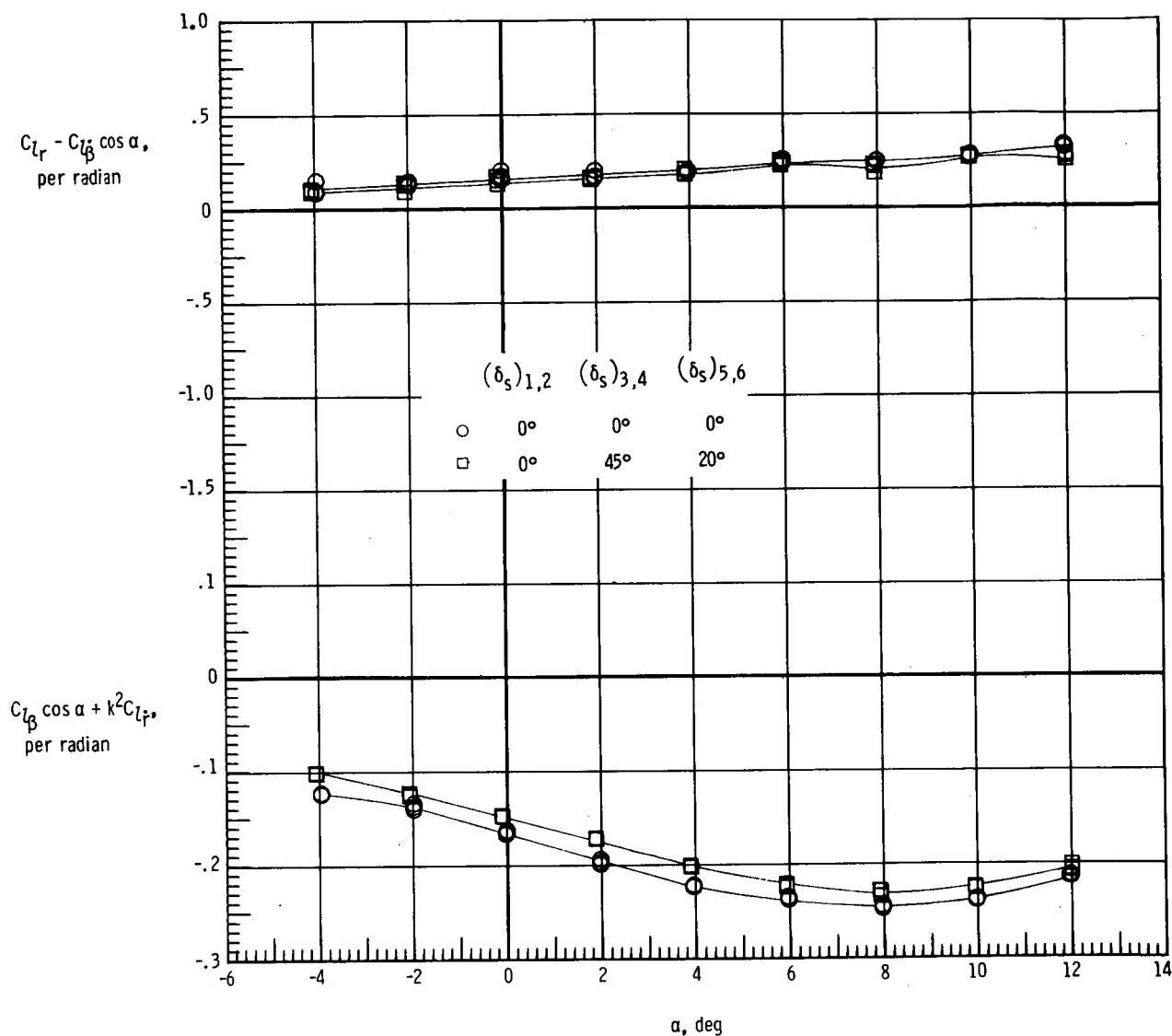
(a)   M = 0.2.

Figure 24.- Effect of spoiler deployment on rolling moment due to yaw-rate parameter and on effective dihedral parameter of ALT configuration. $i_O = 6^O$; unfaired struts; tail cone on.

(b) M = 0.4.

Figure 24.- Continued.
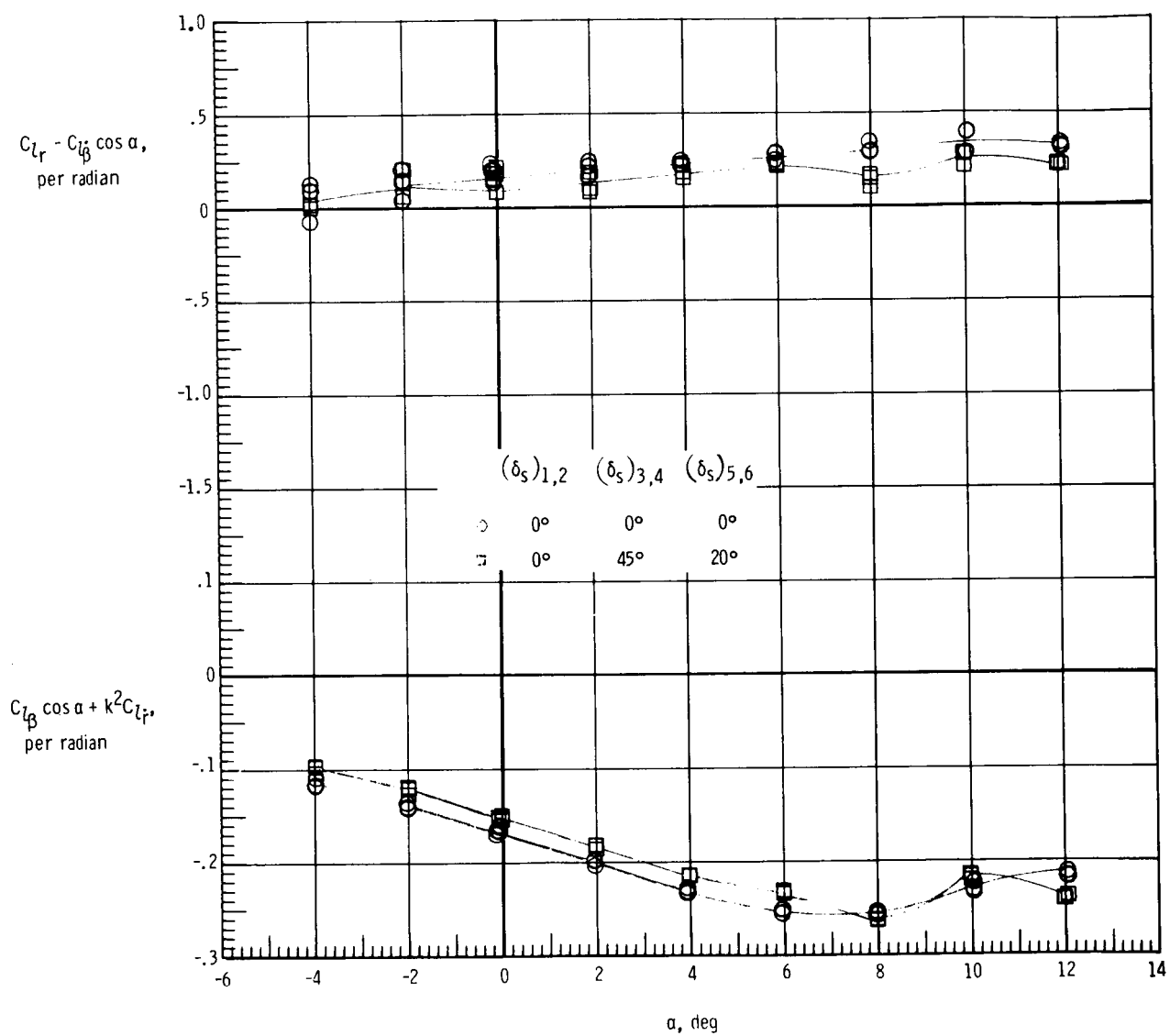
(c) M = 0.5.

Figure 24.- Concluded.
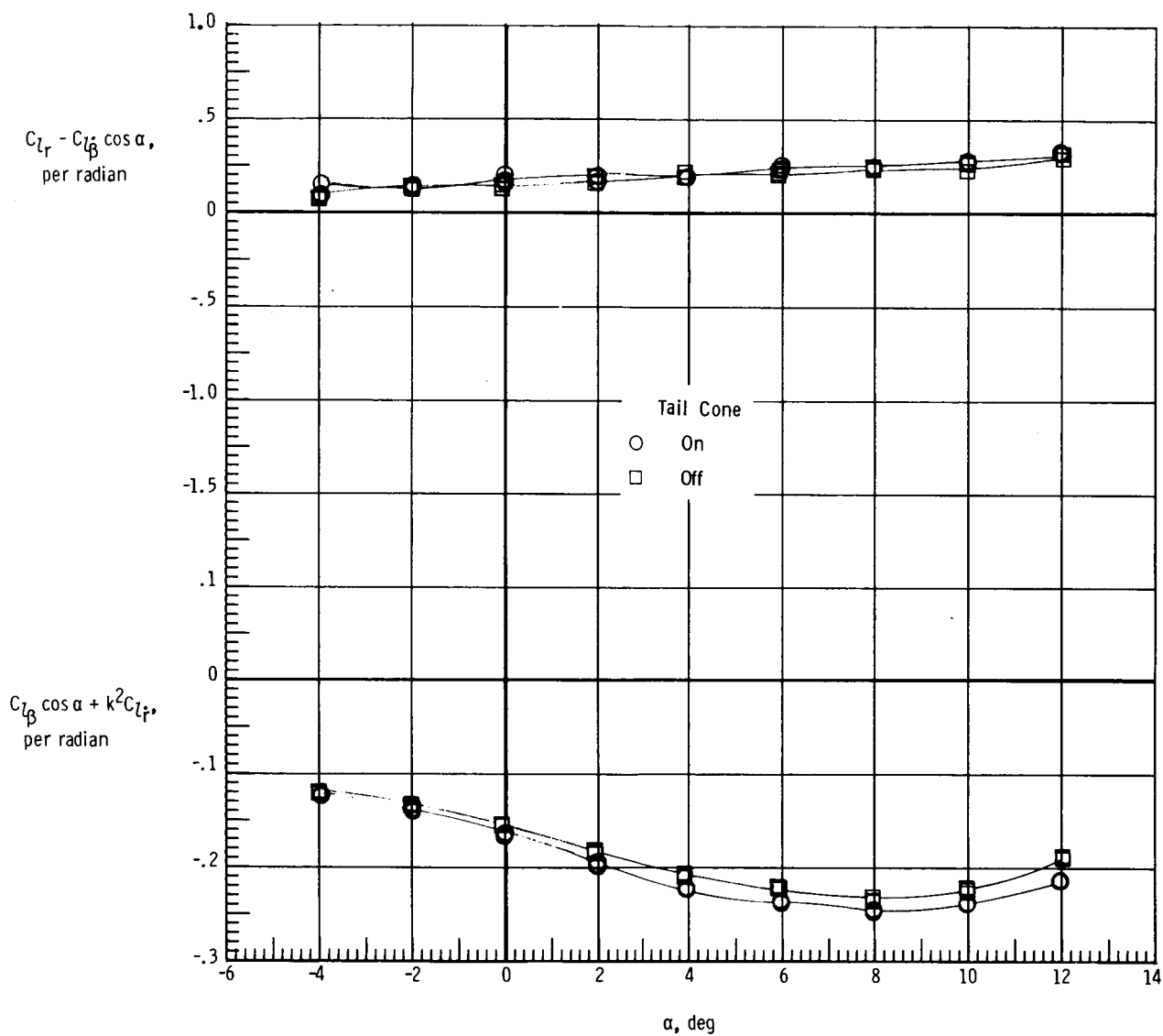
(a)   M = 0.2.

Figure 25.- Effect of tail cone on rolling moment due to yaw-rate parameter and effective dihedral parameter of ALT configuration. $i_0 = 6^0$; unfaired struts.
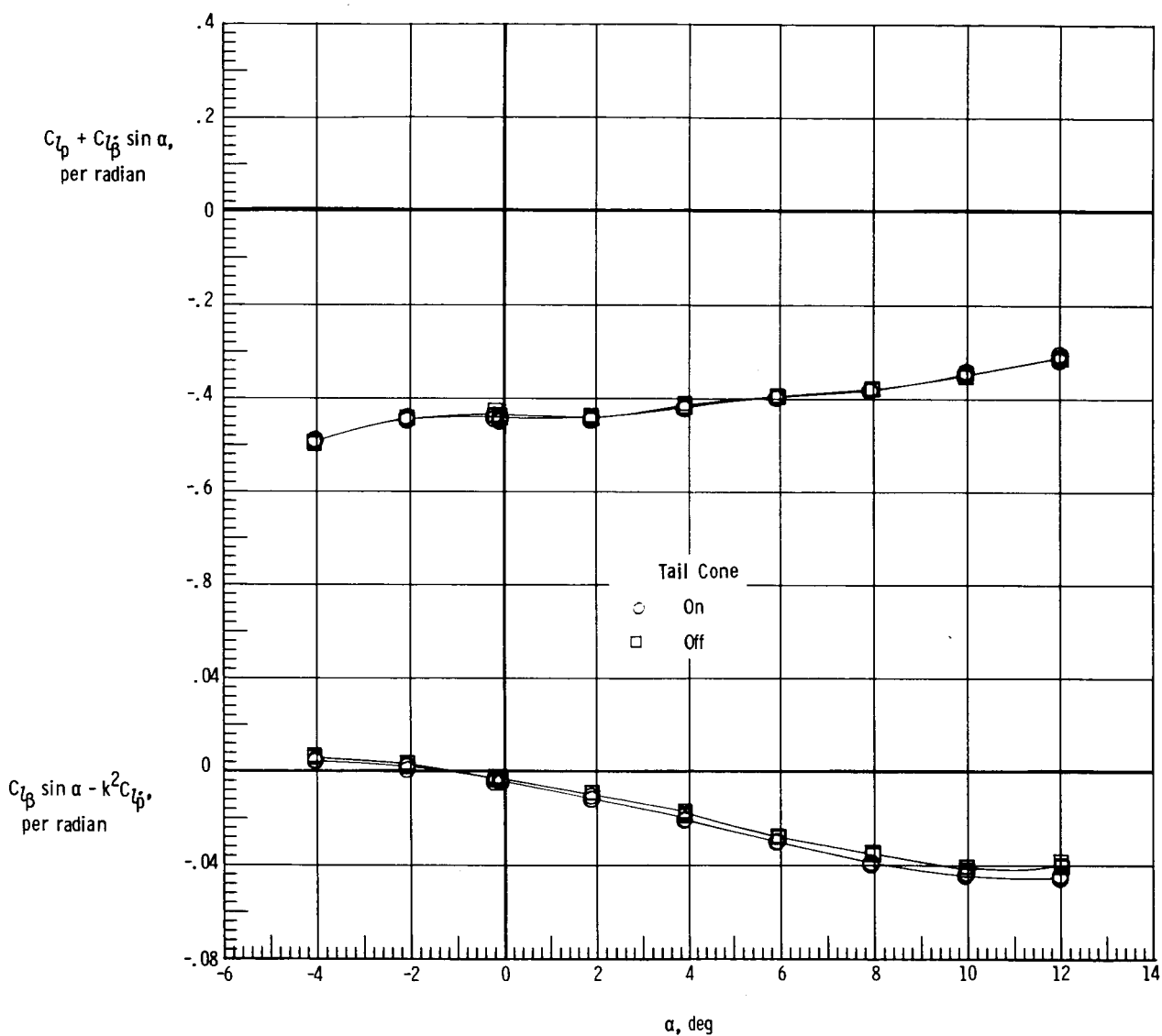
(b)   M = 0.4.
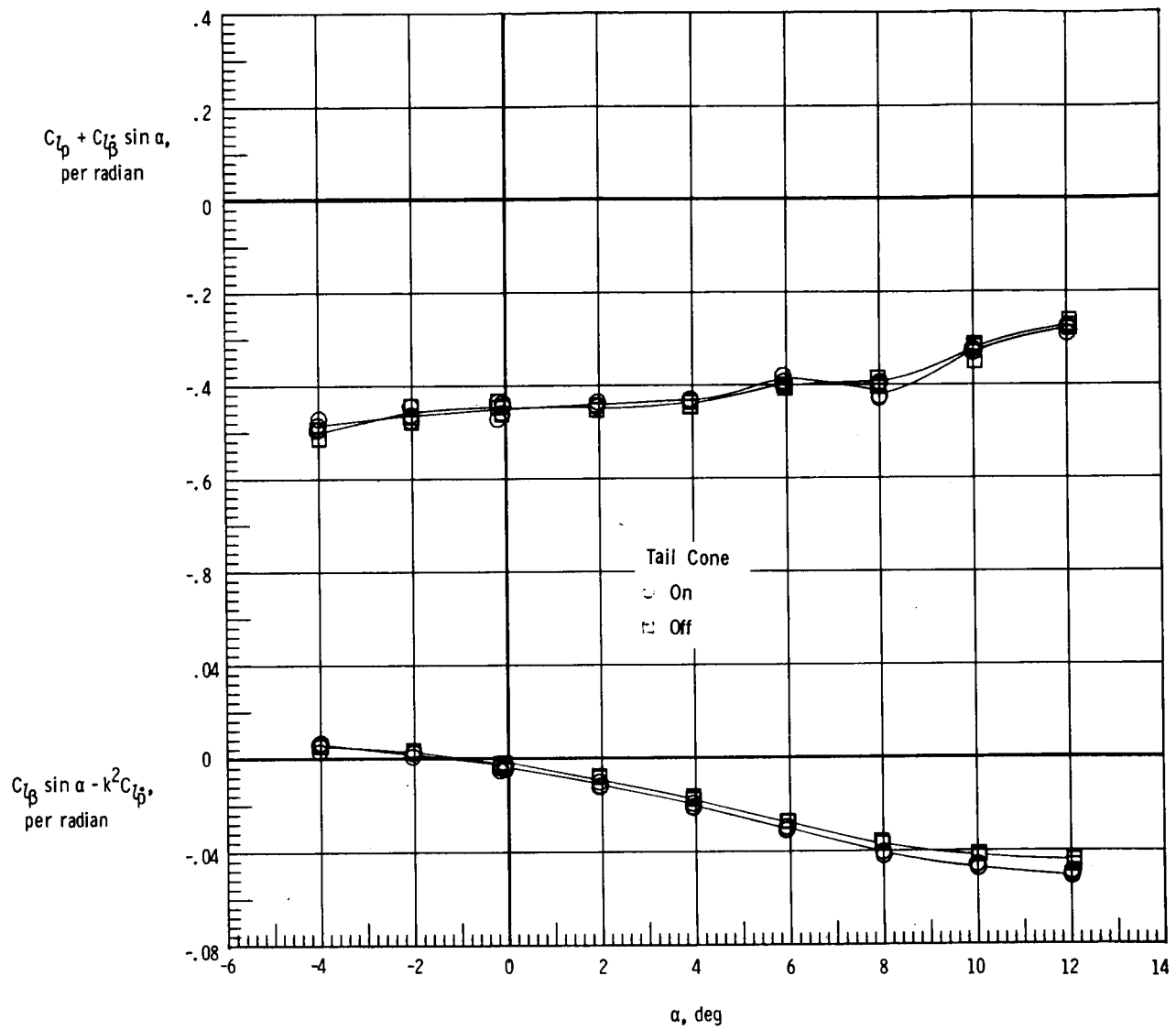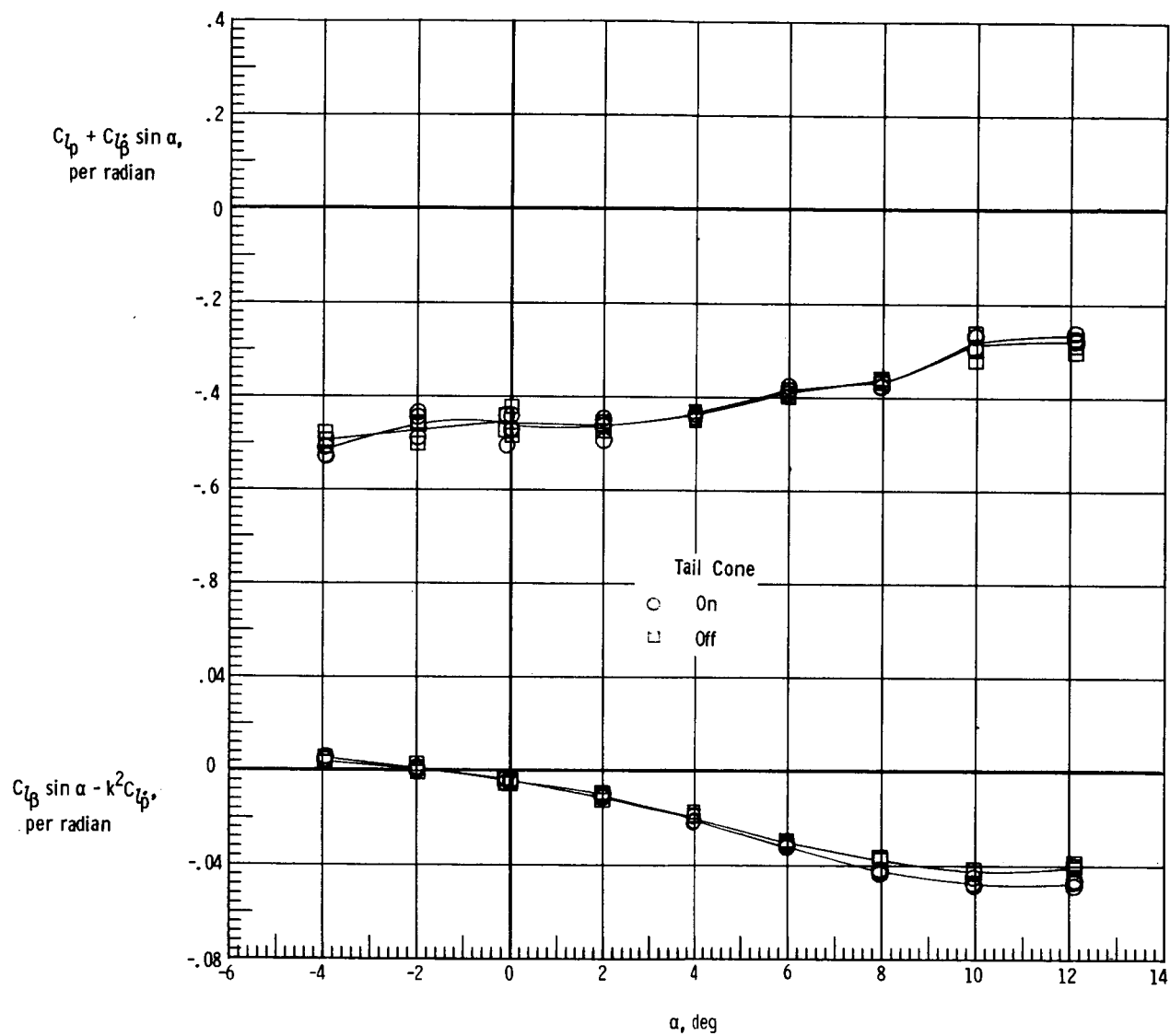
Figure 25.- Continued.

(c) M = 0.5.

Figure 25.- Concluded.
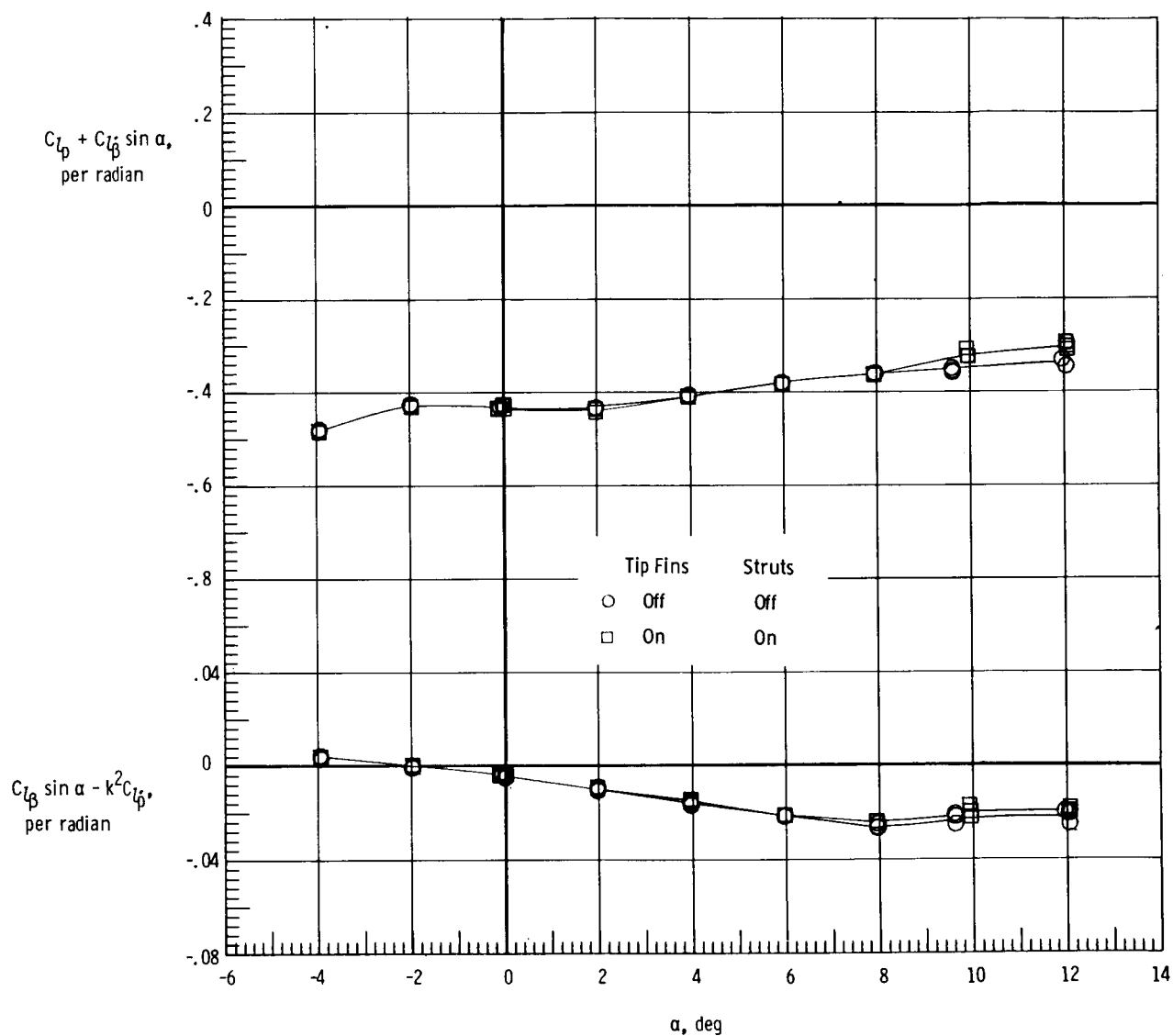
(a) M = 0.2.

Figure 26.- Effect of tip fins and struts on damping-in-roll parameter and on rolling moment due to roll-displacement parameter of basic 747. Unfaired struts.
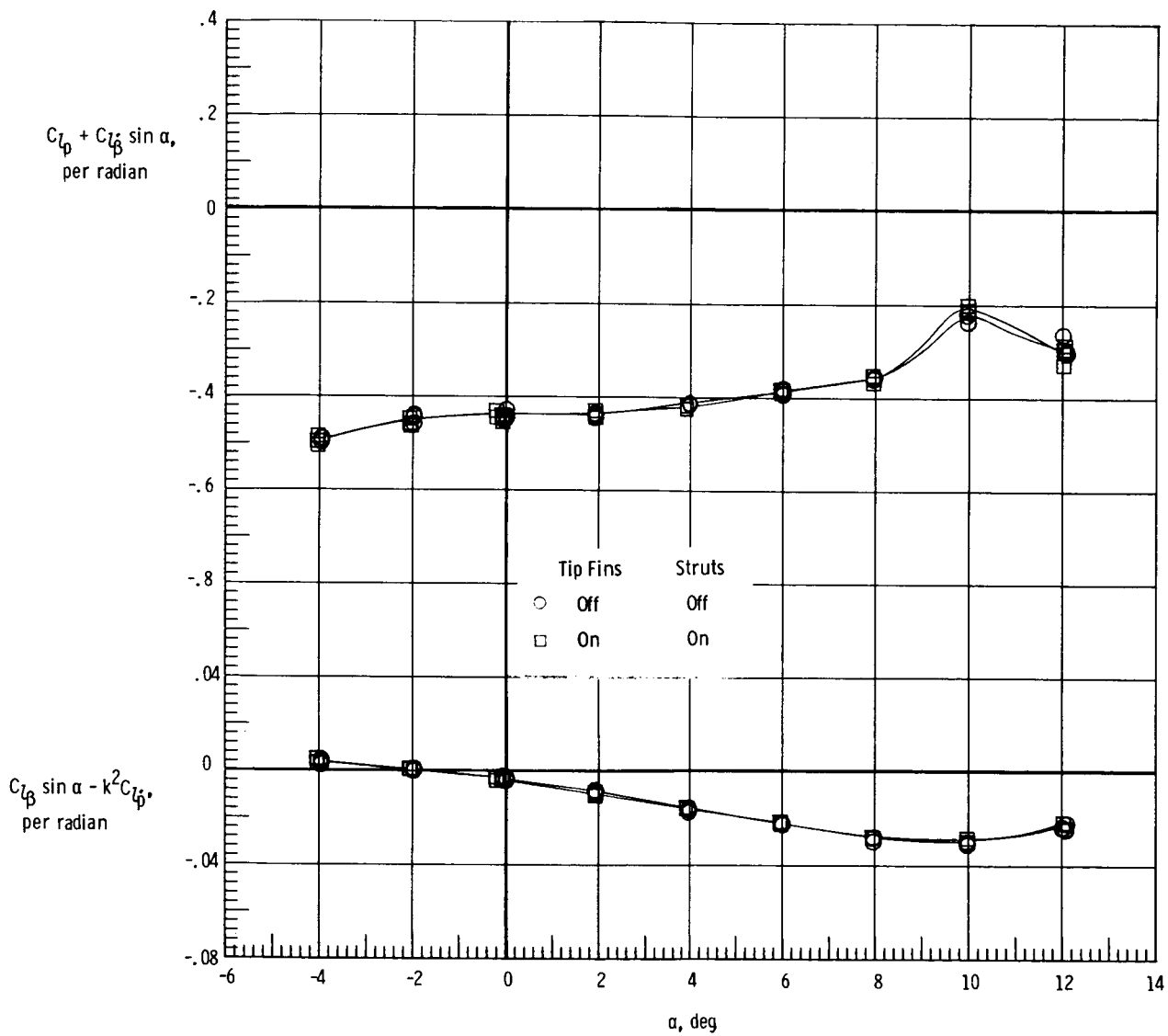
(b)   M = 0.4.

Figure 26.- Continued.

(c)   M = 0.5.

Figure 26.- Concluded.

(a) M = 0.2.

Figure 27.- Effect of orbiter and orbiter incidence on damping-in-roll parameter
and on rolling moment due to roll-displacement parameter of modified 747.
Unfaired struts; tail cone on.
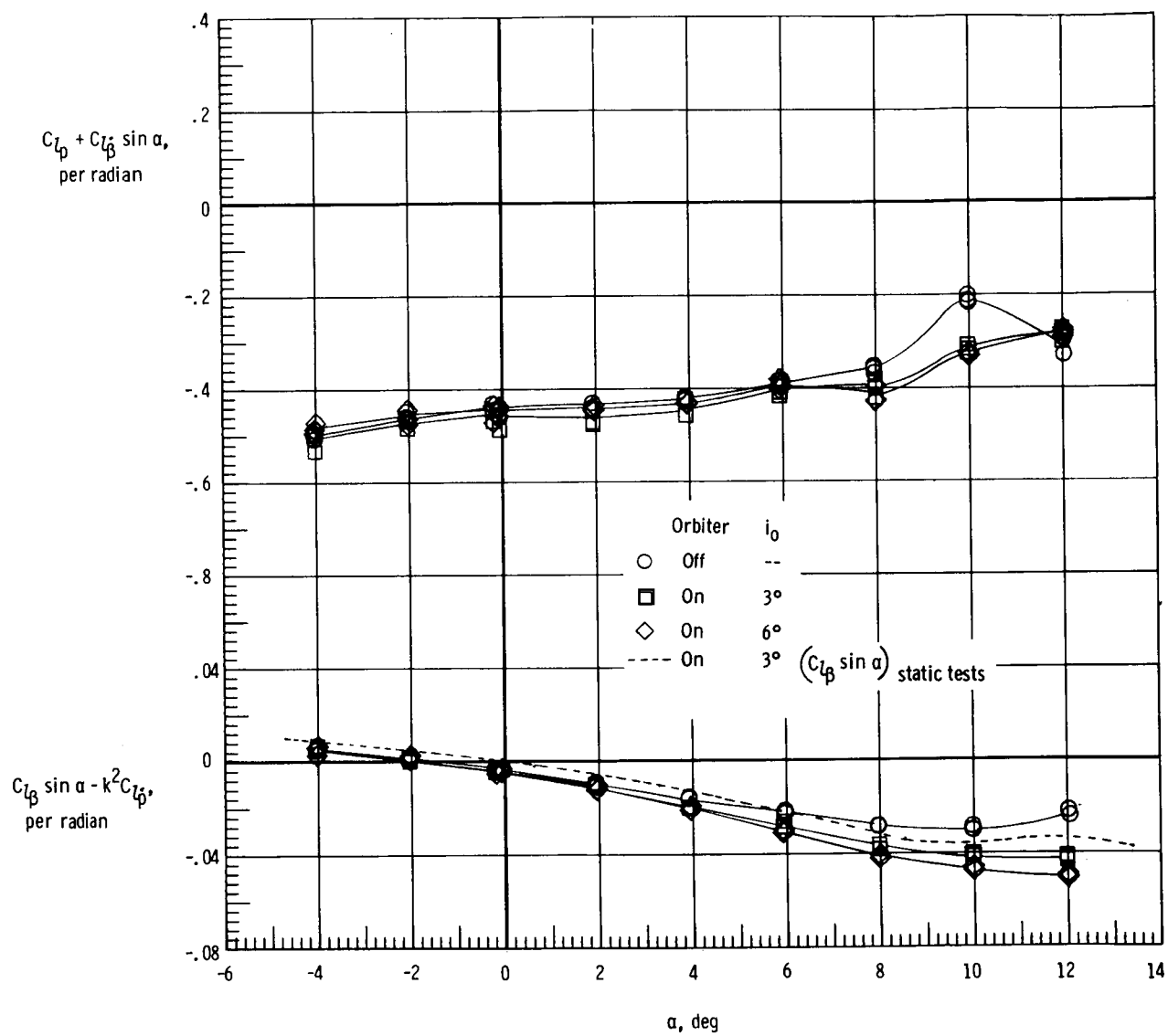
(b) M = 0.4.

Figure 27.- Continued.
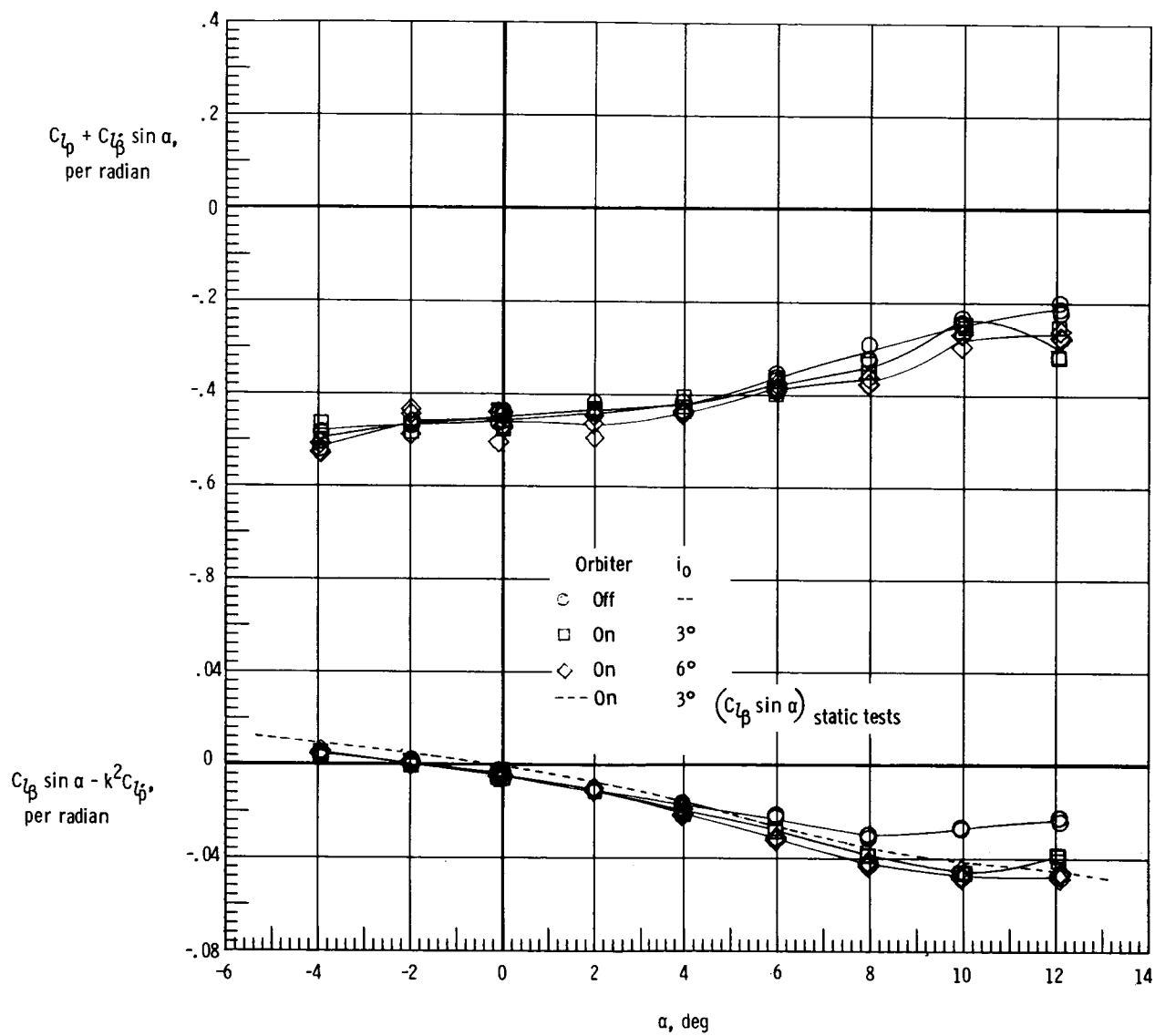
(c)   M = 0.5.

Figure 27.- Concluded.

(a) M = 0.2.

Figure 28.- Effect of spoiler deployment on damping-in-roll parameter and on rolling moment due to roll-displacement parameter of ALT configuration. $i_0 = 6°$; unfaired struts; tail cone on.
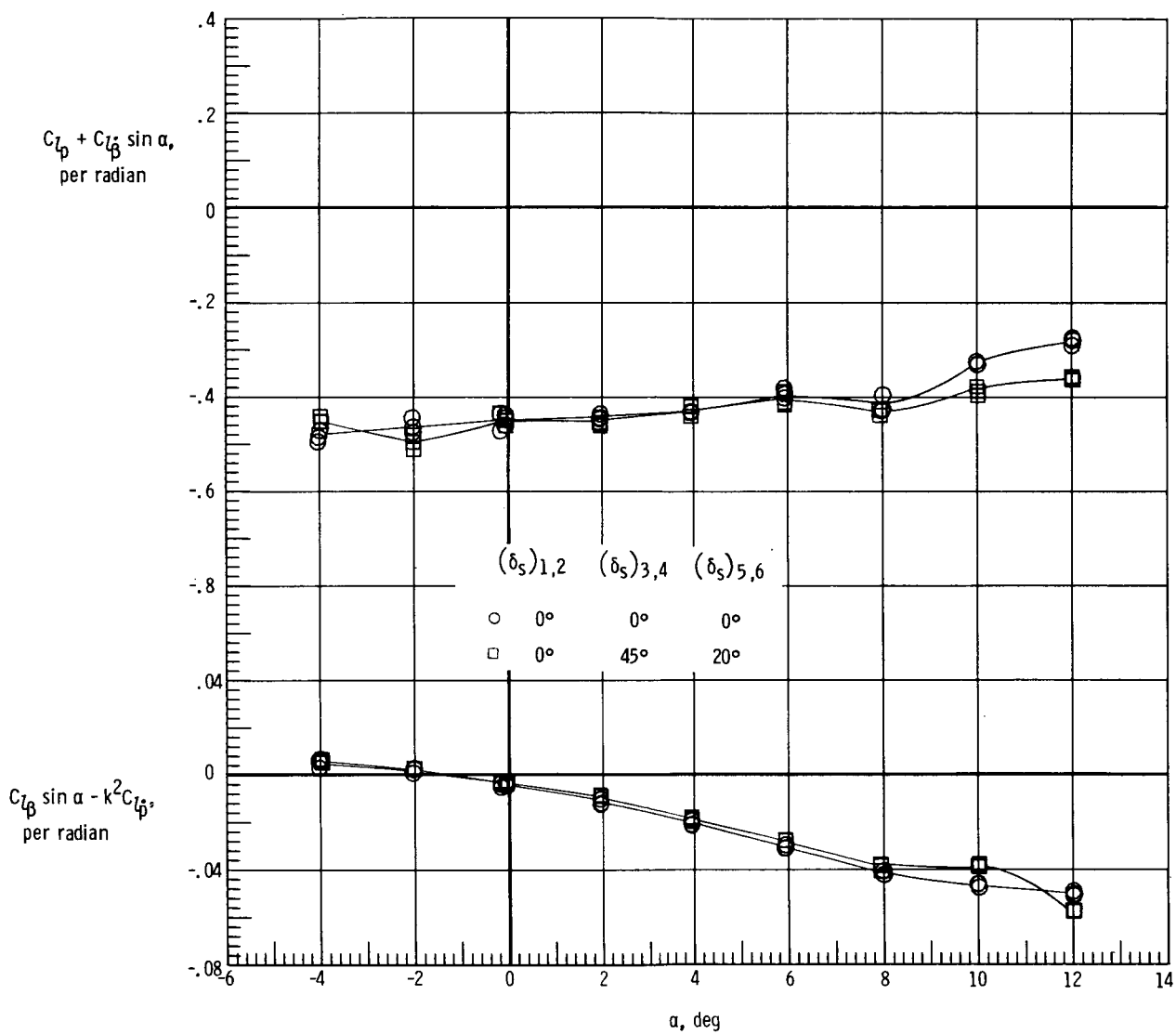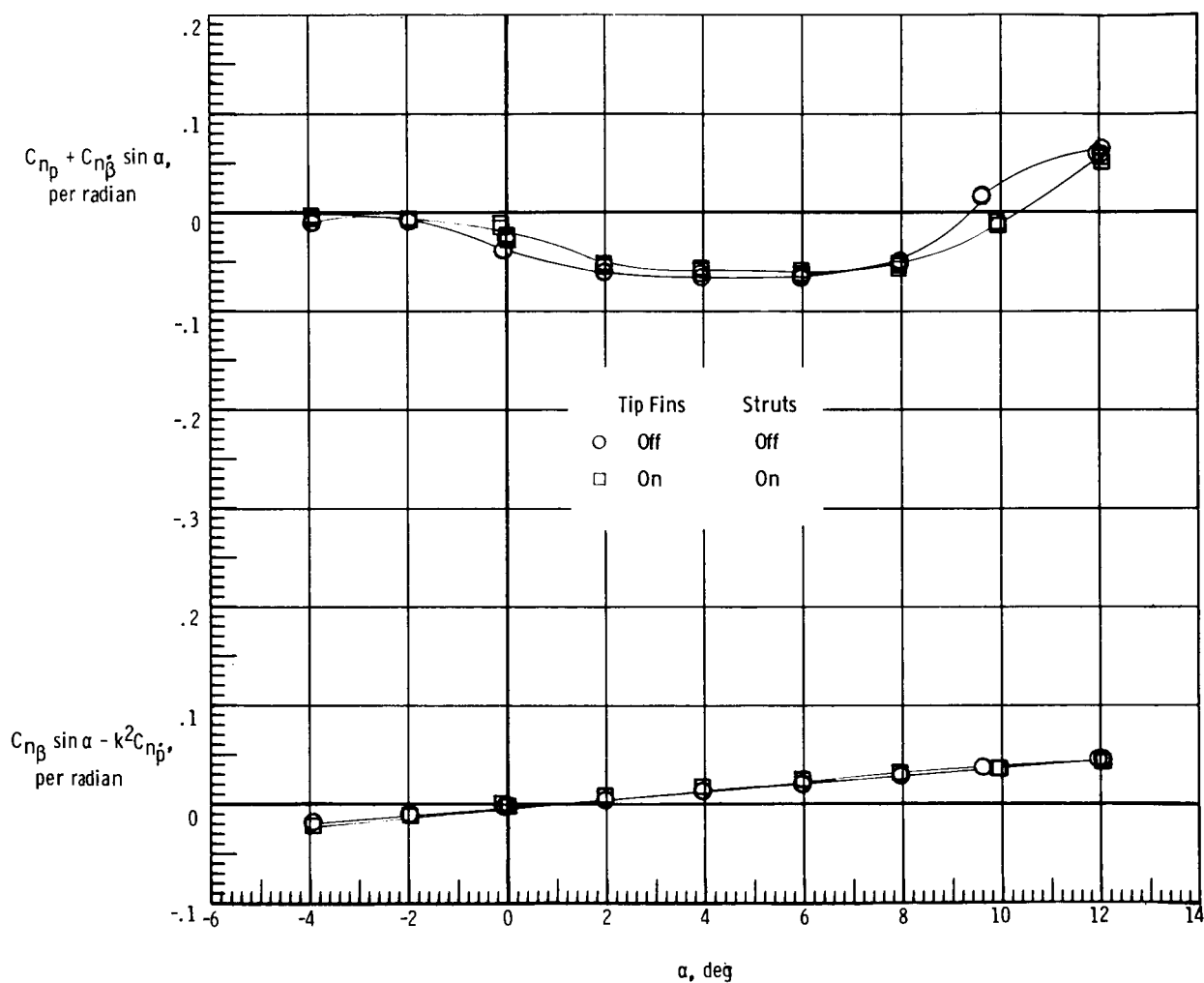
(b) M = 0.4.

Figure 28.- Continued.

(c)   M = 0.5.

Figure 28.- Concluded.

(a) M = 0.2.

Figure 29.- Effect of tail cone on damping-in-roll parameter and on rolling
moment due to roll-displacement parameter of ALT configuration. $i_0 = 6^o$;
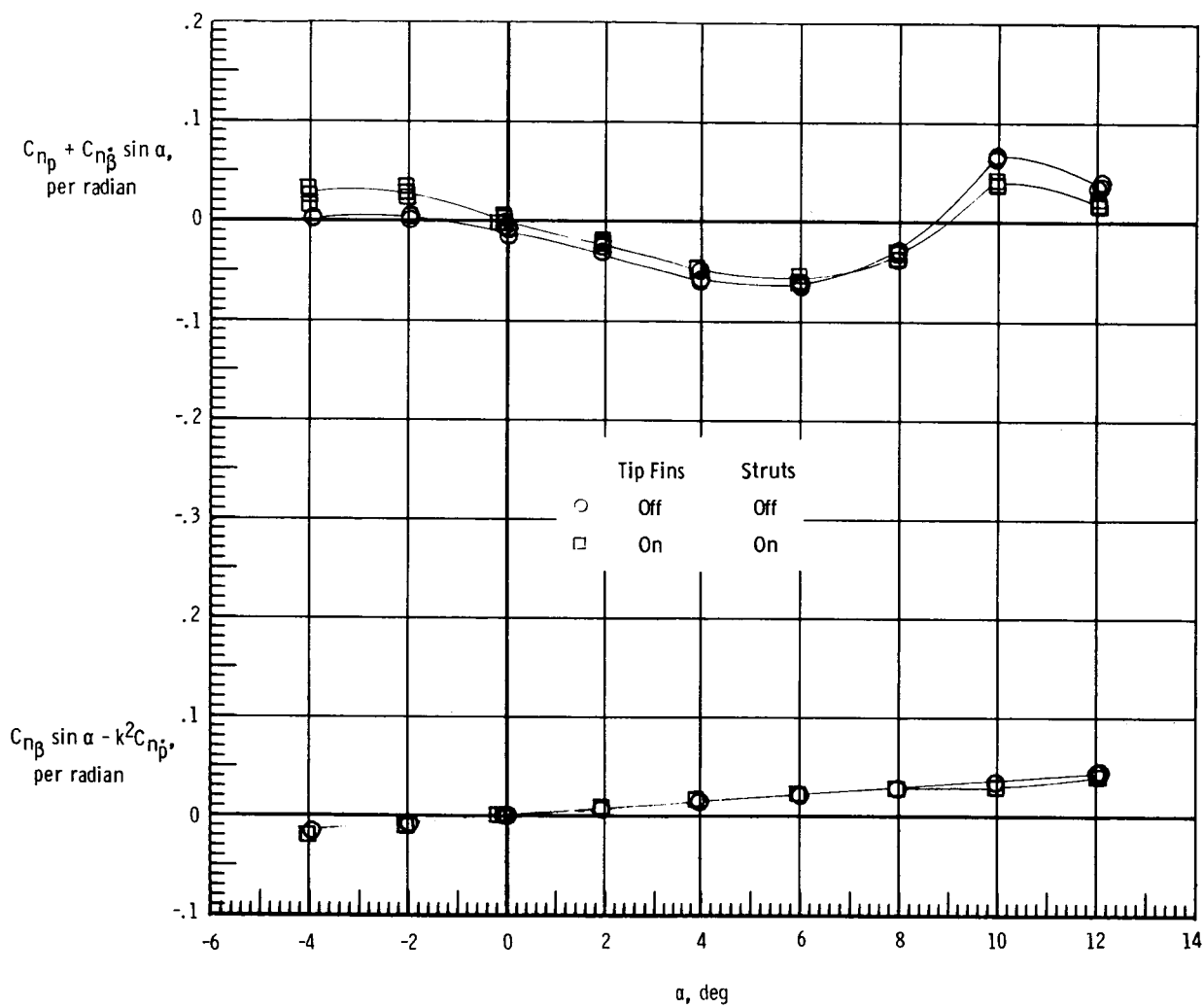unfaired struts.

(b) M = 0.4.

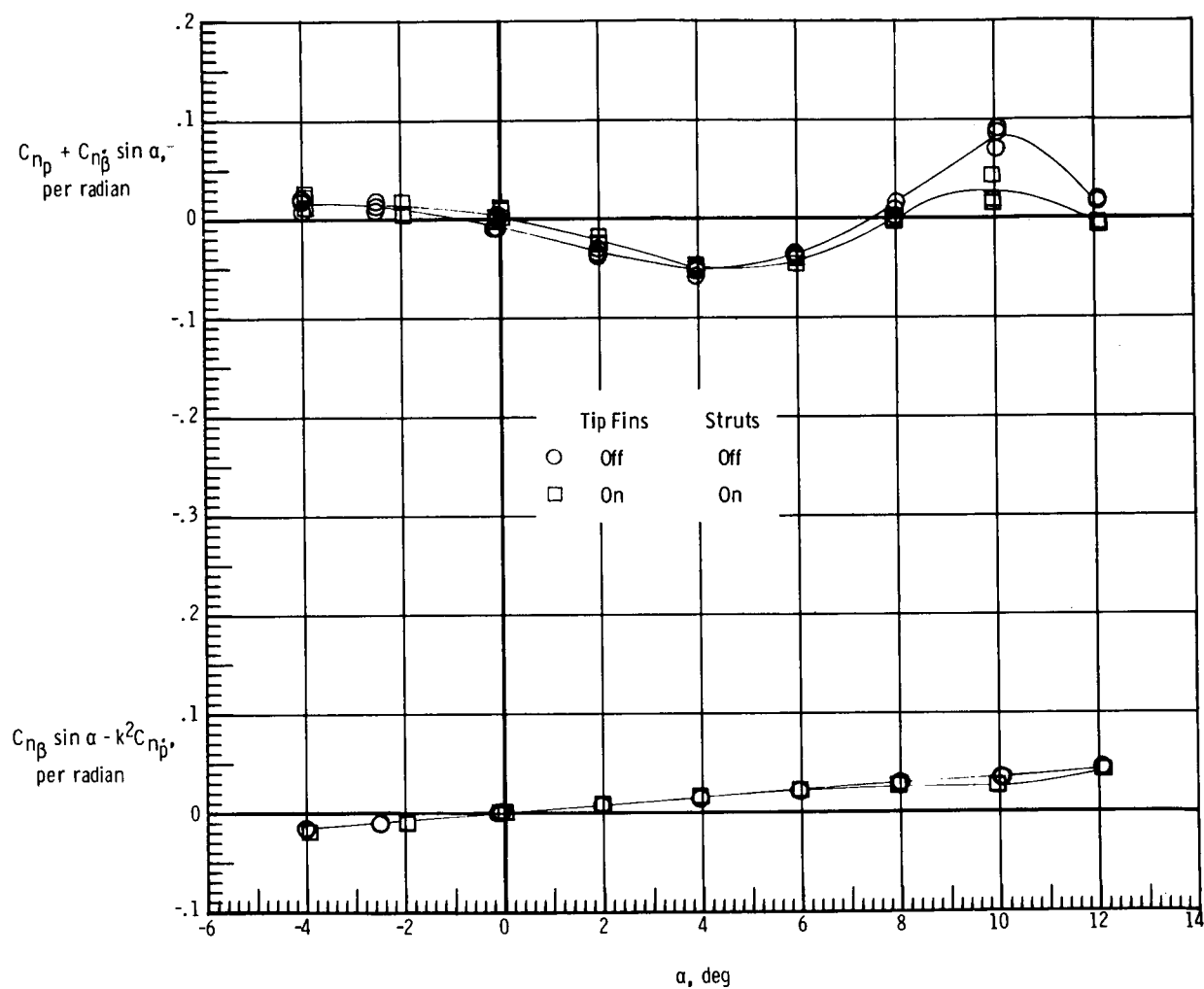Figure 29.- Continued.

(c) M = 0.5.

Figure 29.- Concluded.

(a) M = 0.2.

Figure 30.- Effect of tip fins and struts on yawing moment due to roll-rate
    parameter and on yawing moment due to roll-displacement parameter of
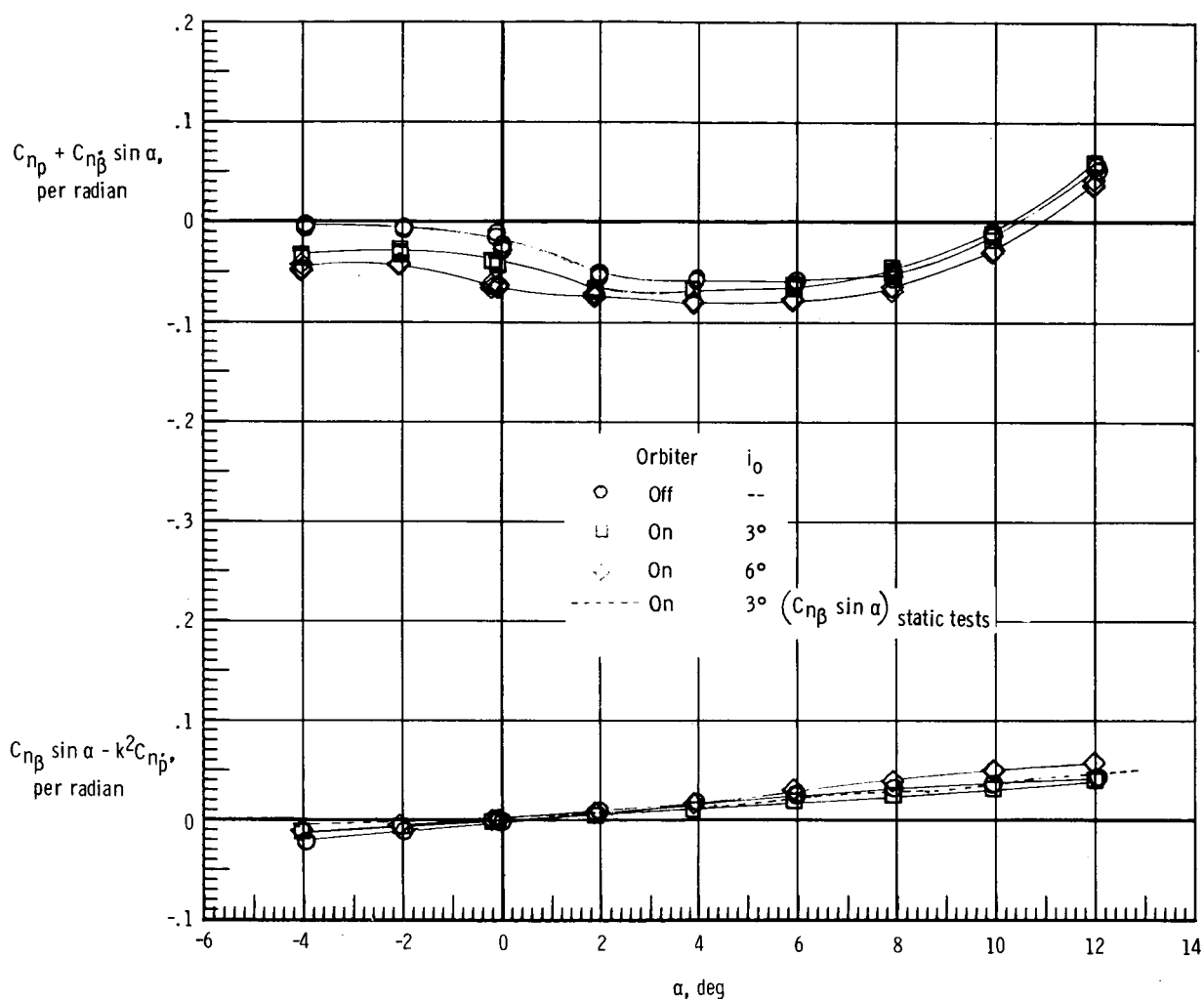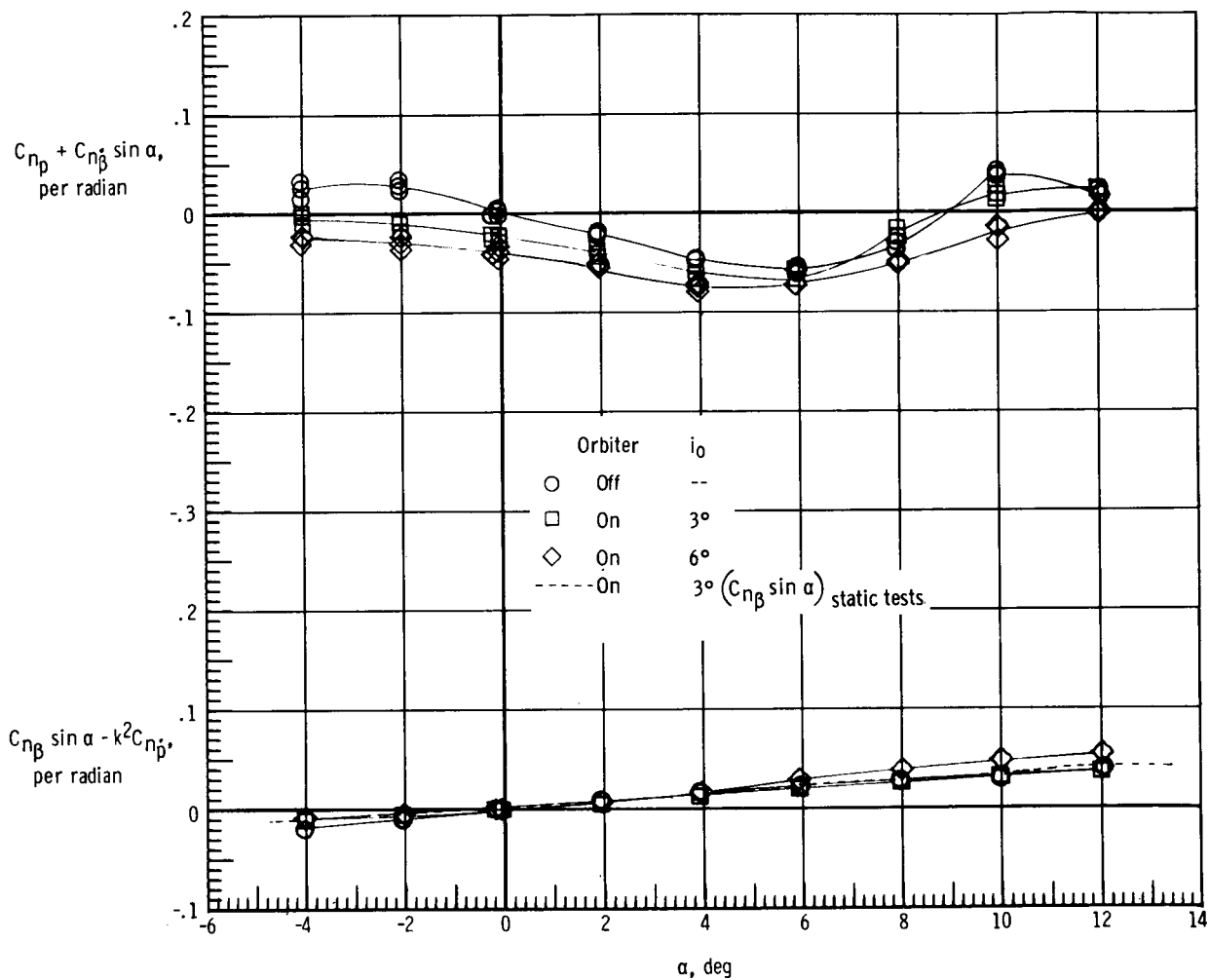   basic 747. Unfaired struts.

(b) M = 0.4.

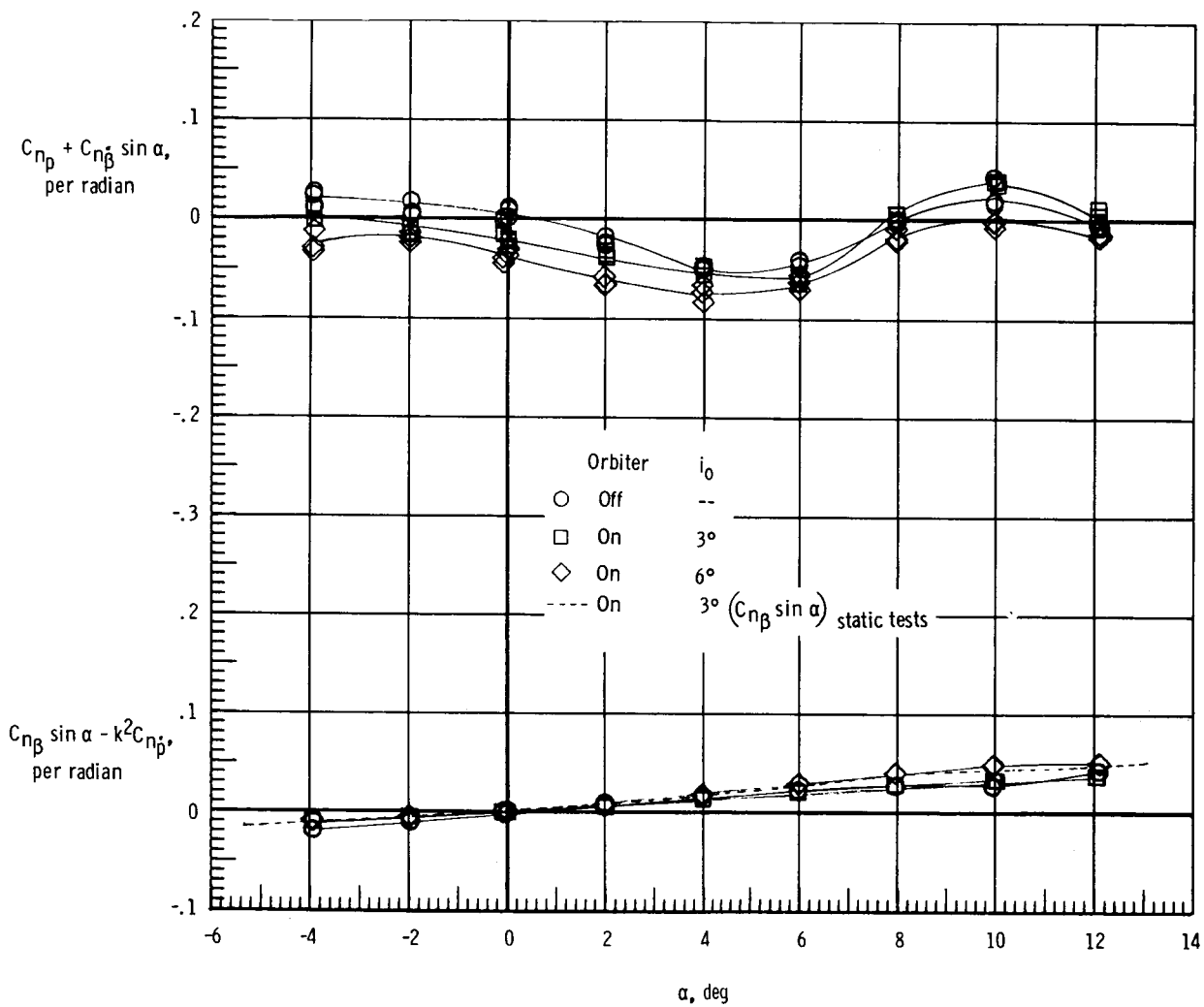Figure 30.- Continued.

(c) M = 0.5.

Figure 30.- Concluded.

(a) M = 0.2.

Figure 31.- Effect of orbiter and orbiter incidence on yawing moment due to roll-rate parameter and on yawing moment due to roll-displacement parameter of modified 747. Unfaired struts; tail cone on.
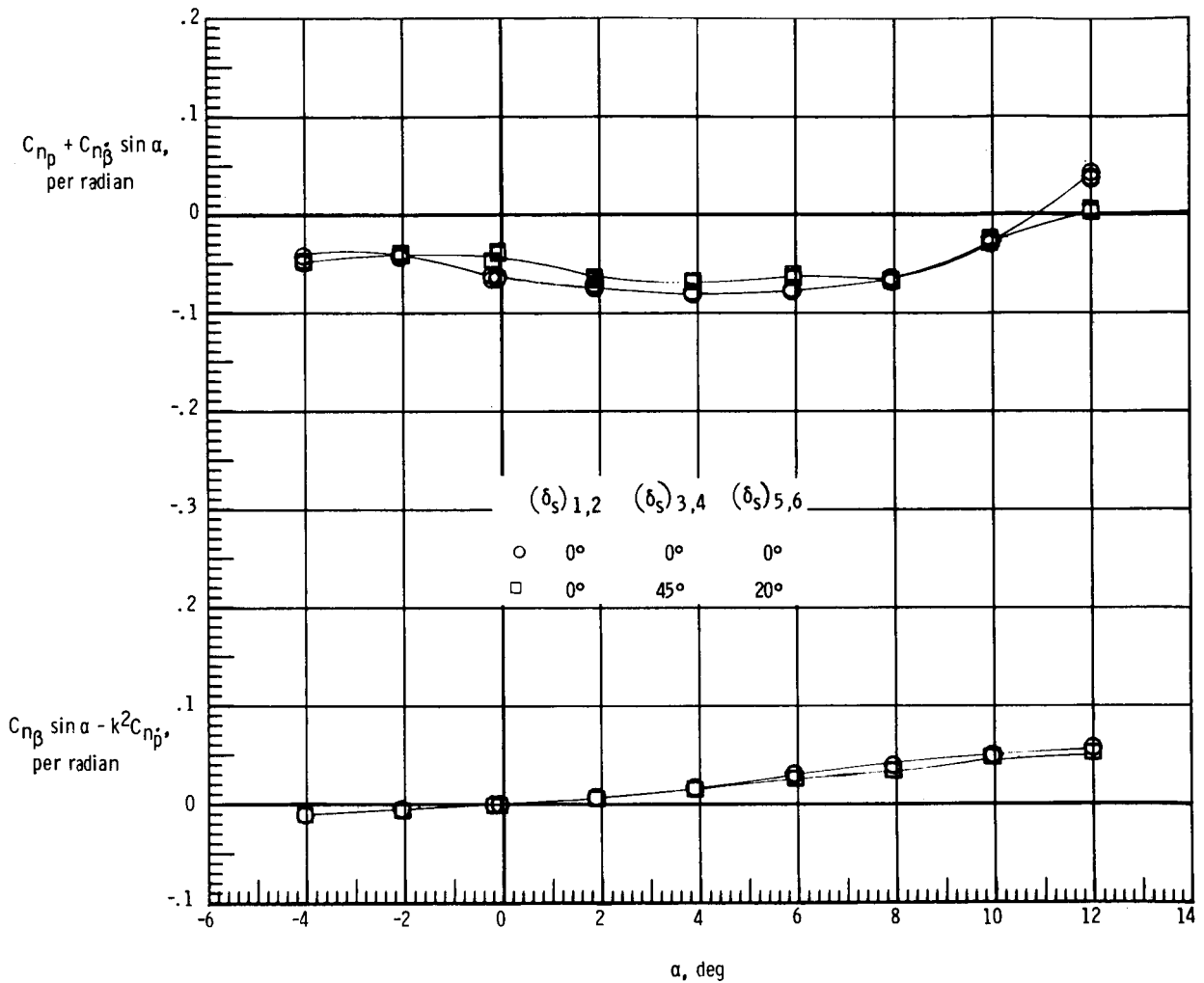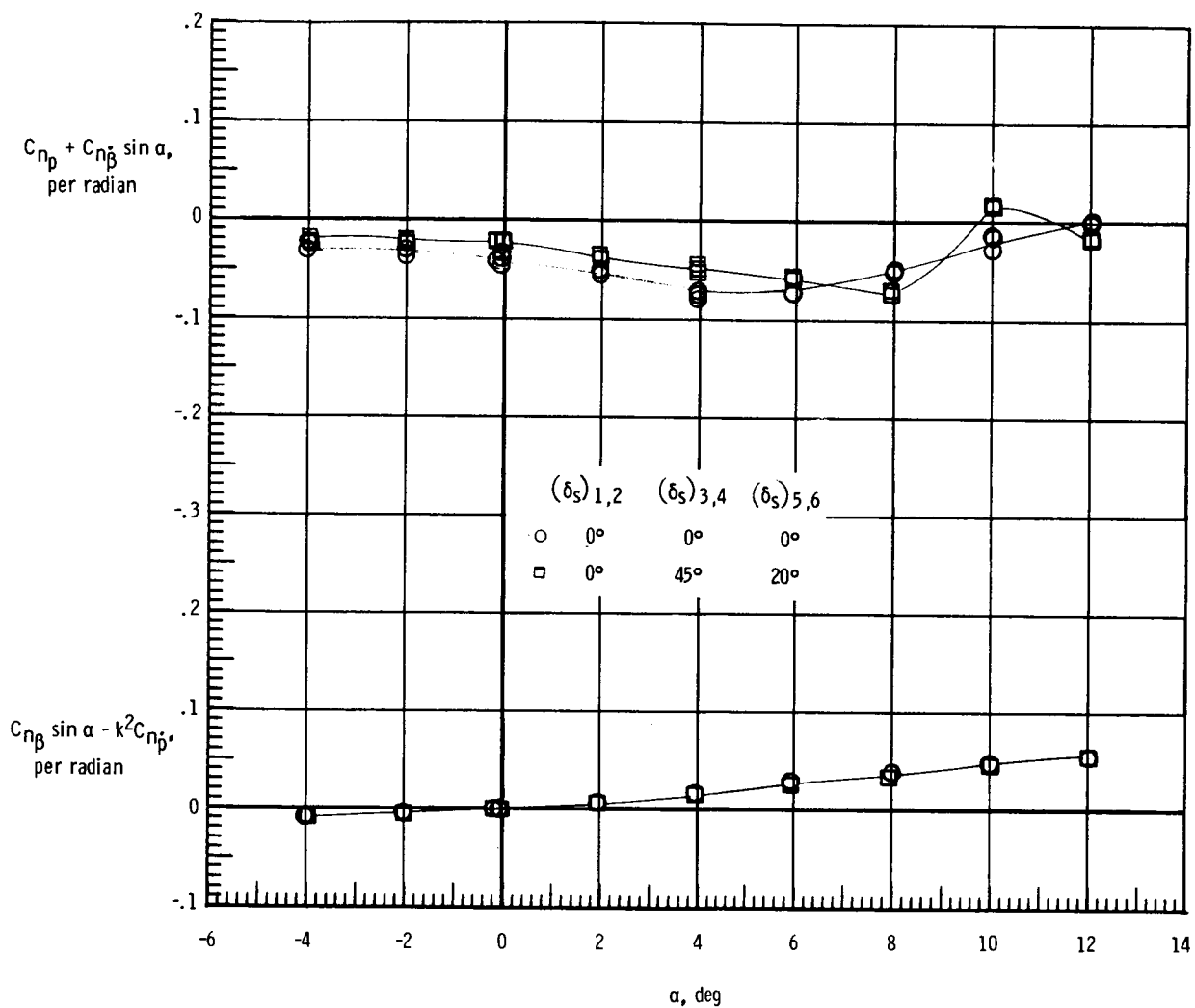
(b)   M = 0.4.

Figure 31.- Continued.

.2

.1

$C_{n_p} + C_{n_{\dot\beta}} \sin\alpha,$
per radian

0

-.1

-.2

-.3

Orbiter	i_o
○ Off	--
□ On	3°
◇ On	6°
---- On	3° $(C_{n_\beta} \sin\alpha)$ static tests

.2

.1

$C_{n_\beta} \sin\alpha - k^2 C_{n_{\dot p}},$
per radian

0

-.1

-6   -4   -2   0   2   4   6   8   10   12   14
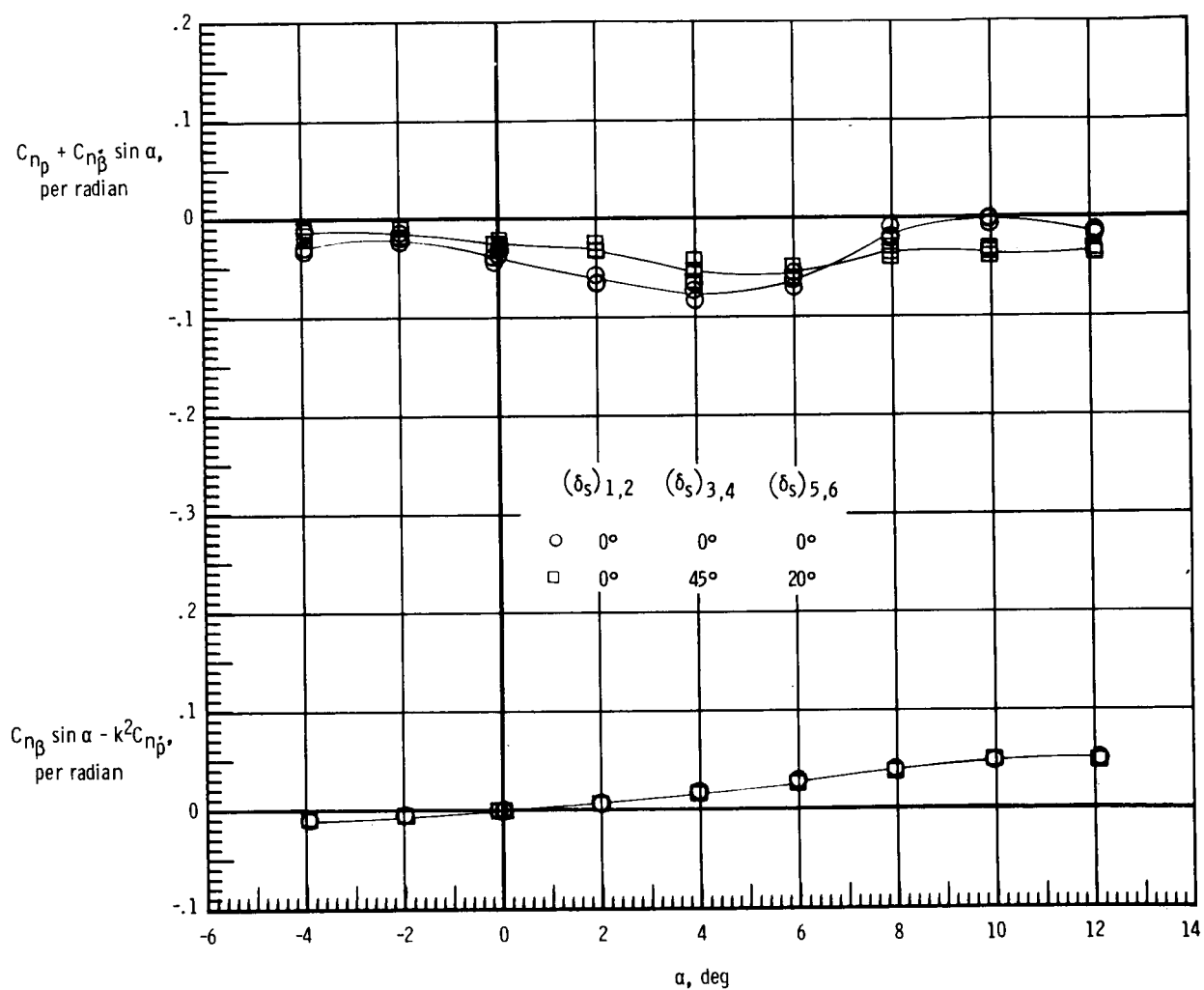
α, deg

(c)   M = 0.5.

Figure 31.- Concluded.

(a) M = 0.2.

Figure 32.- Effect of spoiler deployment on yawing moment due to roll-rate
parameter and on yawing moment due to roll-displacement parameter of
ALT configuration. i_o = 6°; unfaired struts; tail cone on.
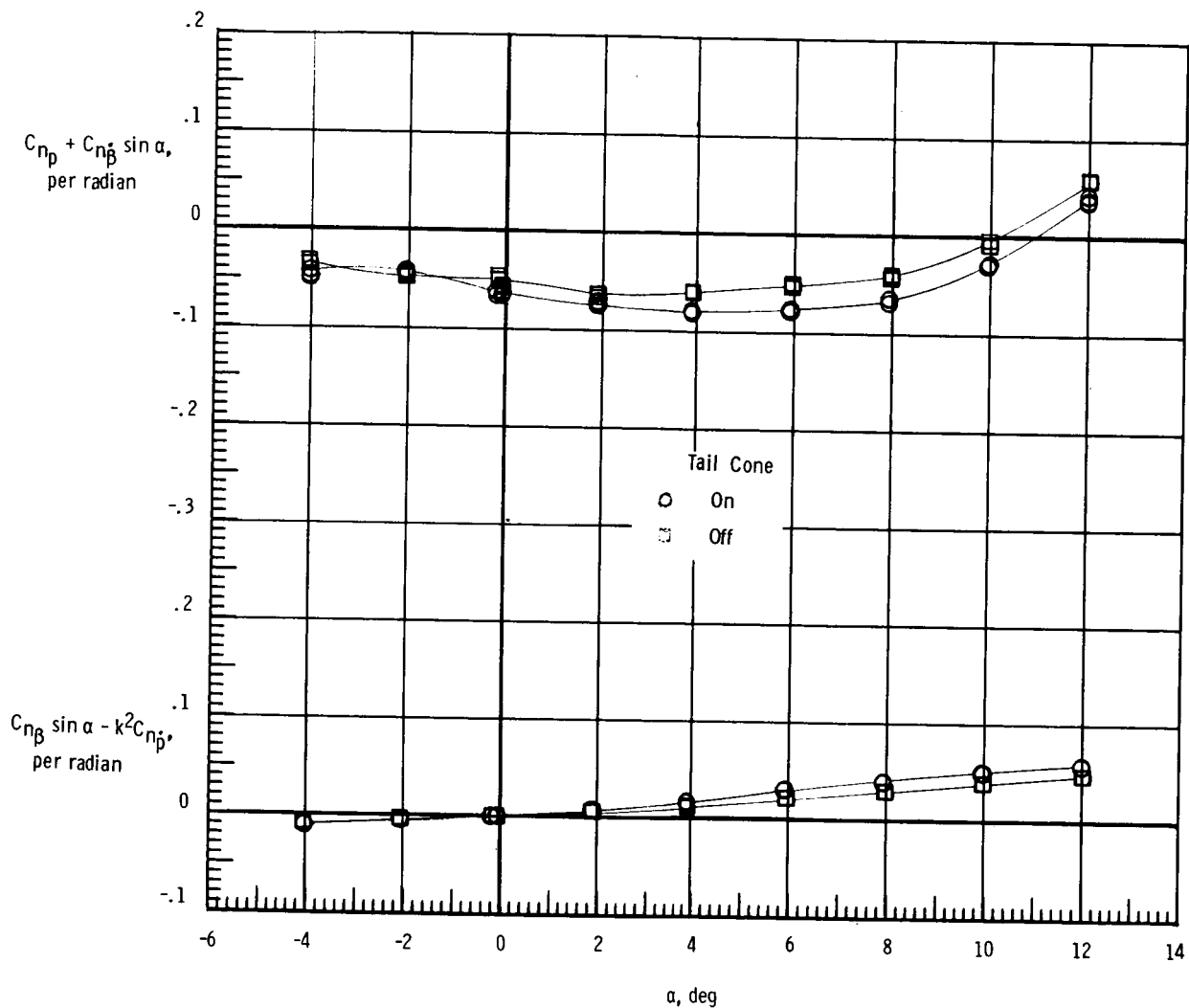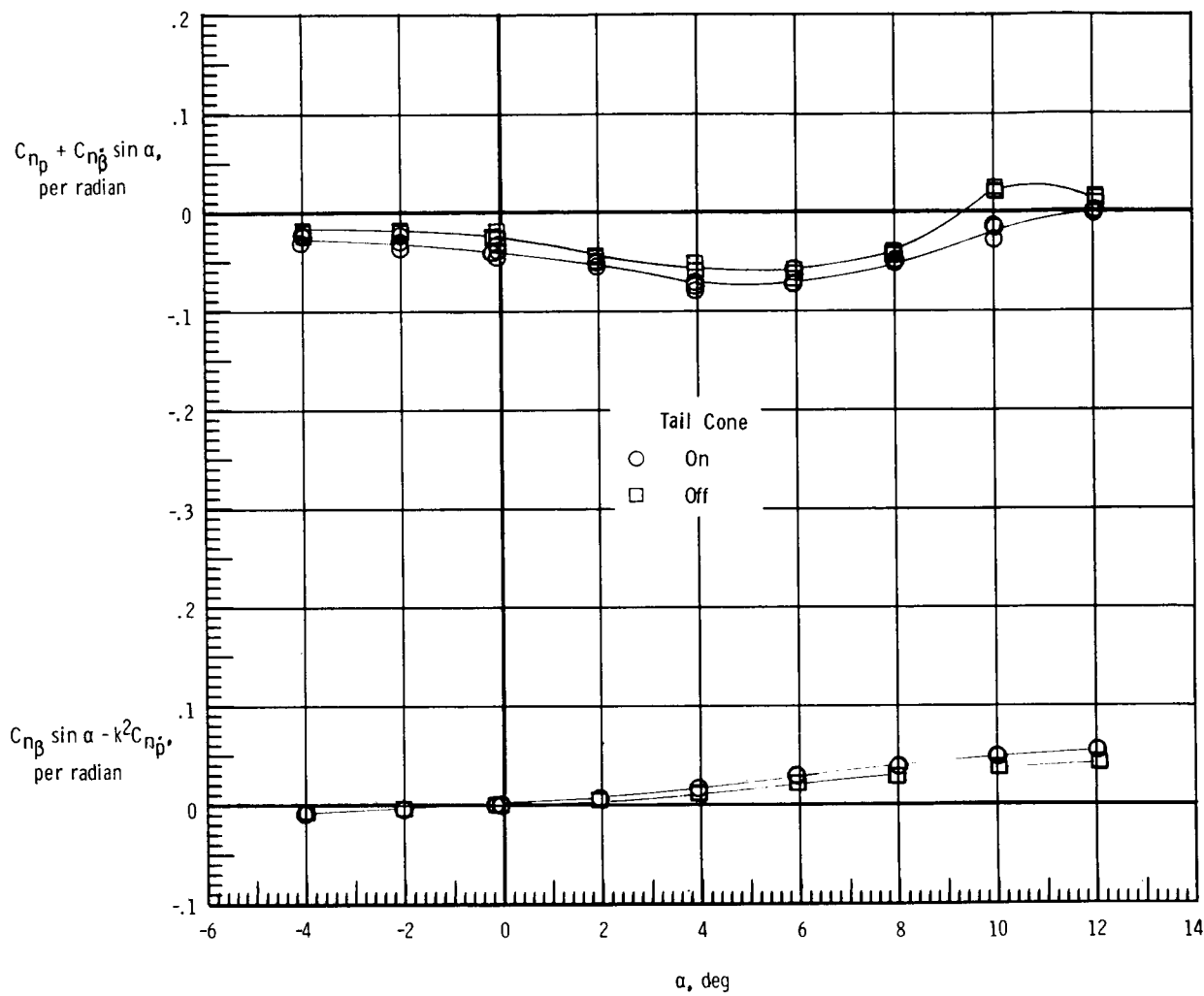
(b) M = 0.4.

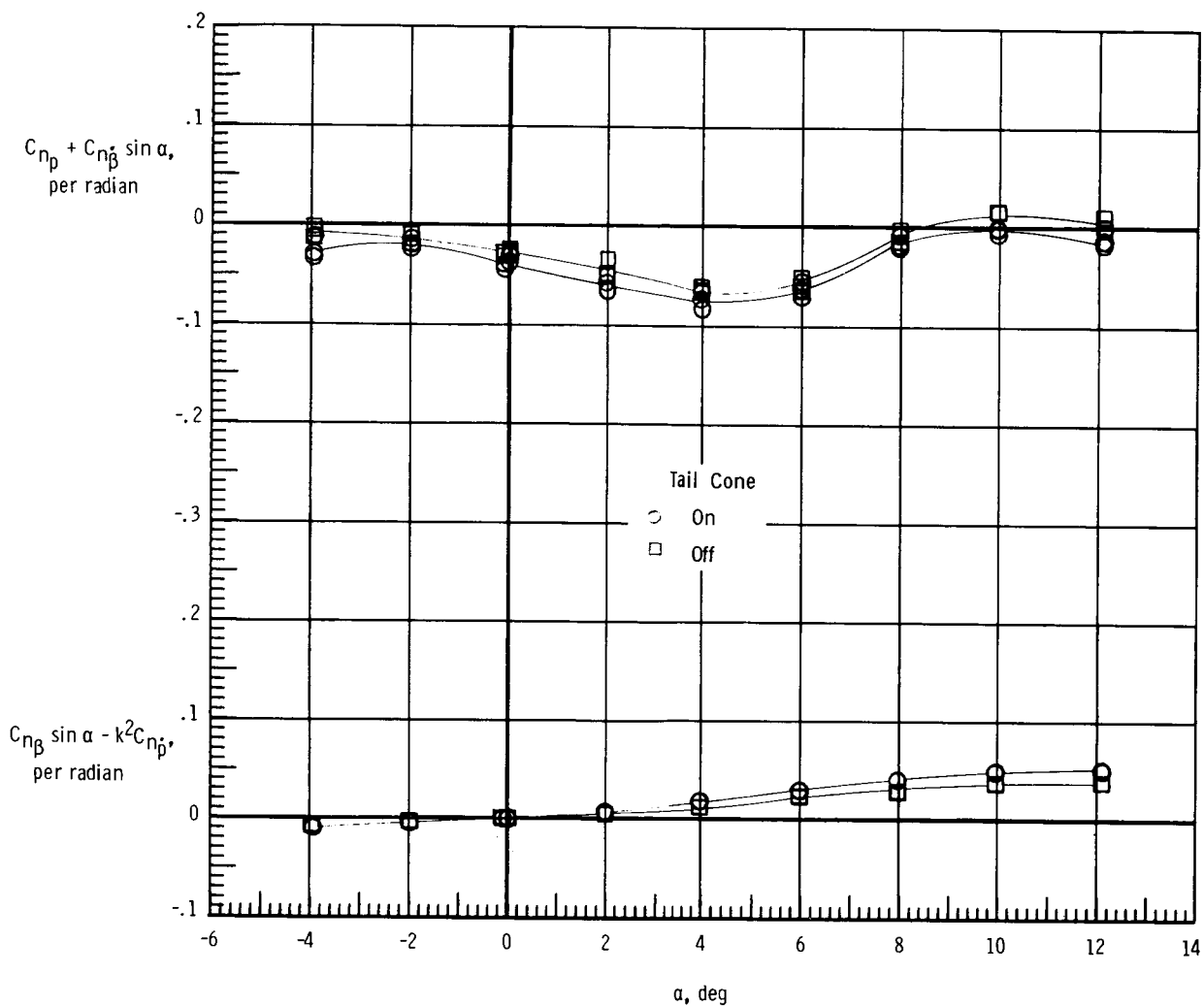Figure 32.- Continued.

(c) M = 0.5.

Figure 32.- Concluded.

(a) M = 0.2.

Figure 33.- Effect of tail cone on yawing moment due to roll-rate parameter and on yawing moment due to roll-displacement parameter of ALT configuration. $i_o = 6°$; unfaired struts.

(b)   M = 0.4.

Figure 33.- Continued.

(c) M = 0.5.

Figure 33.- Concluded.